Illuminating Subduction Systems: 50 years of limited geophysical success and what to do with so many remaining challenges

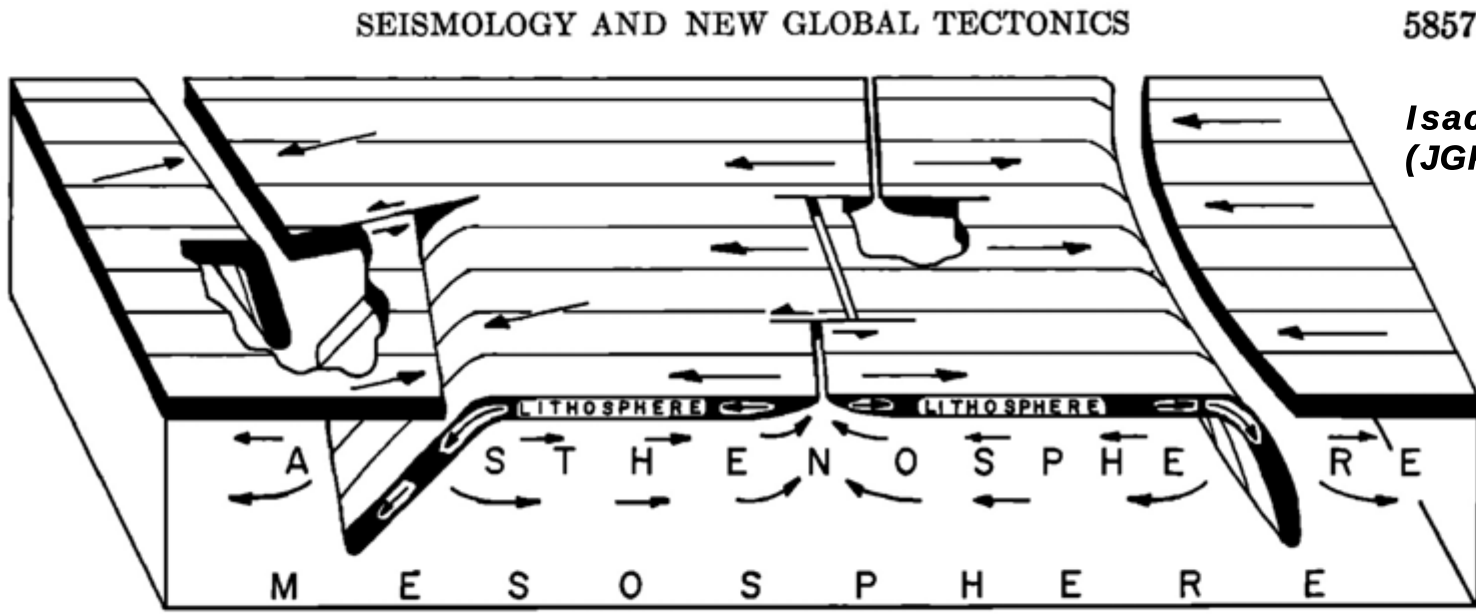

Isacks, Oliver, Sykes (JGR 1968)

César R. Ranero (ICREA at CSIC, Barcelona)

Ingo Grevemeyer, Jason Morgan, Valenti Sallares, Roland von Huene

Colloque: 50 years of Plate Tectonics: Then, Now, Beyond. **Paris 25-26 June 2018**

Subducted slabs beneath the eastern Indonesia–Tonga region: insights from tomography

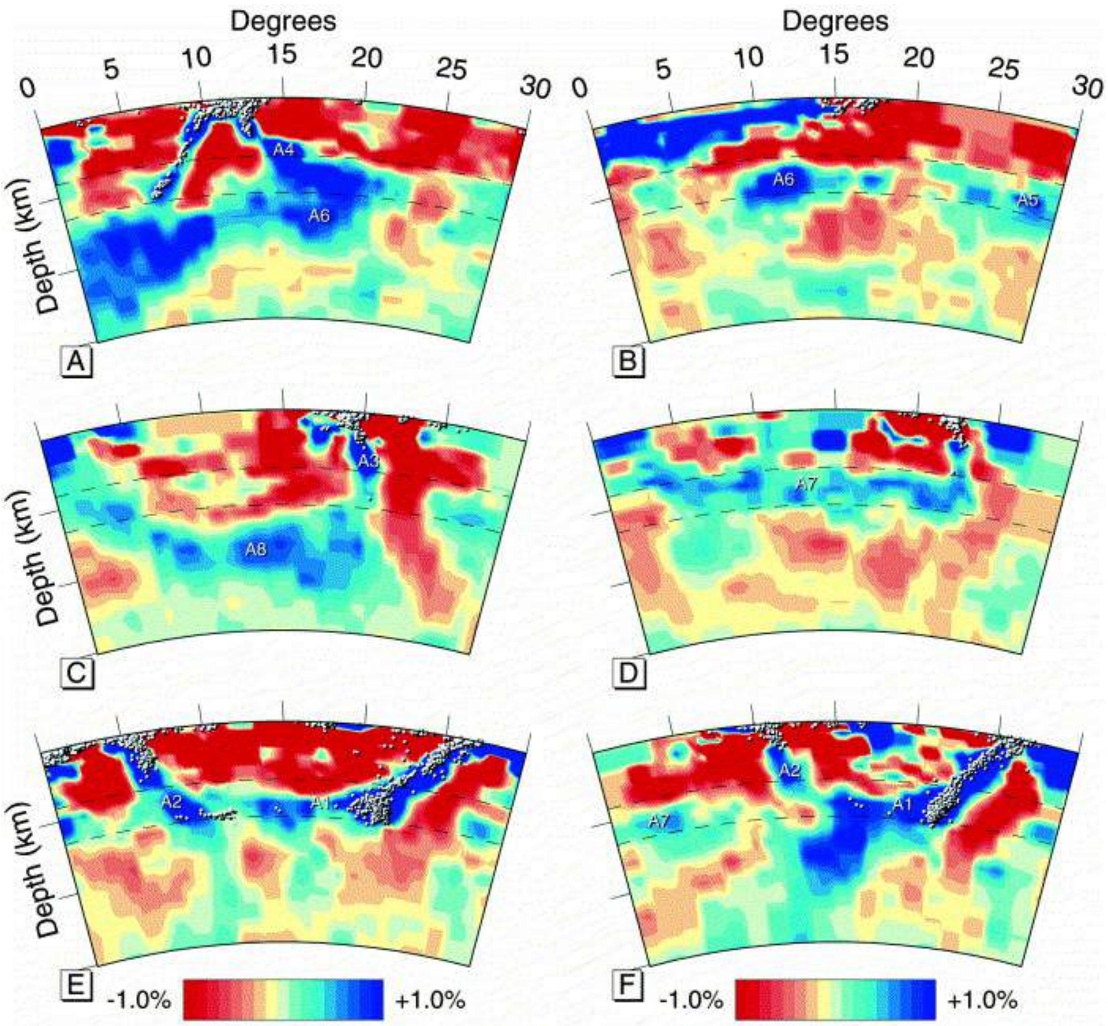

Hall & Spakman
EPSL 2002

Barcelona CSI
Center for Subsurface Imaging

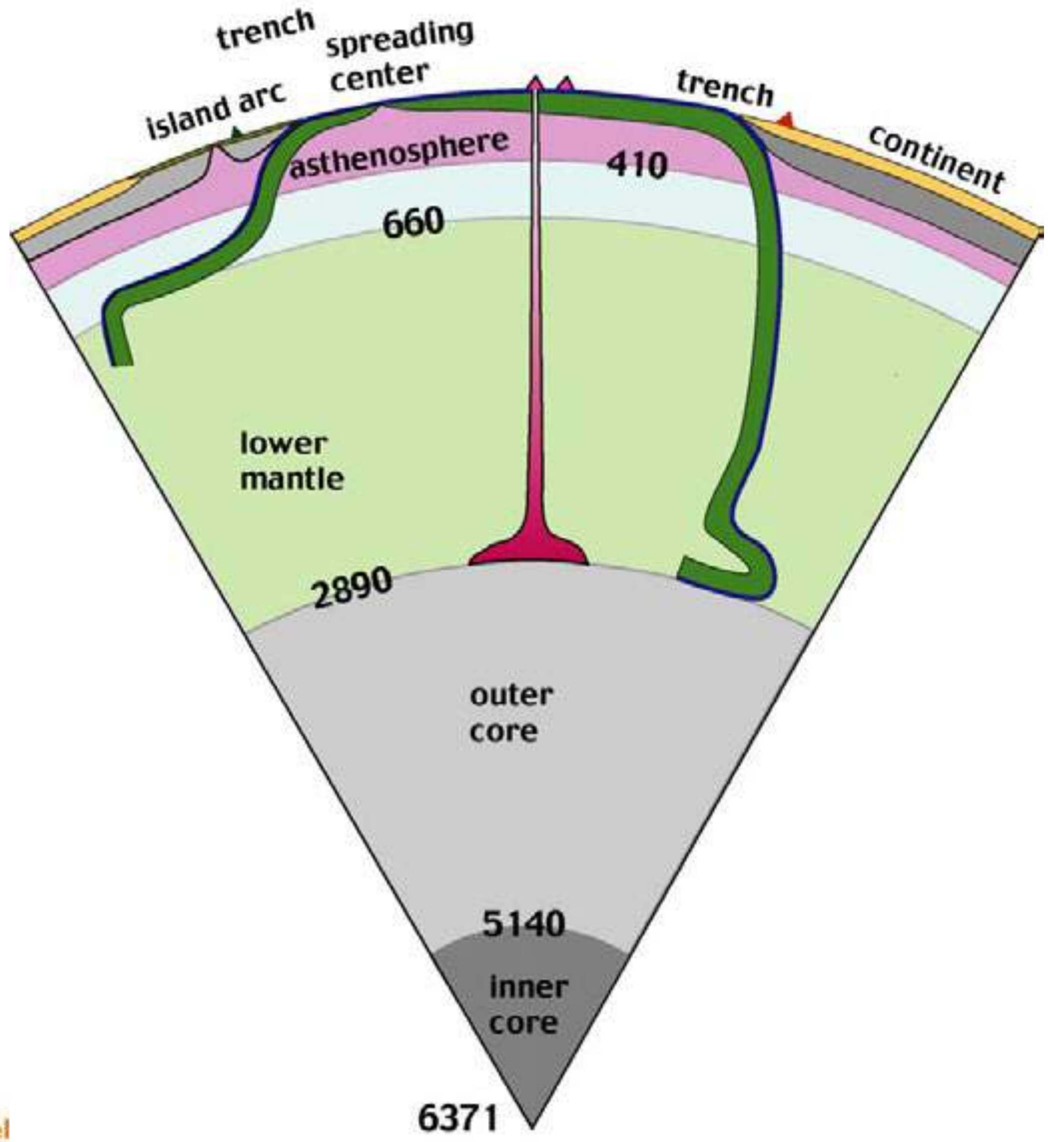

Barcel
Center for Subsurface Imaging

Recycling at subduction zones:

INPUTS:
Volume, structure, composition/fluid content

Pelagic and Detrital Sediment

Accretion/Tectonic erosion (V, S, C/F)

Oceanic crust (S, C/F)

Oceanic mantle (S, C/F)

Regions of concentrated deformation and exchange of materials, fluids and volatiles

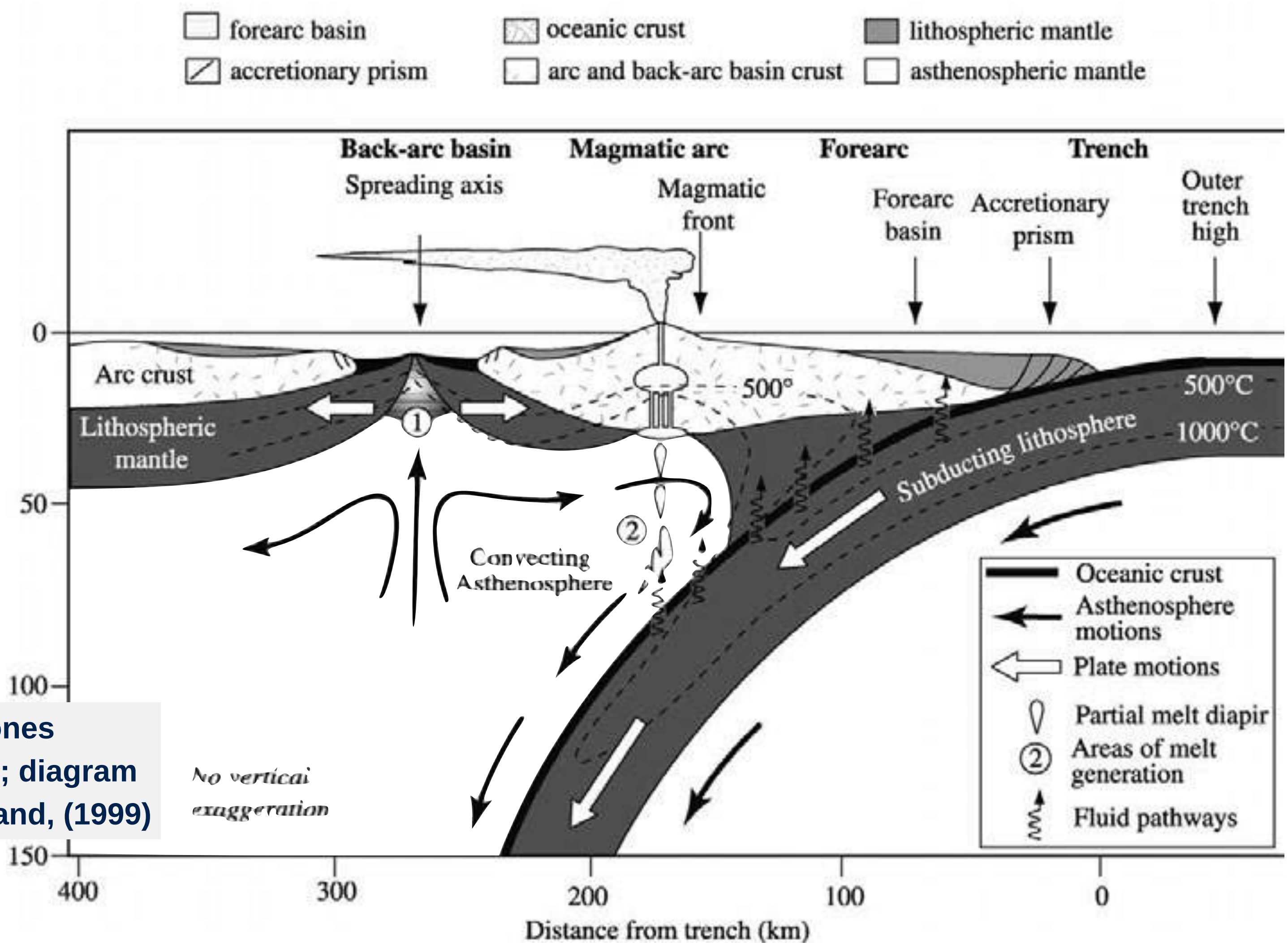

Stern, Subduction Zones (Rev. Geophys, 2002); diagram adapted from Lallemand, (1999)

Barcelona CSI
Center for Subsurface Imaging

Three major topics for the 21st century

- Earthquakes and Slow Slip Phenomena at the mega-thrust interplate fault.
- Fluids across the forearc, and their (speculative) relation to deformation.
- The incoming plates of subduction zones.
- What do to next to advance?

1. Earthquakes and Slow Slip Phenomena at the mega-thrust interplate fault.

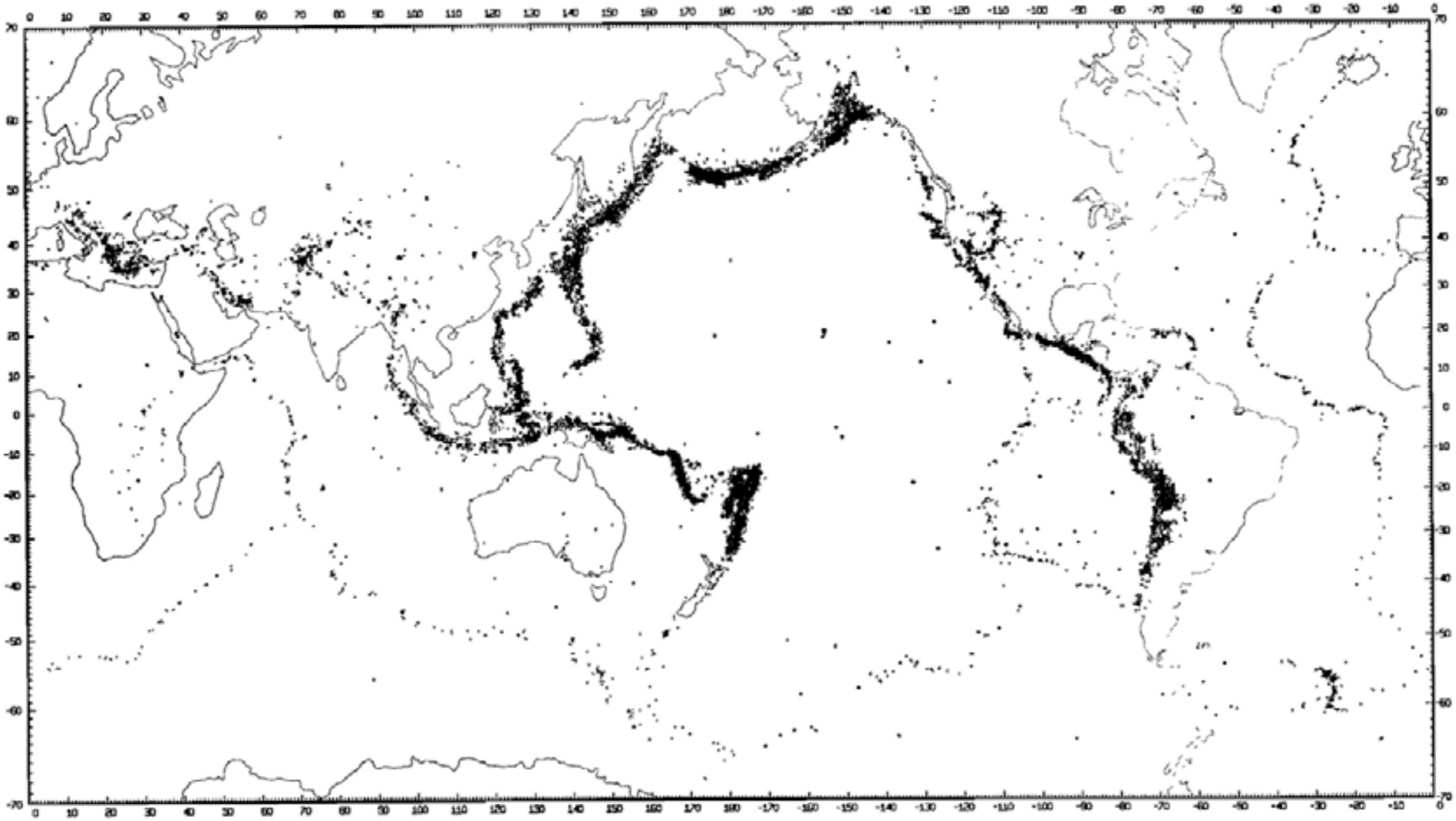

Fig. 15. Worldwide distribution of all earthquake epicenters for the period 1961 through 1967 as reported by U. S. Coast and Geodetic Survey [after *Barazangi and Dorman*, 1968]. Note continuous narrow major seismic belts that outline aseismic blocks; very narrow, sometimes steplike pattern of belts of only moderate activity along zones of spreading; broader very active belts along zones of convergence; diffuse pattern of moderate activity in certain continental zones.

EQ. recurrence & seismic gaps

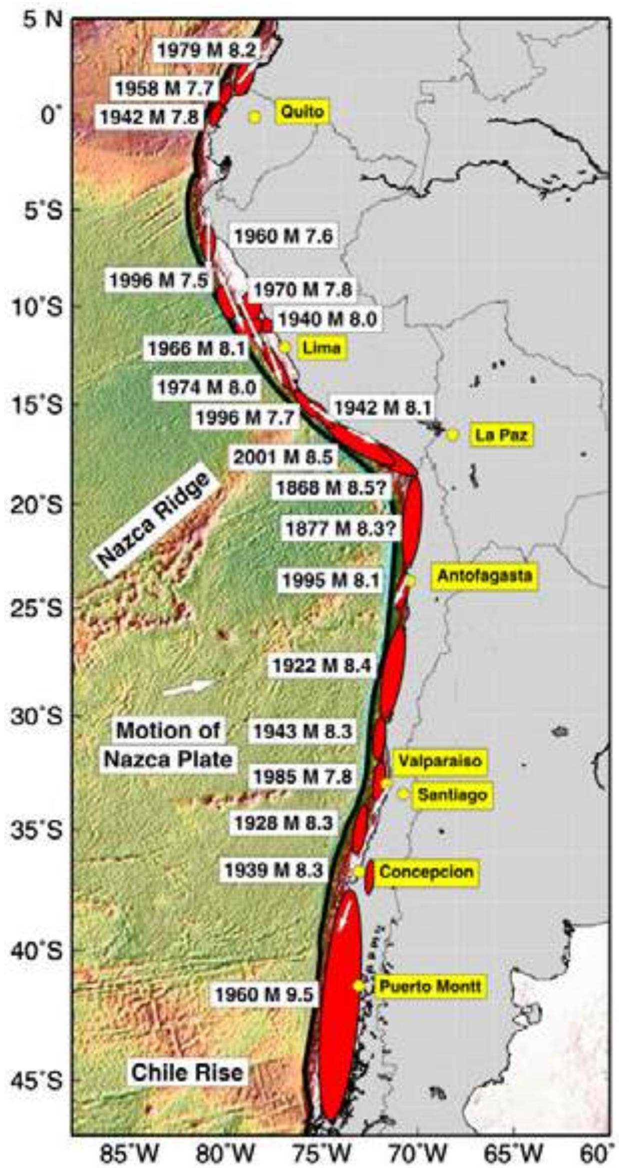

Pritchard et al., JGR 2007

Barcelona CSI
Center for Subsurface Imaging

The complex mechanical behaviour of faults

Slip on fault during 2004 Sumatra Mw9.2 EQ

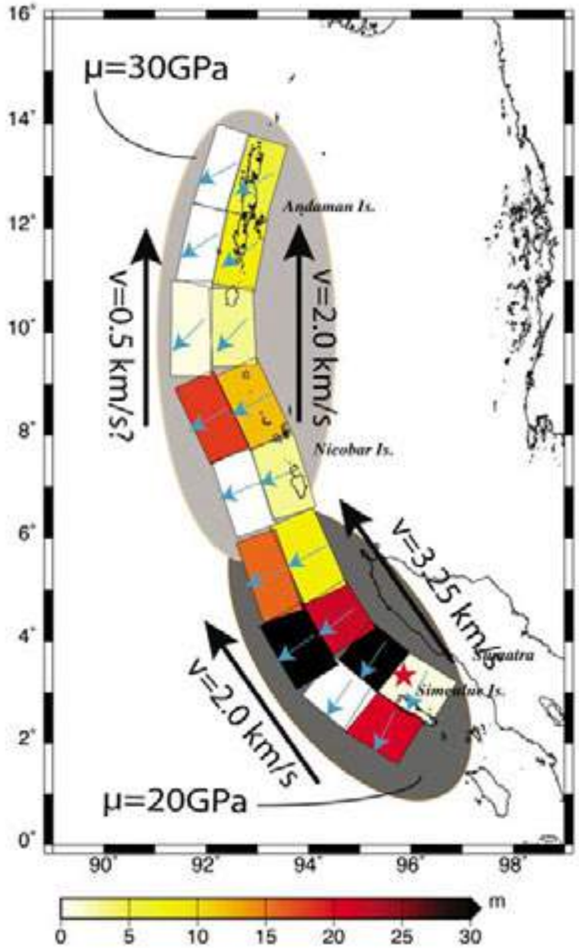

Lorito (Nature Geos. 2010)

Slip on fault during 2011 Tohoku-Oki Mw9 EQ

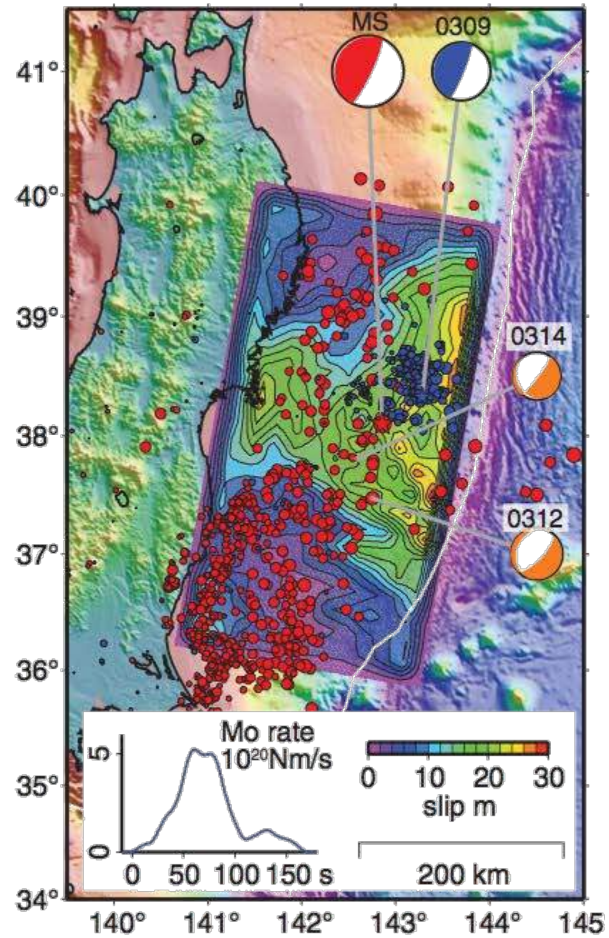

Ide et al., Science 2011

Barcel
Center for Subsurface Imaging

Broken Paradigms

"Almost all the recent EQ have violated some theories of where and when great earthquakes can occur and what their consequences can be." (*Lay, Nature 2012*).

Outdated conceptual models of where Giant EQ may occur

Young plates & Fast convergence (Ruff & Kanamori 1980)	2004 Andaman Mw9.2 slow convergence
Voluminous sediment in the trench (Ruff, 1984)	2011 Tohoku-Oki Mw9.0 sediment starved
Predict Max. EQ-Mw & recurrence time (Nishenko, USGS-report 1984).	2011 Tohoku-Oki Mw9.0 millennia-scale recurrence

Barcelona CSI
Center for Subsurface Imaging

Slow Slip Phenomena

LFE (red), VLF (orange), and SSE (green) occur in the Nankai trough while ETS (light blue) occur in the Cascadia subduction zone. These follow a scaling relation of $M0 \propto t$, for slow earthquakes. Purple circles are silent earthquakes. Black symbols are slow events listed in the bottom half of Table 1. **a**, Slow slip in Italy[23,24], representing a typical event (circle) and proposed scaling (line). **b**, VLF earthquakes in the accretionary prism of the Nankai trough[26]. **c**, Slow slip and creep in the San Andreas Fault[21,22]. **d**, Slow slip beneath Kilauea volcano[25]. **e**, Afterslip of the 1992 Sanriku earthquake[27]. Typical scaling relation for shallow interplate earthquakes is also shown by a thick blue line.

Ide et al., (Nature 2007)

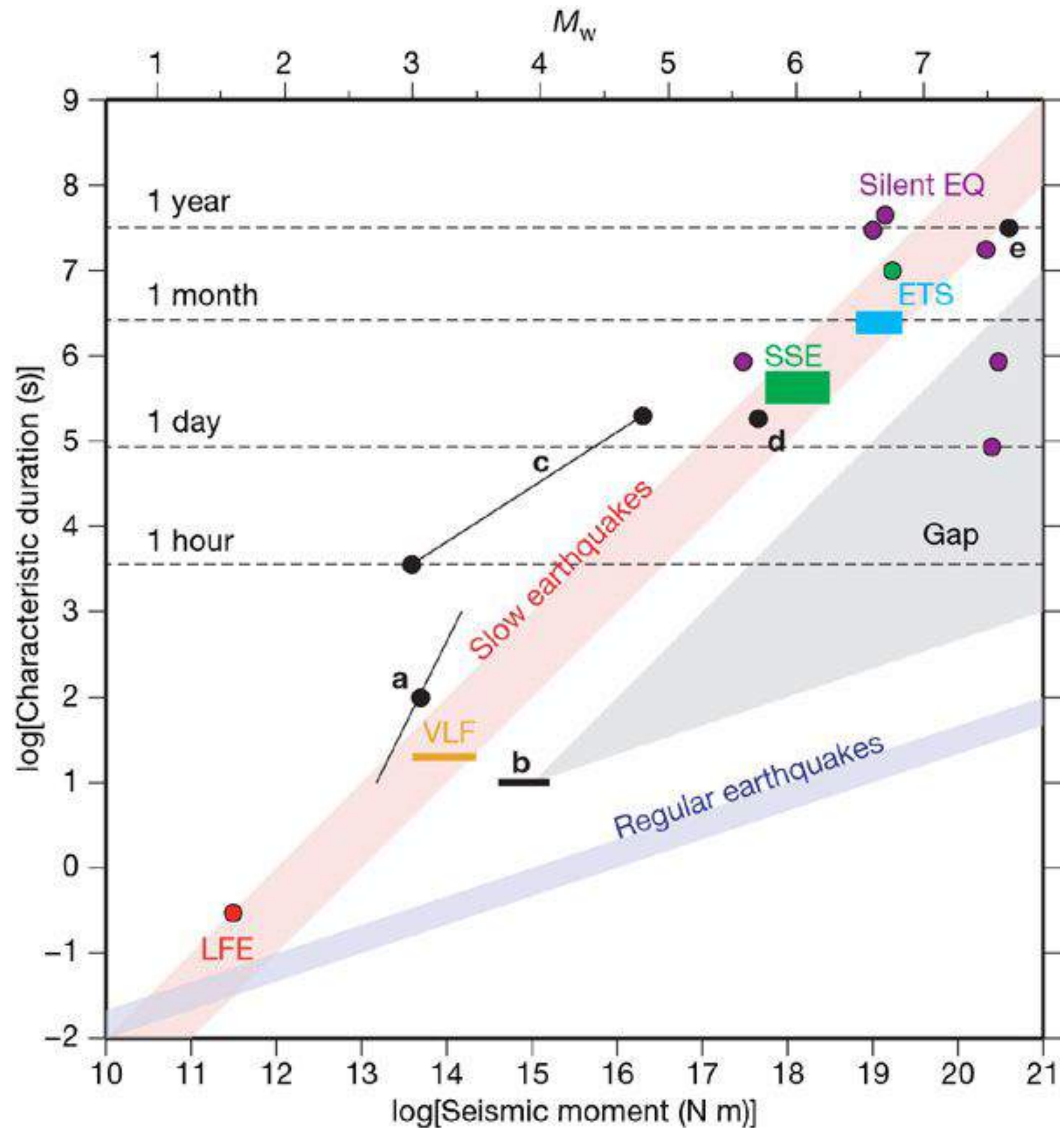

Slow Slip Phenomena

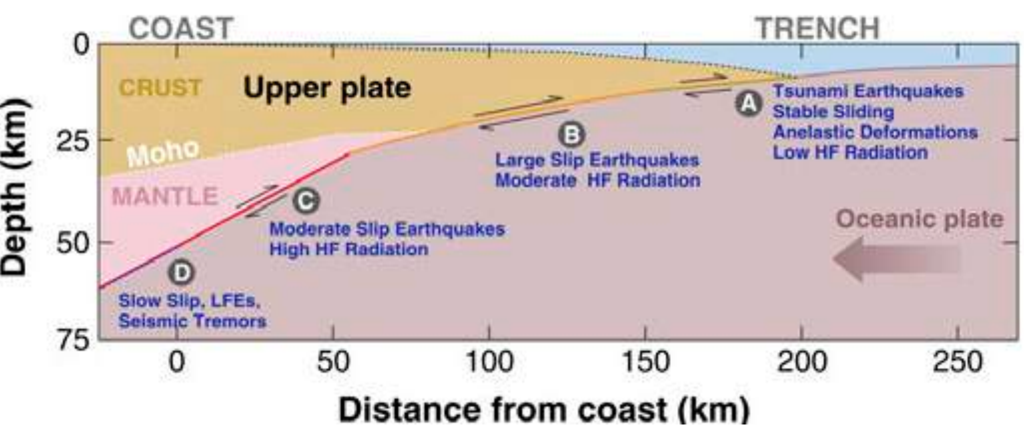

Ye et al. (2016)

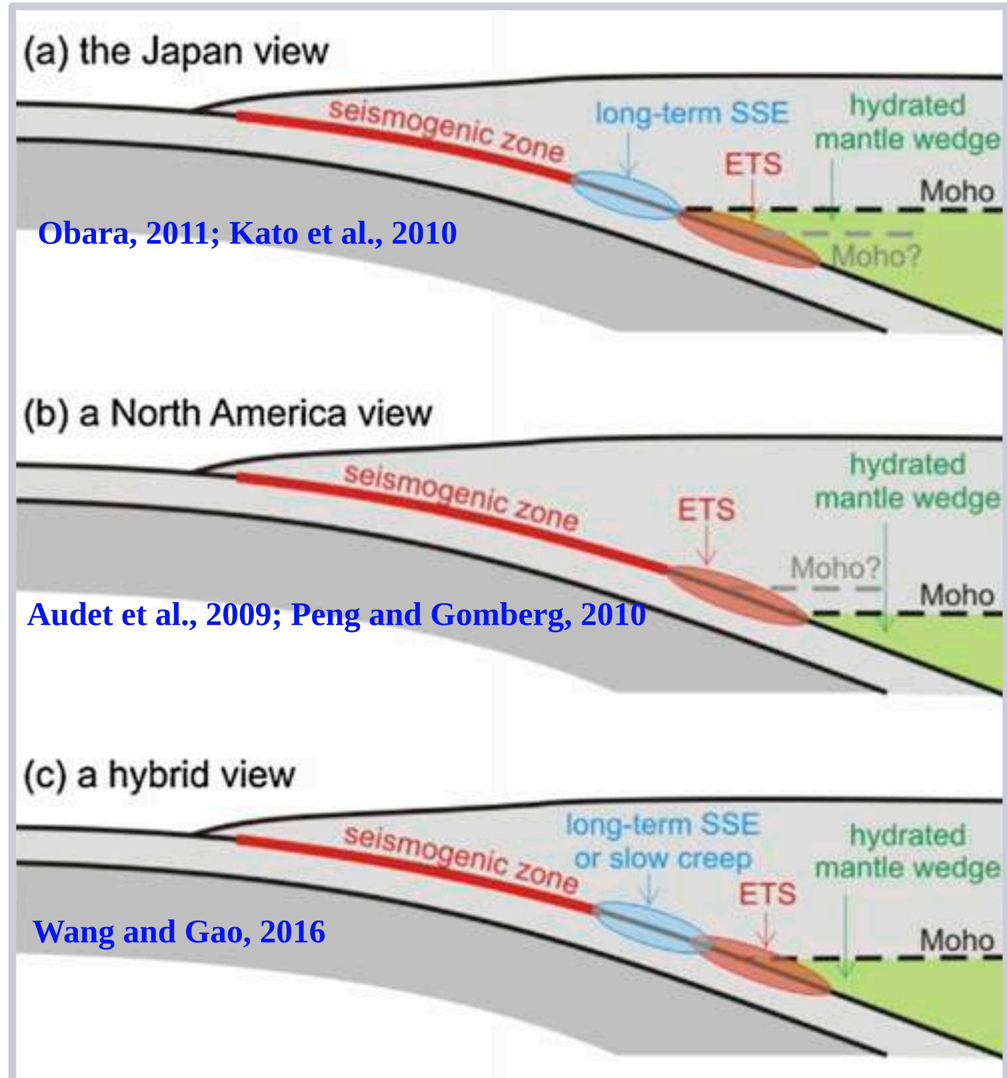

after Wang and Trehu (2016)

Mega-thrust fault and upper plate sampling, characterisation and monitoring

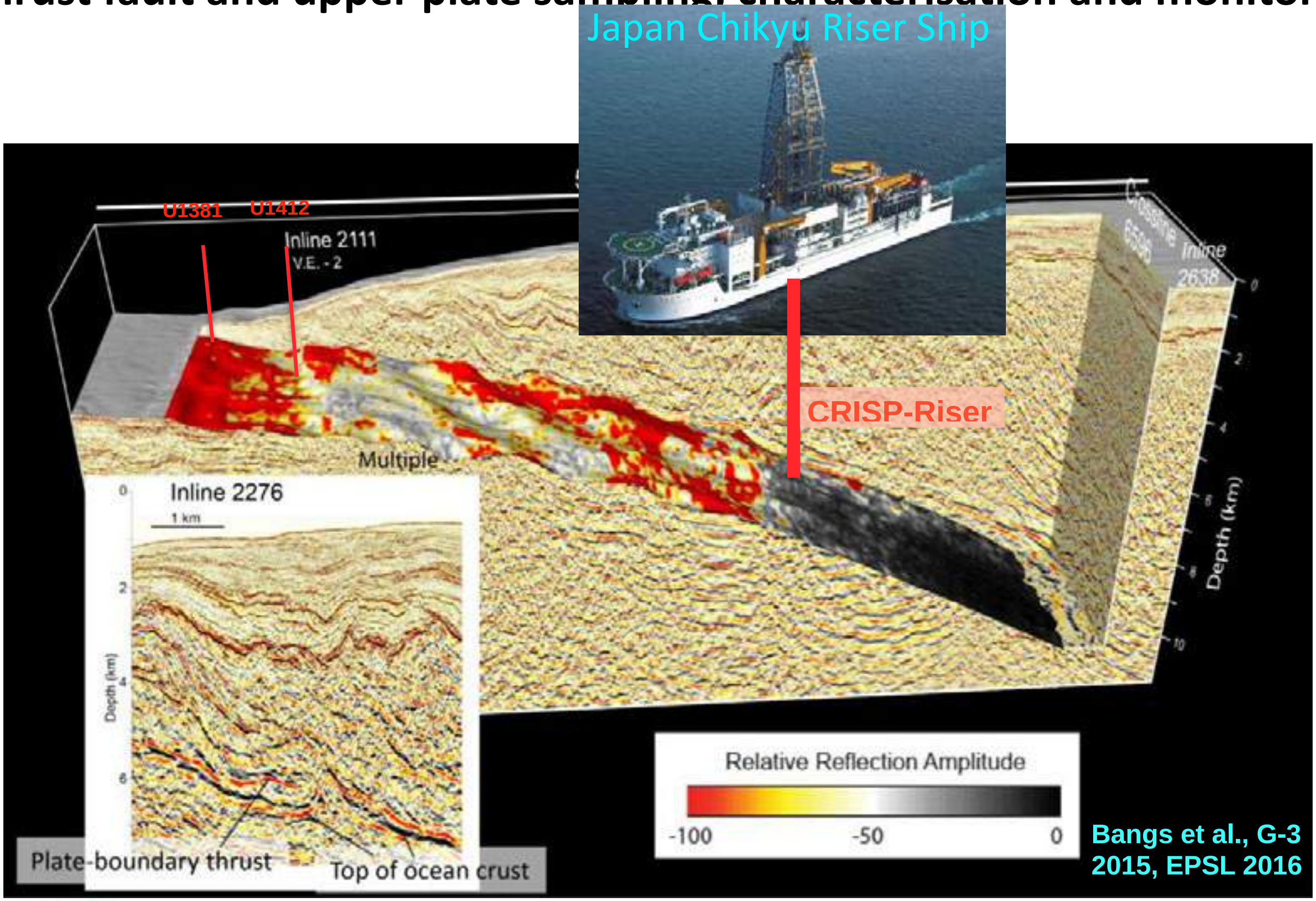

Bangs et al., G-3 2015, EPSL 2016

Understanding EQ nucleation, rupture propagation and arrest

Mega-thrust frictional environment: Fault mechanics

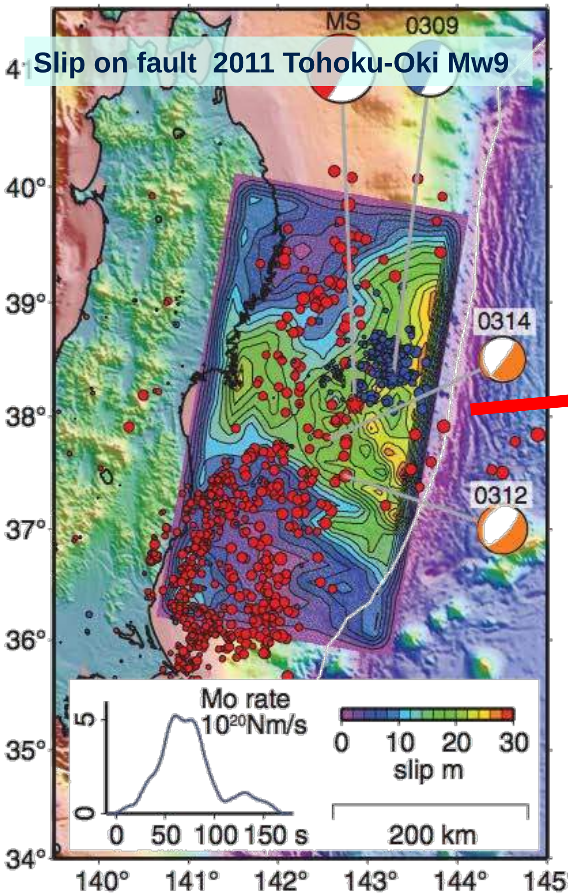

Ide et al., Science 2011

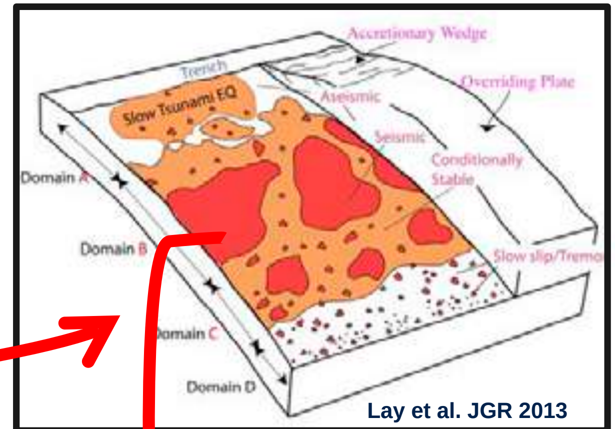

Lay et al. JGR 2013

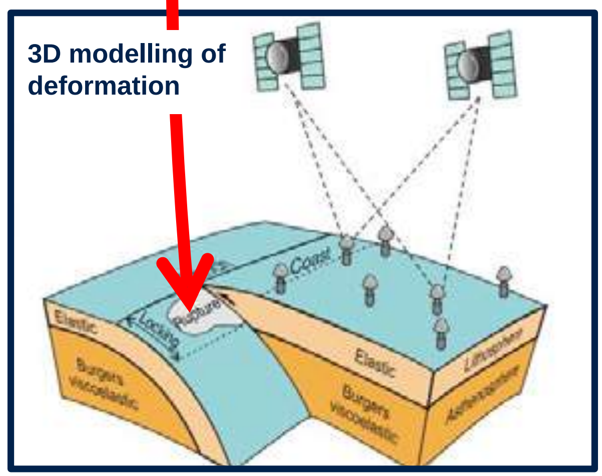

Wang et al., Nature 2012

Barcelona CSI
Center for Subsurface Imaging

Understanding EQ nucleation, rupture propagation, and arrest will require 4D observations

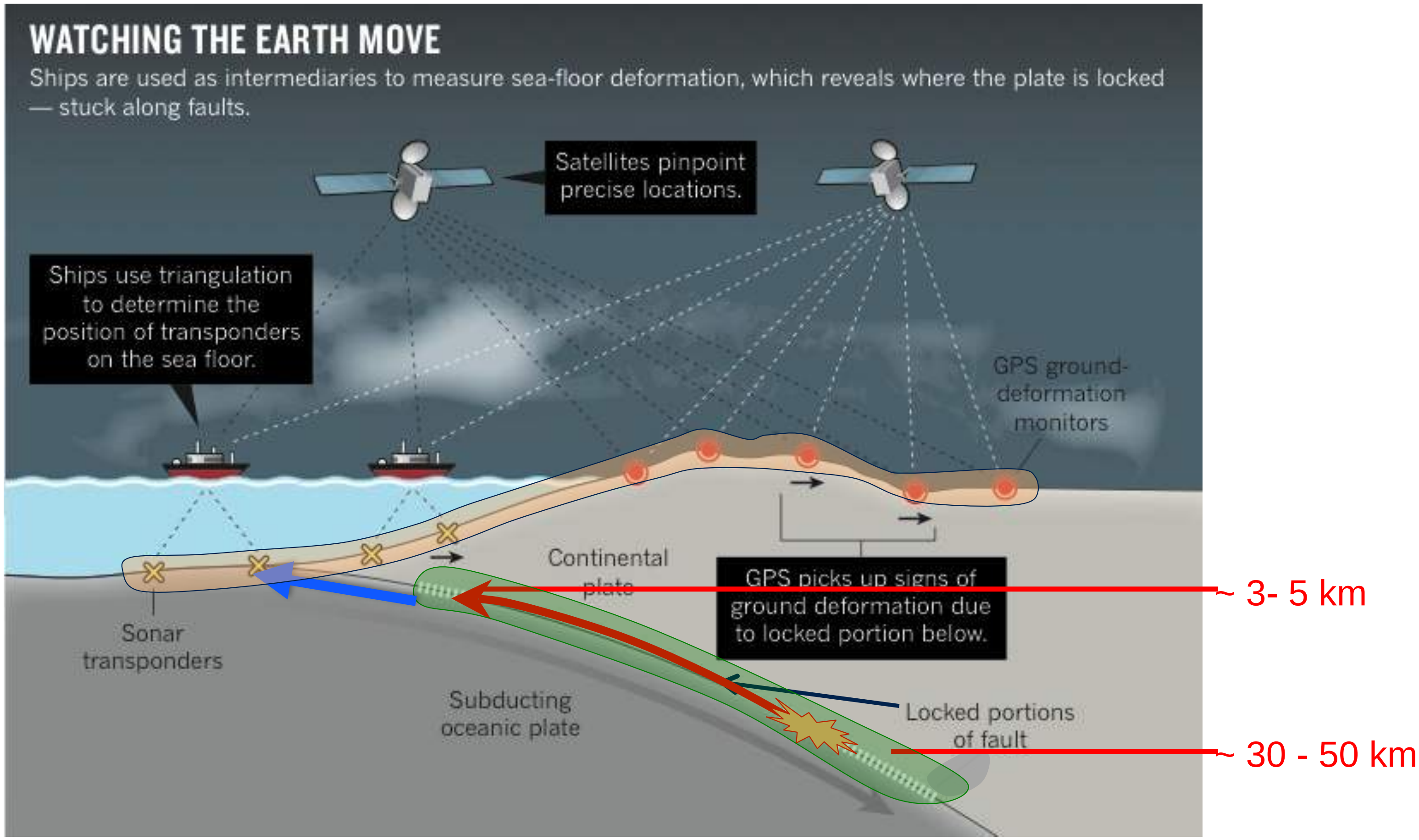

Newman, (Nature 2011)

2. Fluids across the forearc, and their (speculative) relation to deformation

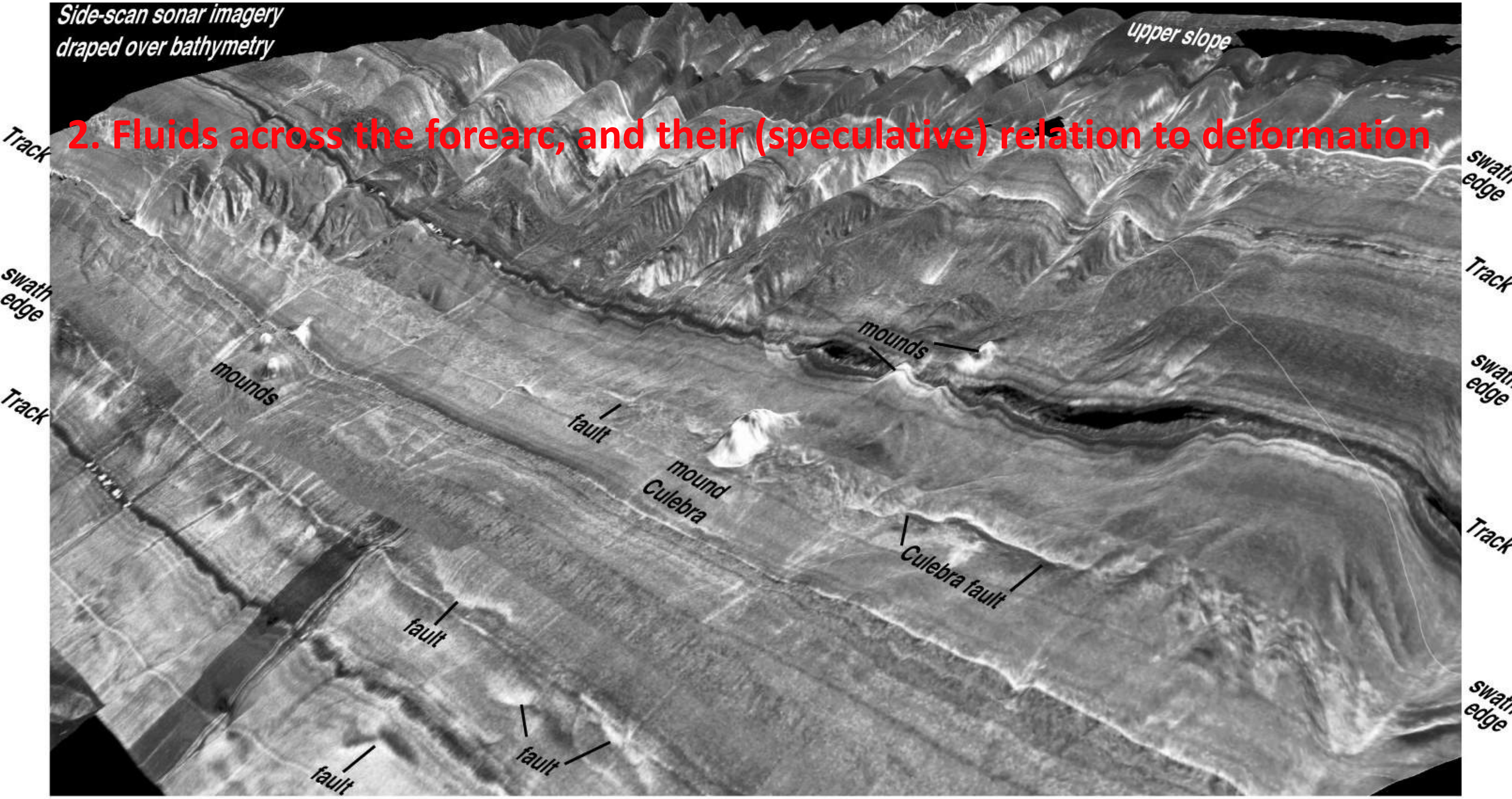

Seepage at the seafloor

Ranero et al., (G-cubed, 2008)

Fluids & deformation

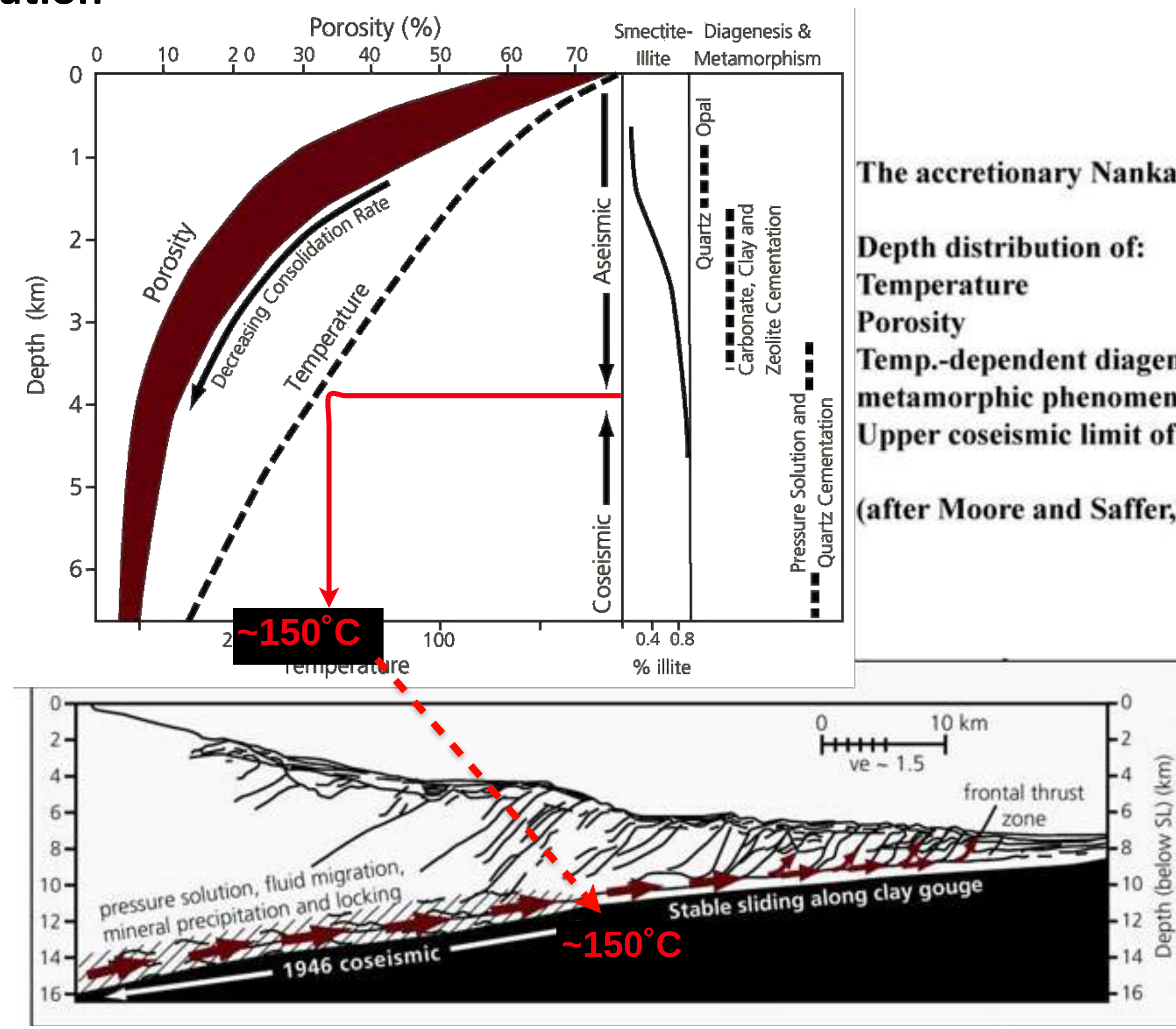

The accretionary Nankai margin

Depth distribution of:
Temperature
Porosity
Temp.-dependent diagenetic and metamorphic phenomena
Upper coseismic limit of 1946 great earthquake

(after Moore and Saffer, 2001)

Figures taken from Margins Science Plan

R. Stern, **Subduction Zones**, Review of Geophysics, 2002

“Review aimed at:

1) Advanced undergraduate or beginning graduate student.

2) Professional not specialised in subduction zones “

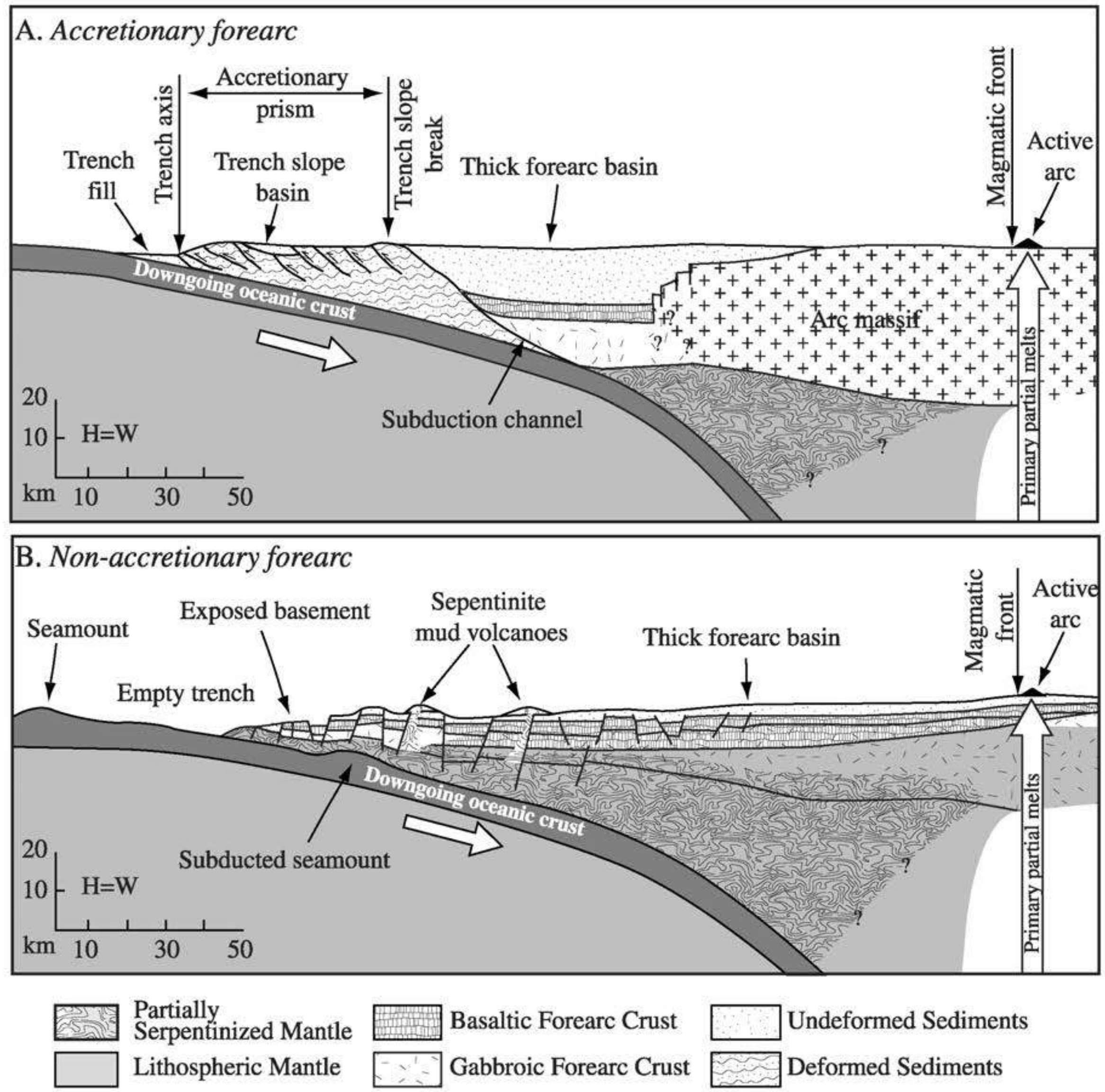

Barcelona CSI
Center for Subsurface Imaging

World Convergent Margins

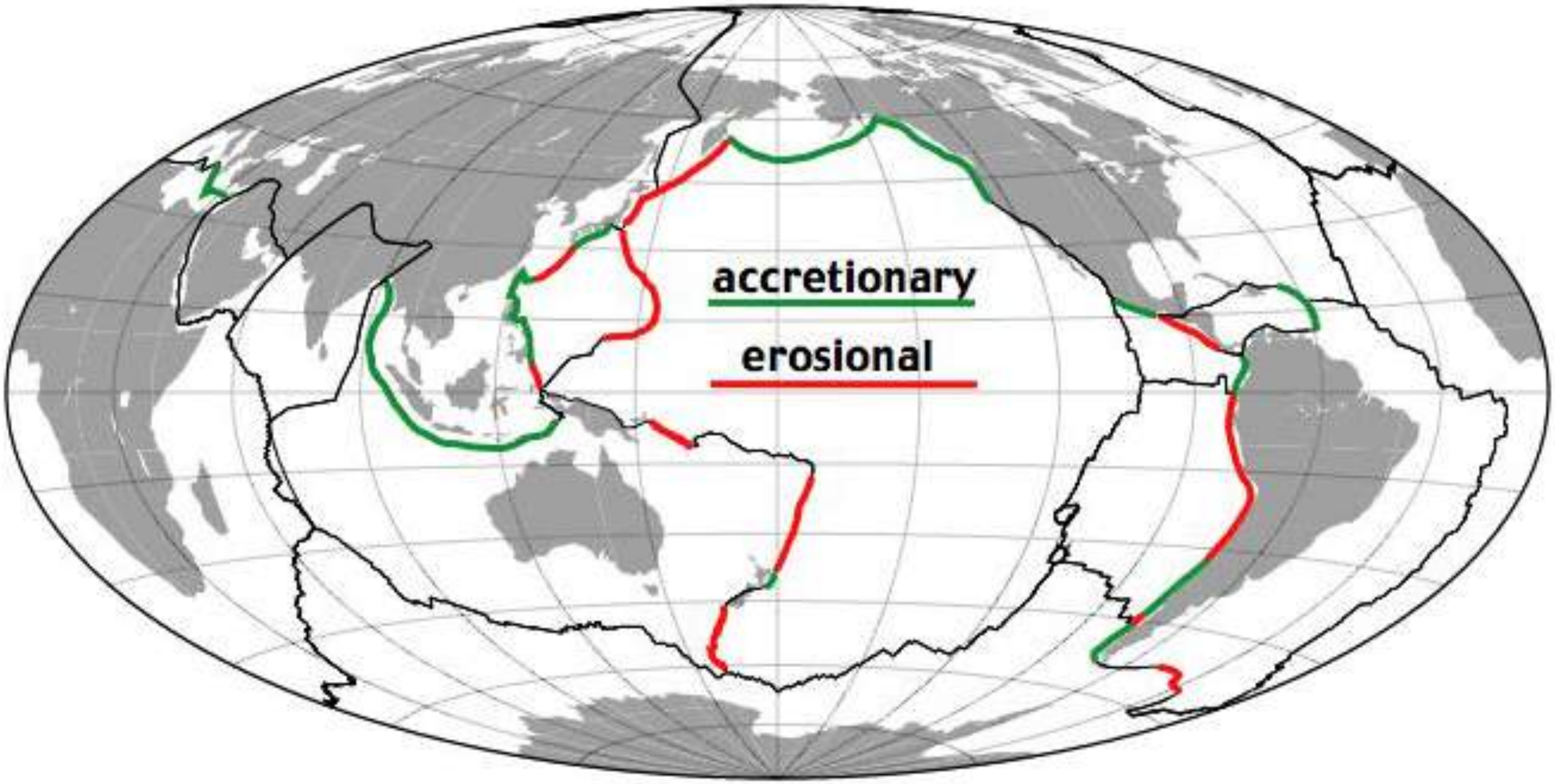

About 50-50%

Barcelona CSI
Center for Subsurface Imaging

Accretionary prism structure is well displayed in seismic images

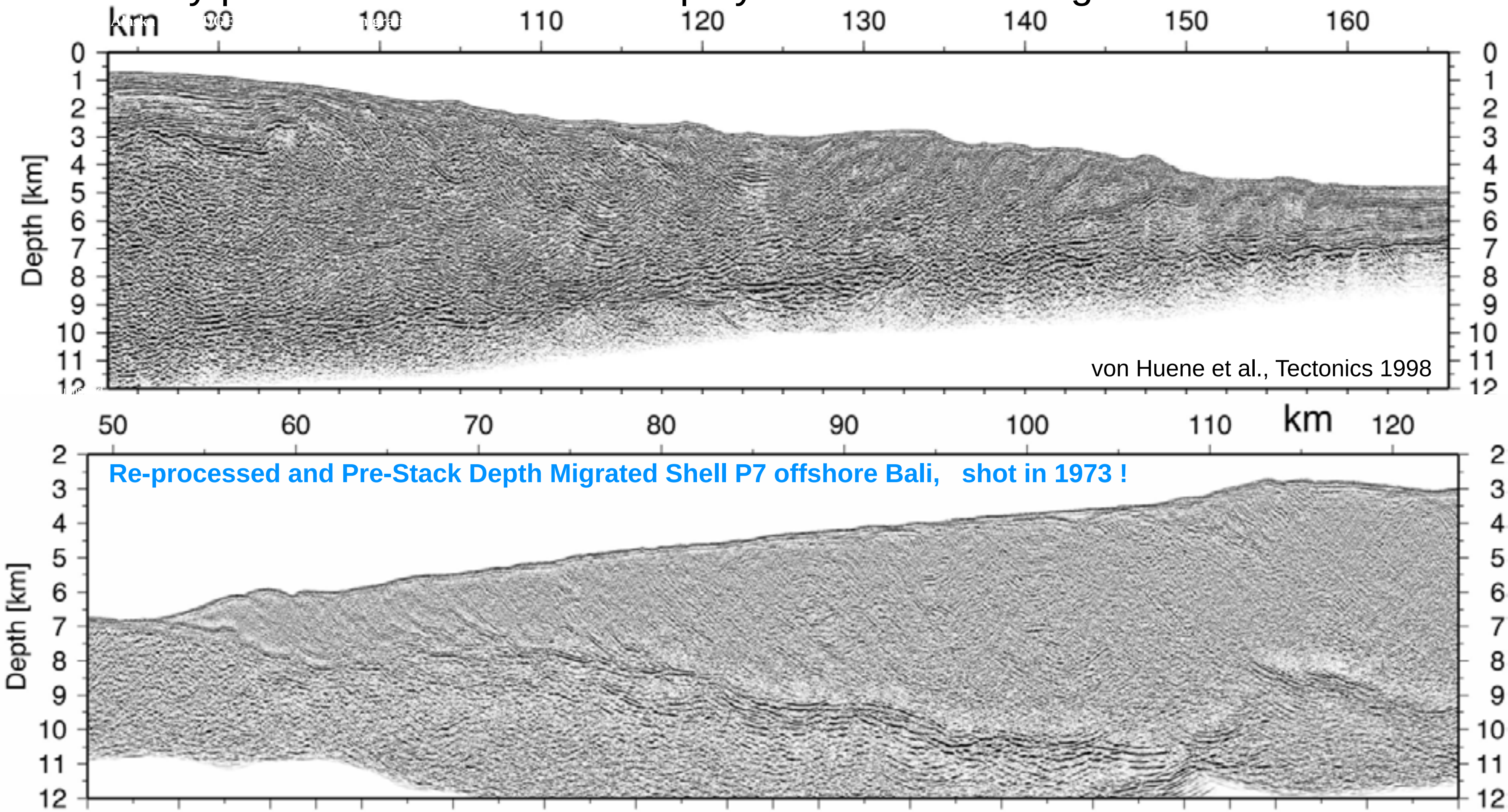

Barcelona CSI
Center for Subsurface Imaging

Ranero, Unpublished

The hydrogeological system of accretionary prisms

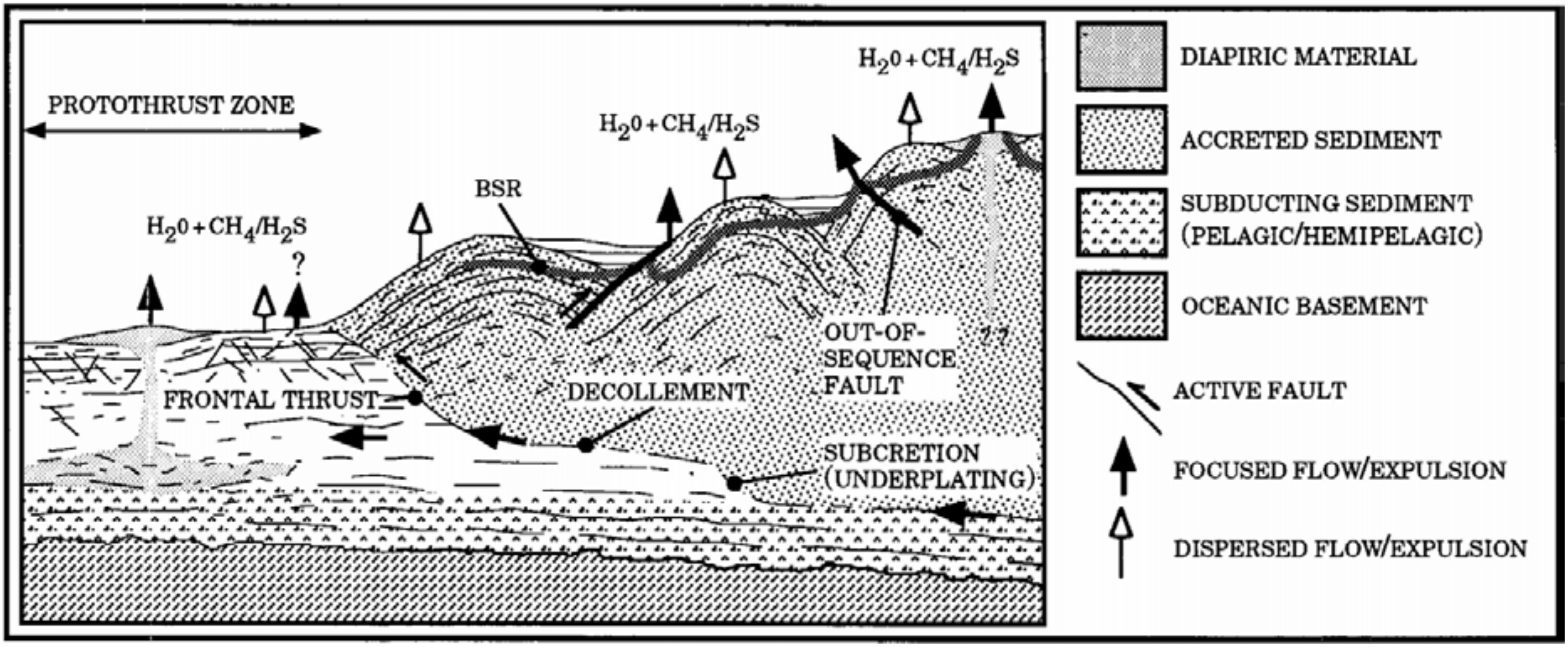

"On most prisms, fluid vents are thought to cover < 1% of the total surface area and although flow rates from active vents are high (10^5-10^{10} mm/yr), their contribution to estimates of total discharge (dispersed plus focused, Table 3) is not apparent." (**Carson and Screaton, Rev. Geophys. 1998**)

Conventional Wisdom in early 2000s:

The hydrogeological system of accretionary prisms is largely controlled by decollement and matrix permeability.

Tectonic erosion at subduction zones

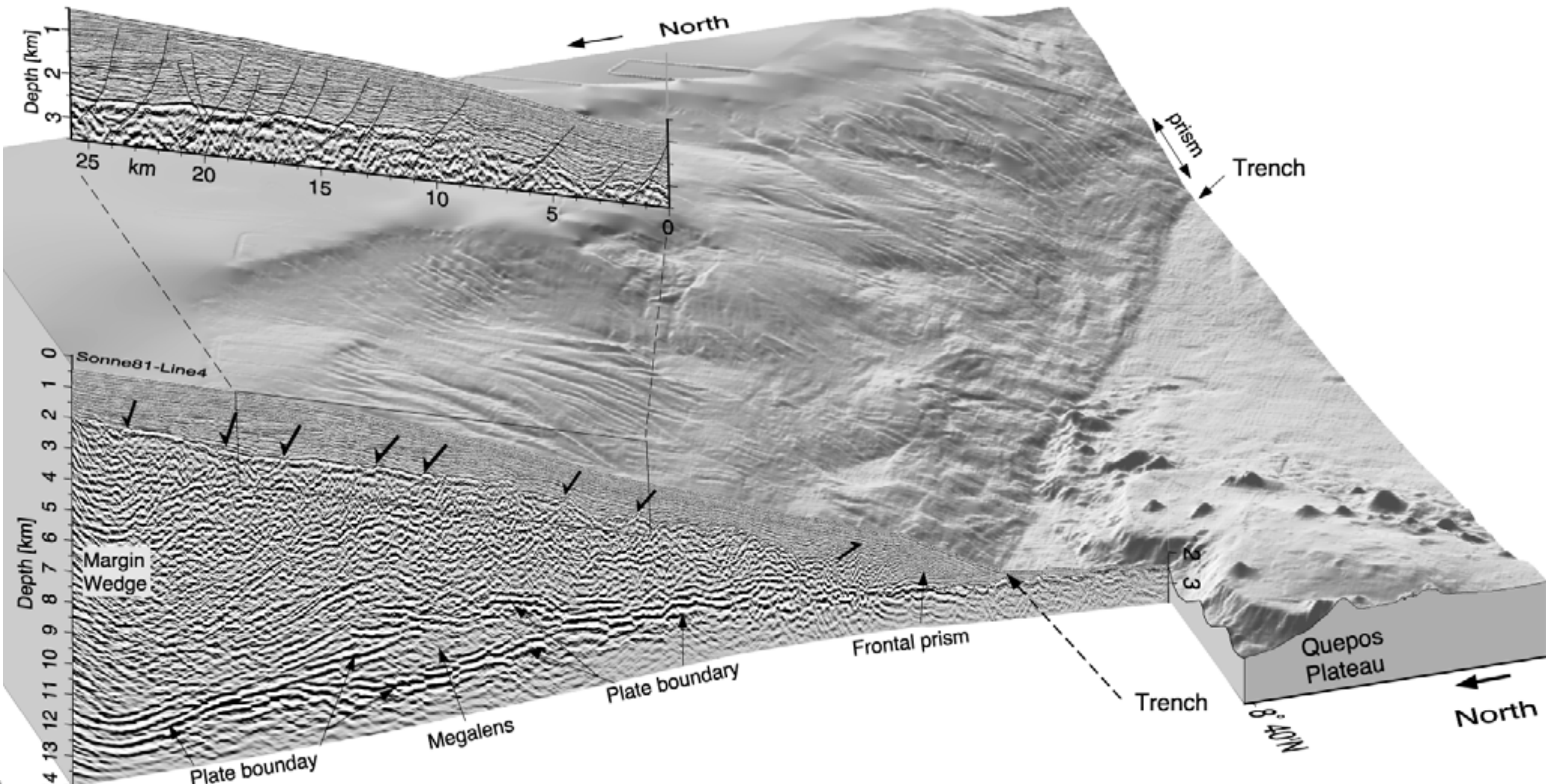

Ranero and von Huene (Nature 2000)

Barcelona CSI
Center for Subsurface Imaging

Conceptual Model for Erosional Plate Boundaries

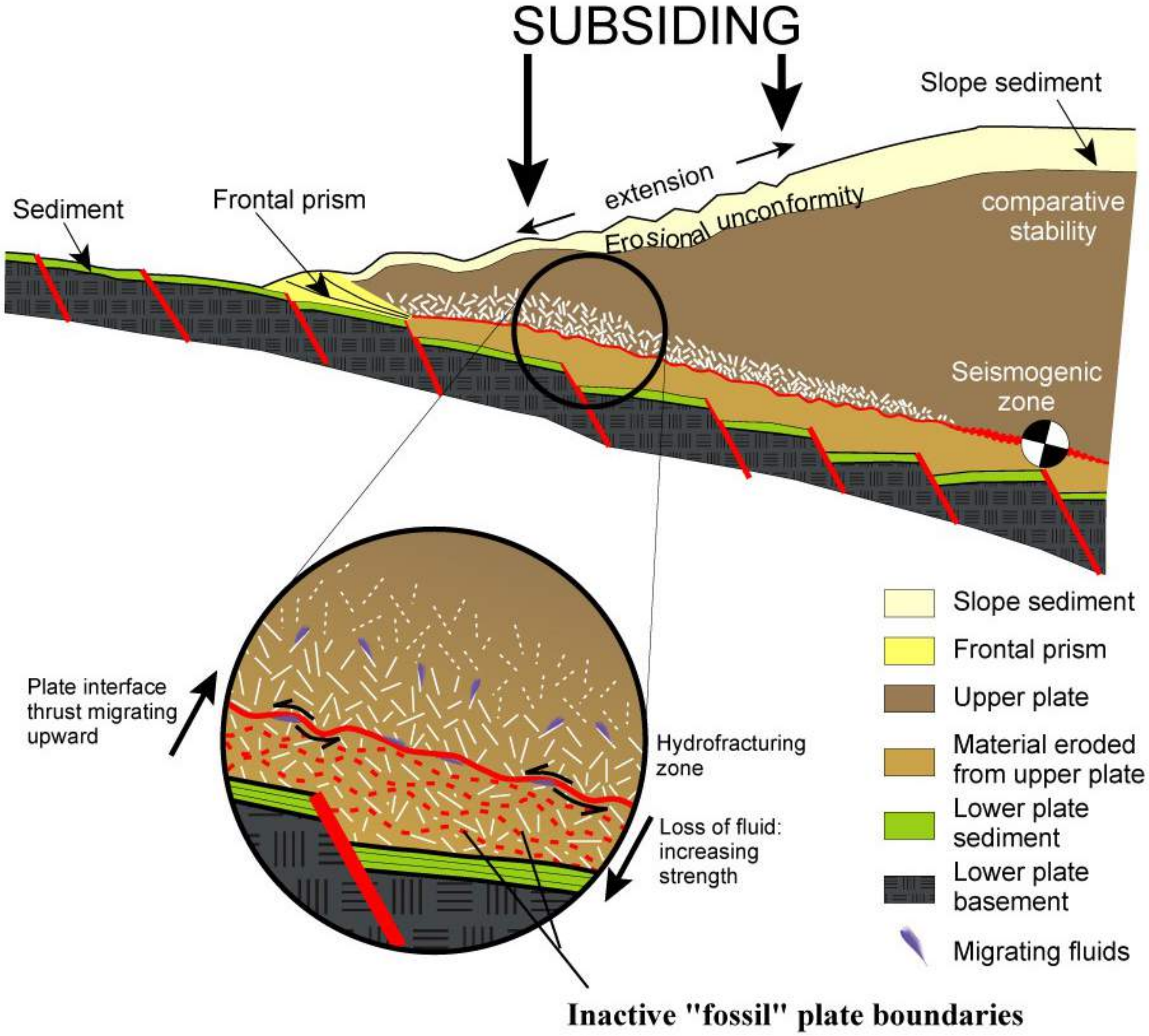

Barcelona CSI
Center for Subsurface Imaging

von Huene, Ranero, Vannucchi, (Geology, 2004)

Seepage at the seafloor

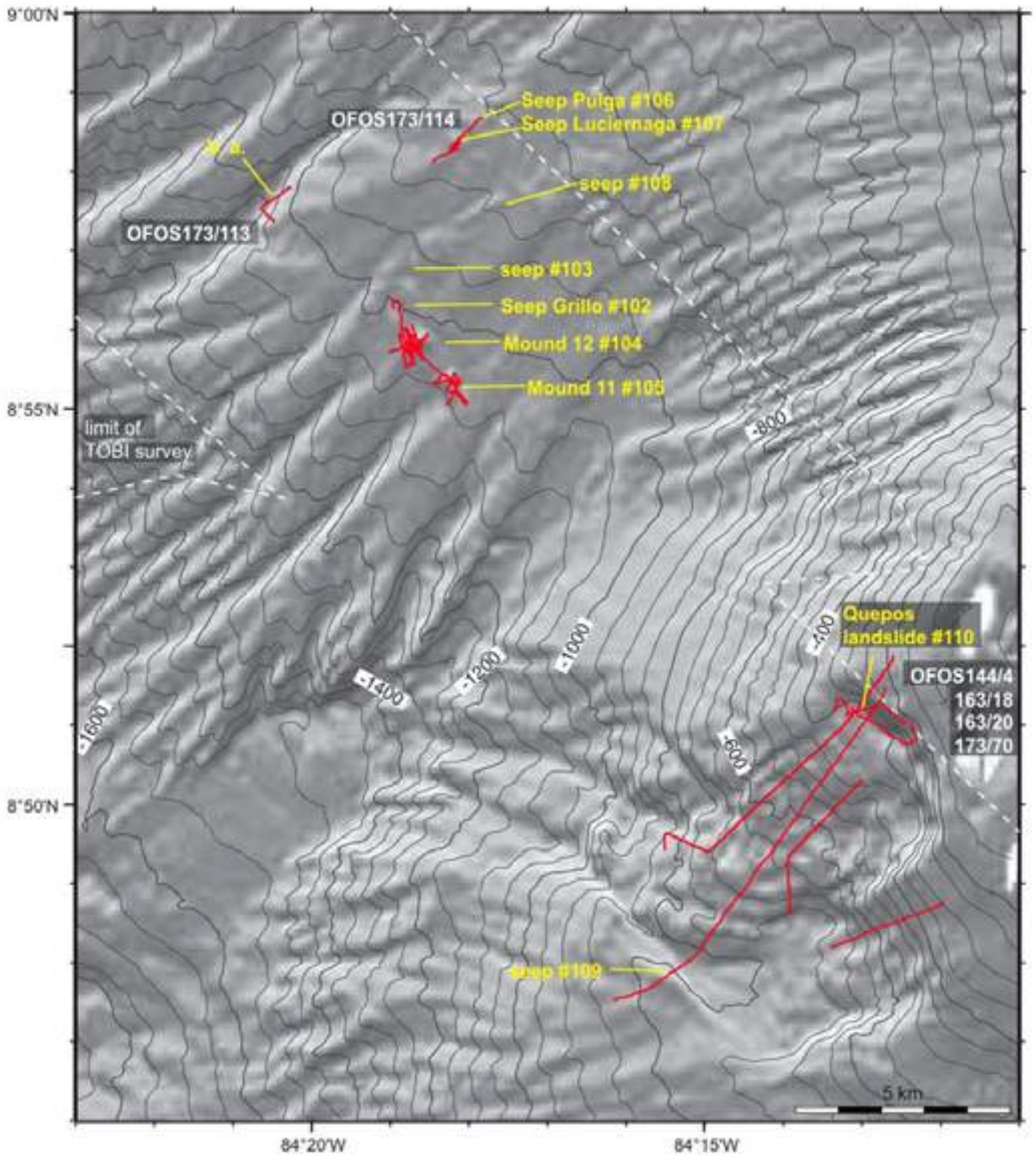

Sahling et al.,
(G-cubed, 2008)

Barcelona CSI
Center for Subsurface Imaging

Seepage at the seafloor

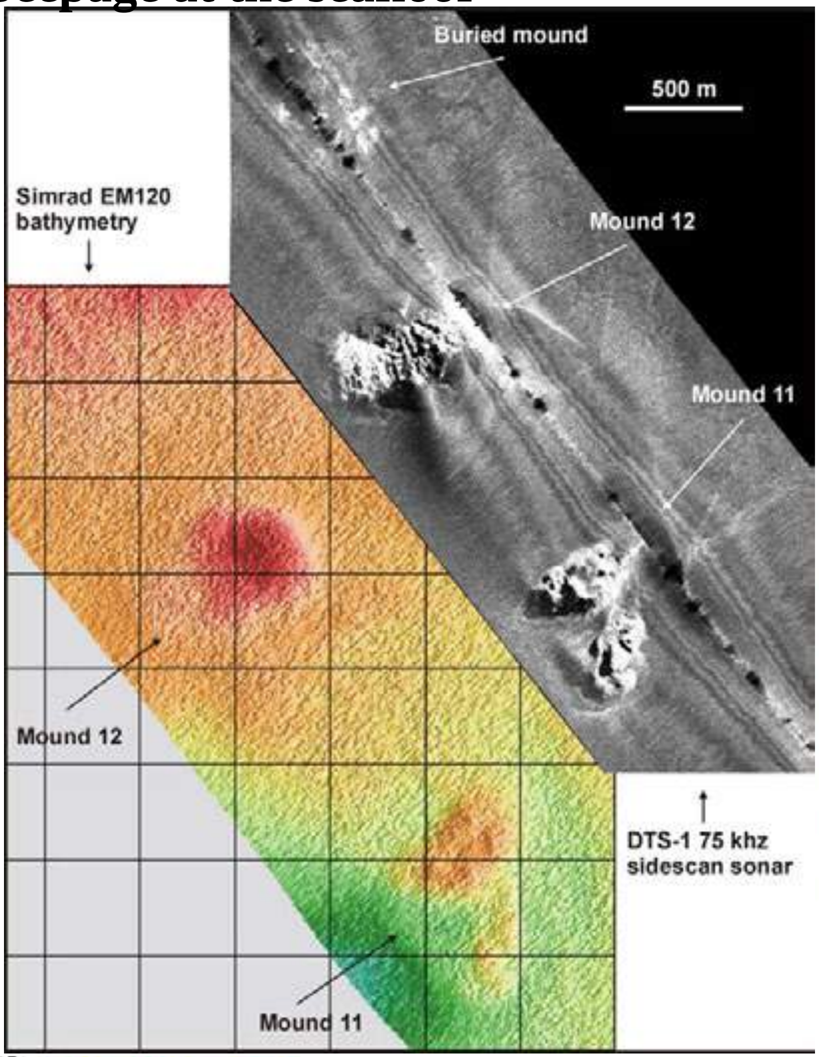

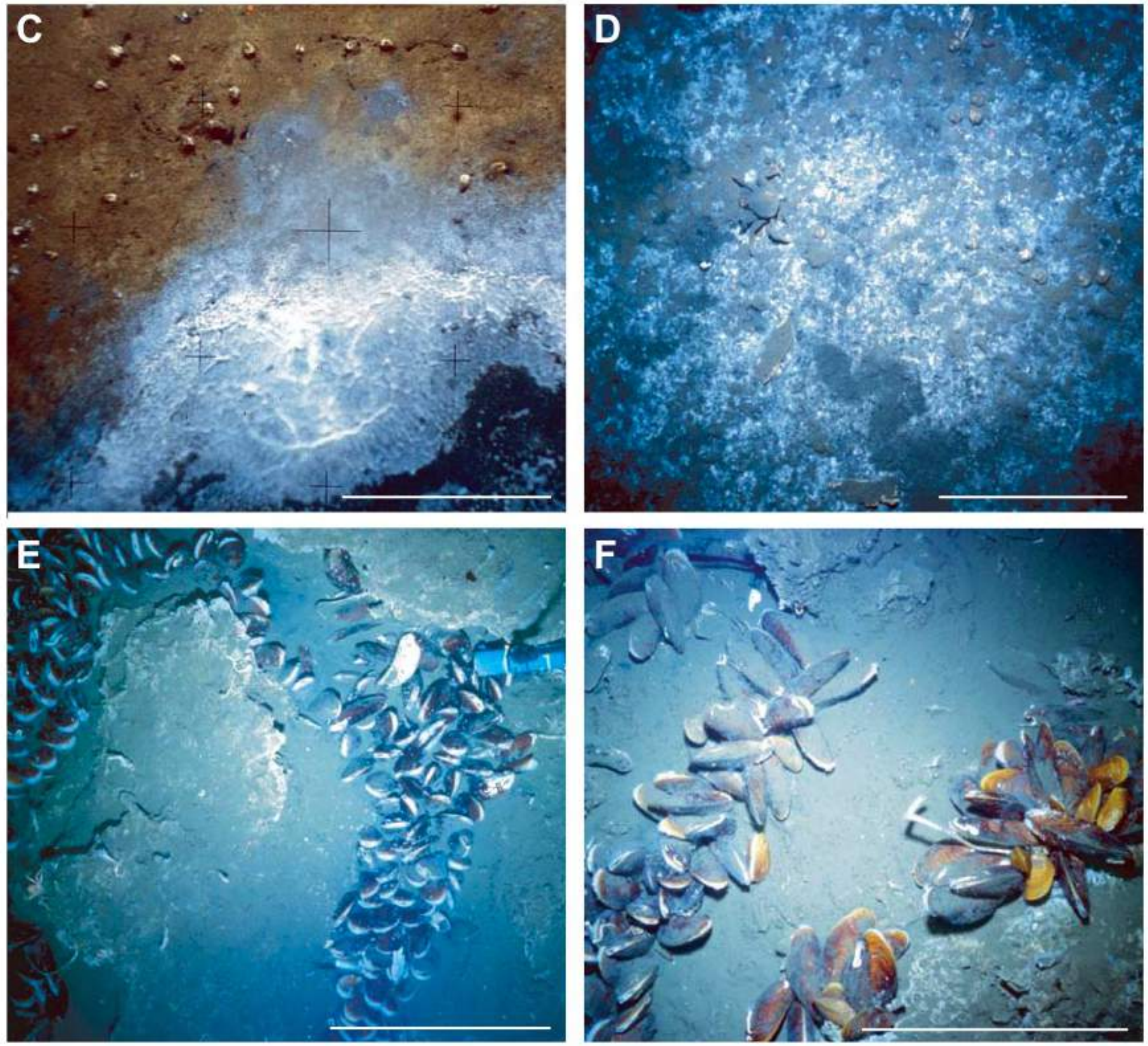

Barcelona CSI
Center for Subsurface Imaging

Sahling et al., G-cubed 2008

Seepage at the seafloor

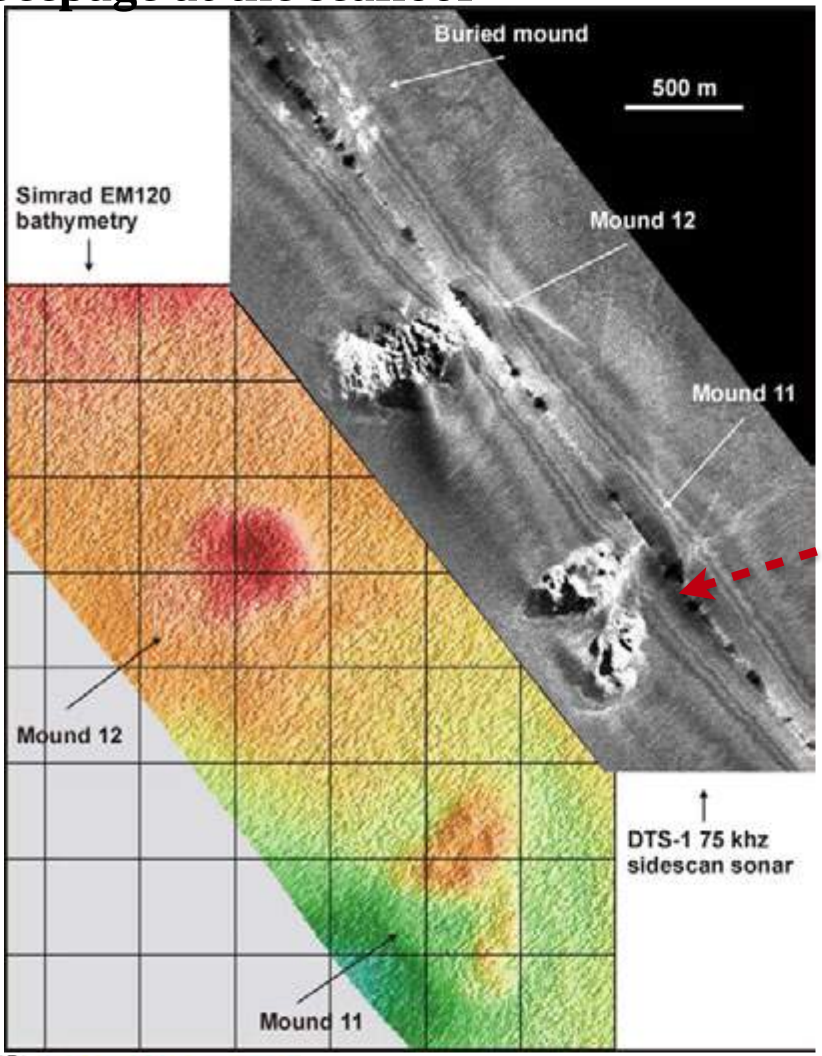

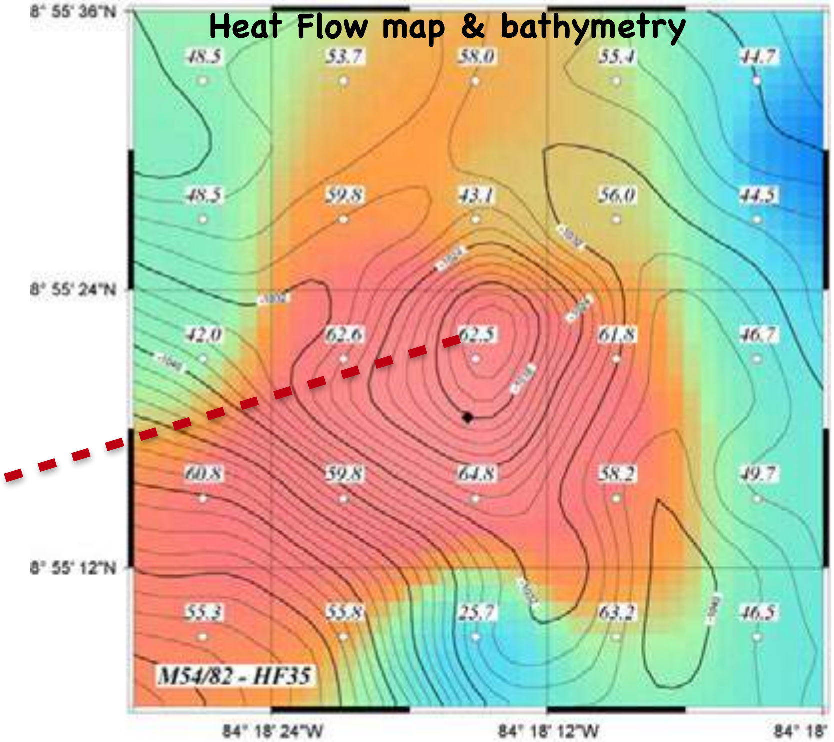

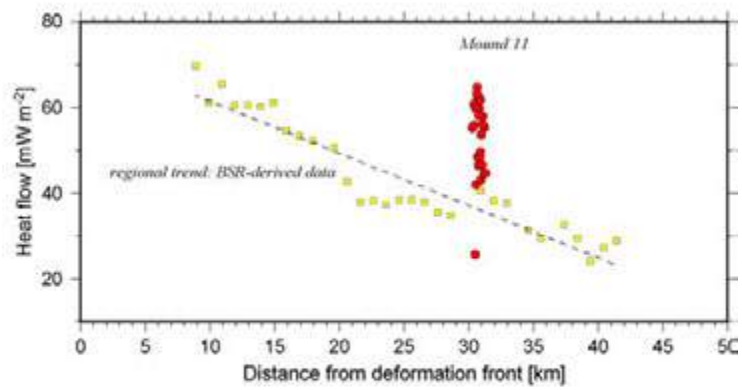

Barcelona CSI
Center for Subsurface Imaging

What kind of fluids discharge at seeps?

Barcelona CSI
Center for Subsurface Imaging

Low Cl indicates fresh water discharging at seafloor seeps

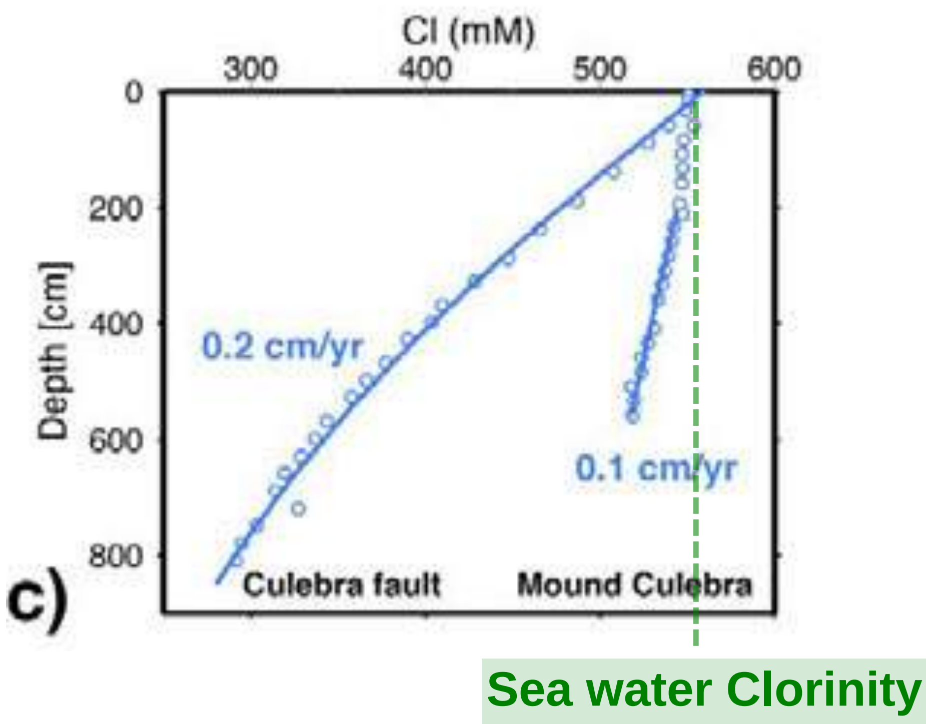

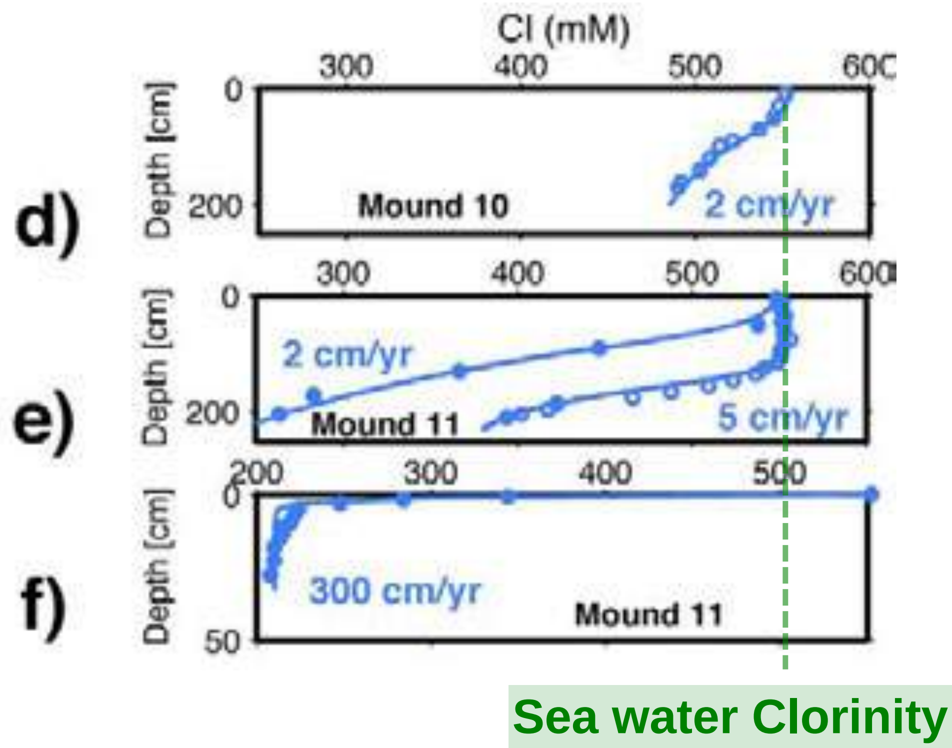

Barcelona CSI
Center for Subsurface Imaging

Ranero et al., G-cubed 2008

Pore water chemistry from seeps and origin of fluids

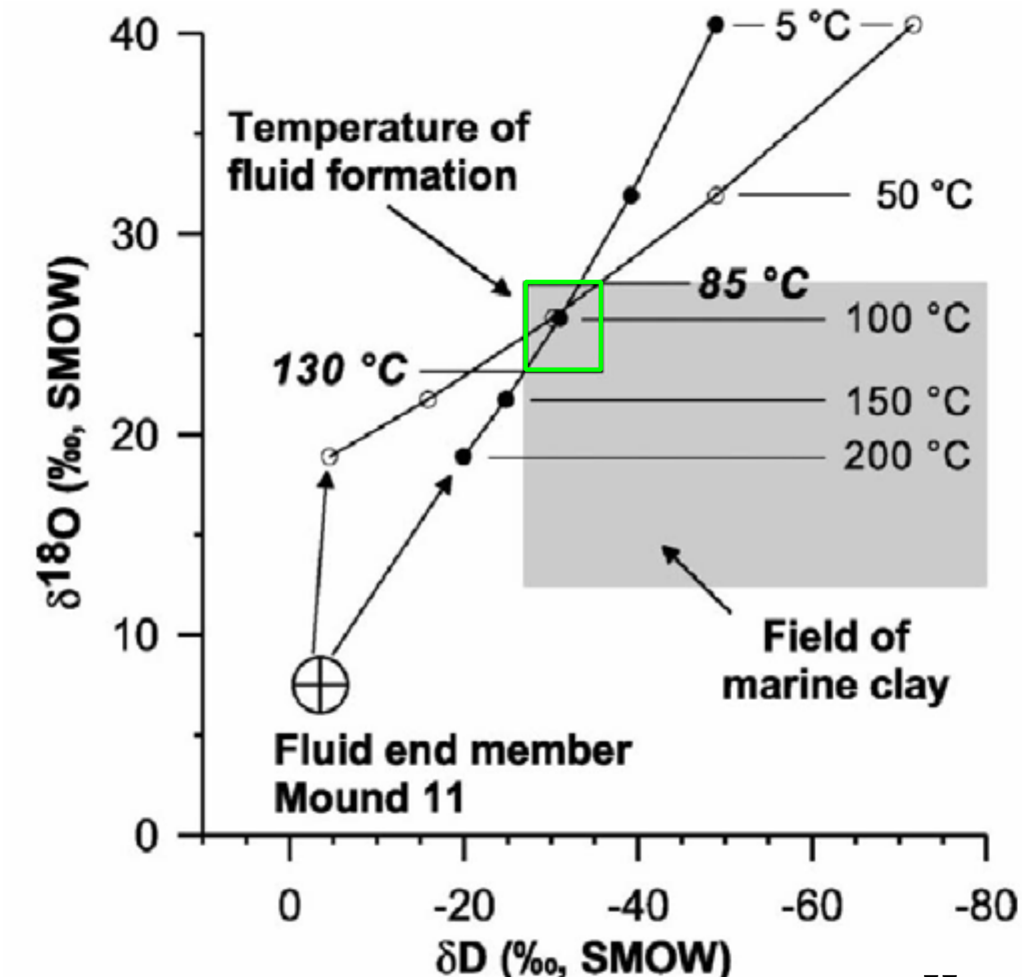

Hensen et al. (Geology 2004)

124 large seepage sites

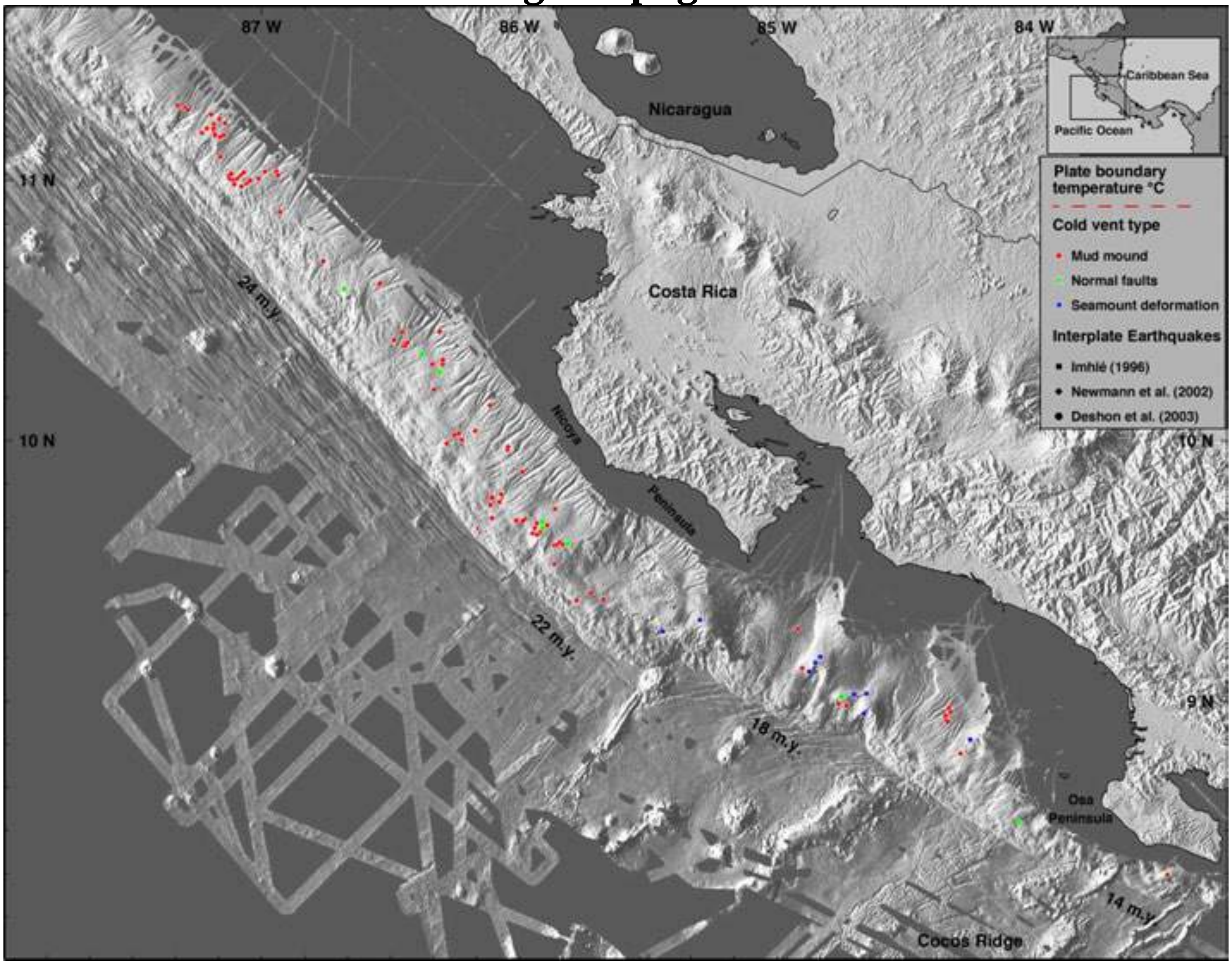

Barcelona CSI
Center for Subsurface Imaging

Temperature along the plate boundary

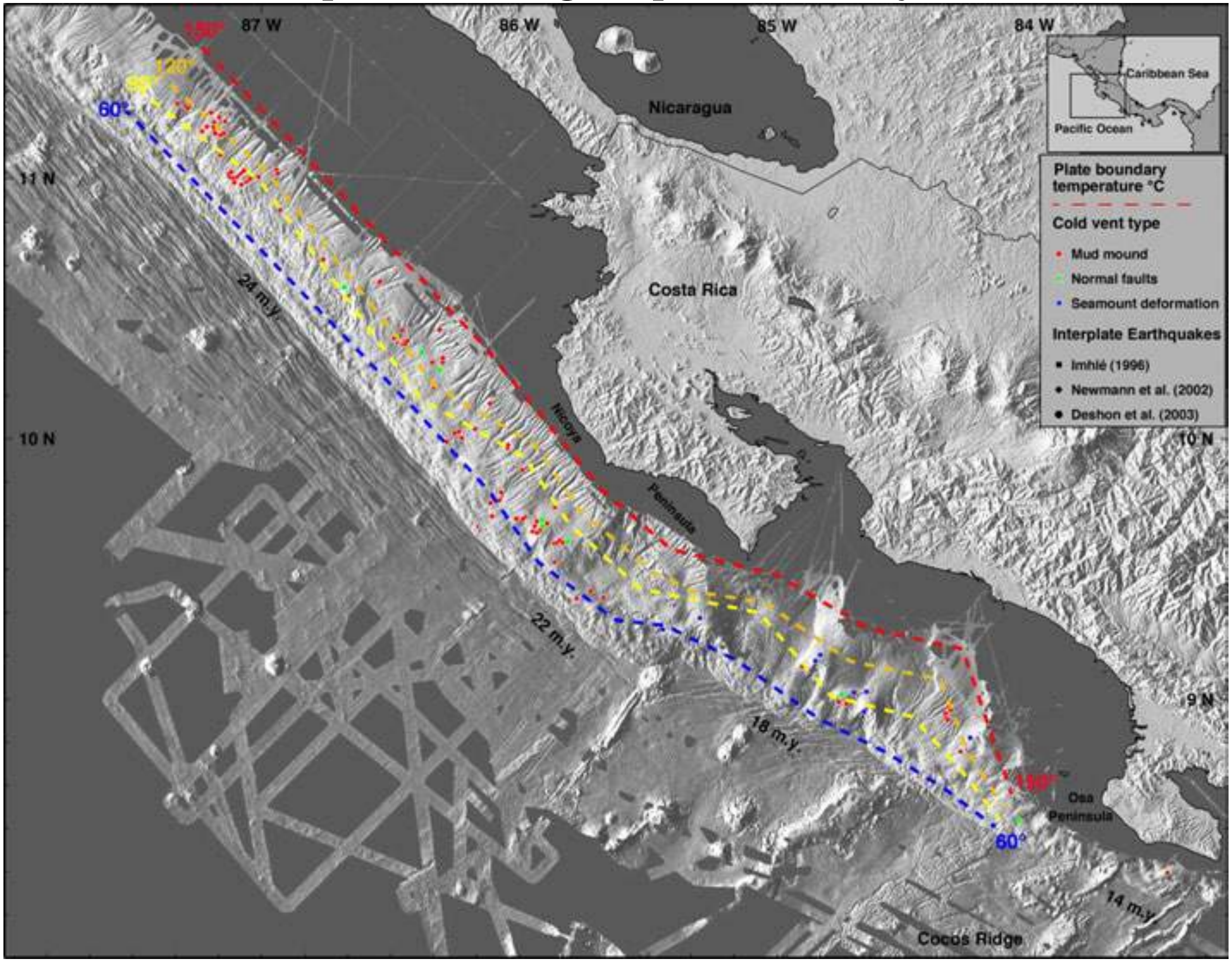

Seismic lines

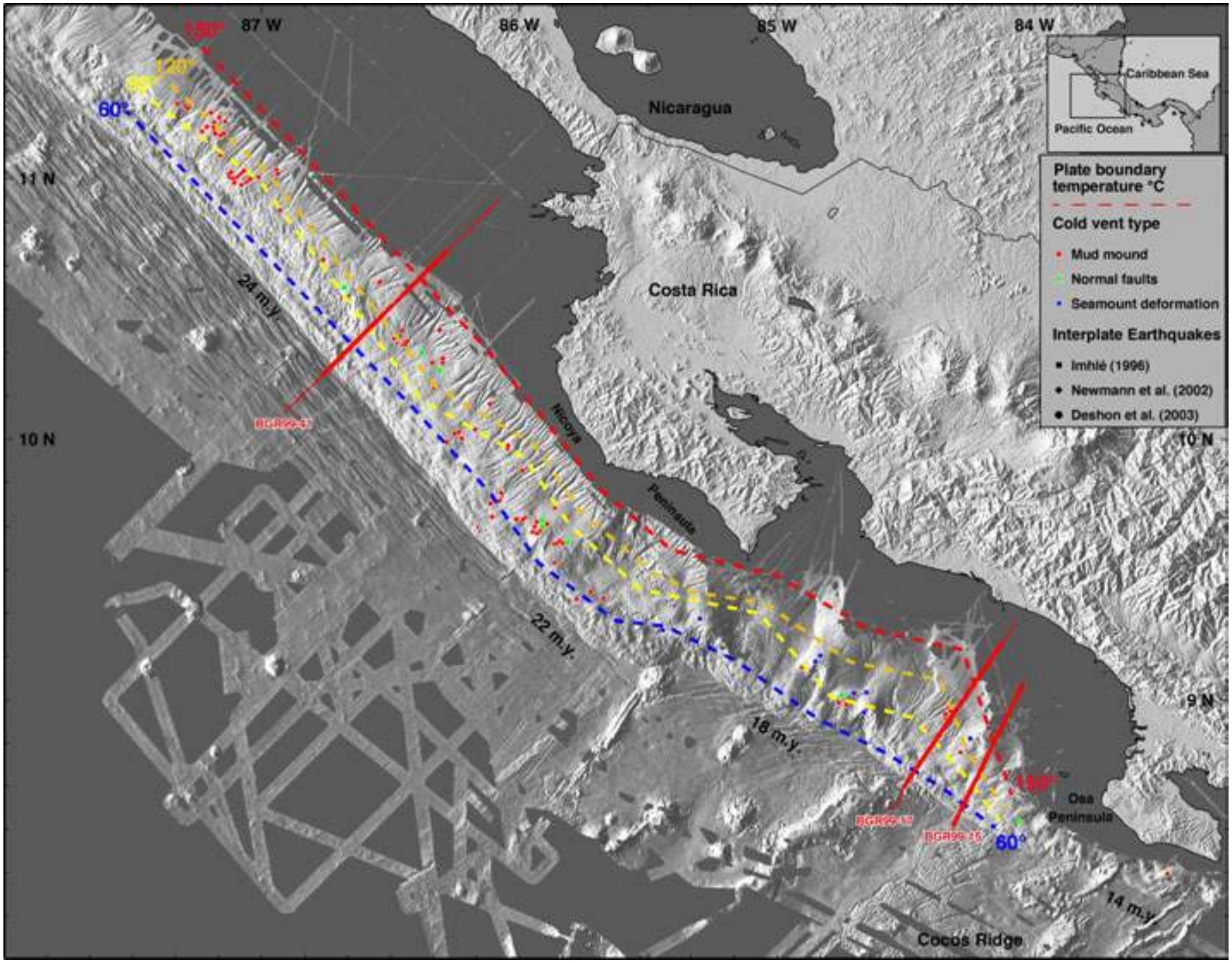

Barcelona CSI
Center for Subsurface Imaging

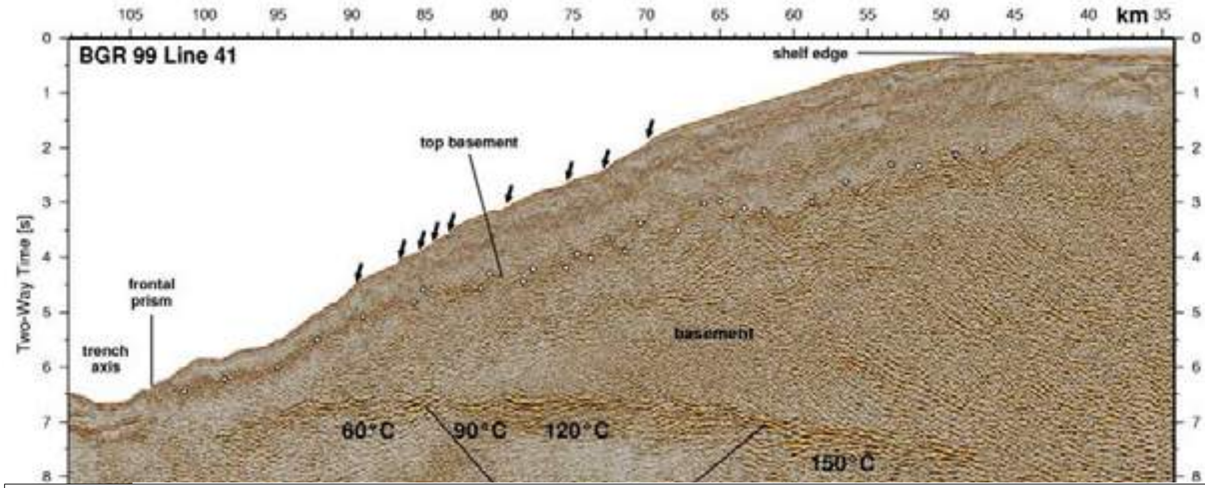

Imaging the region of dehydration of subducting sediment

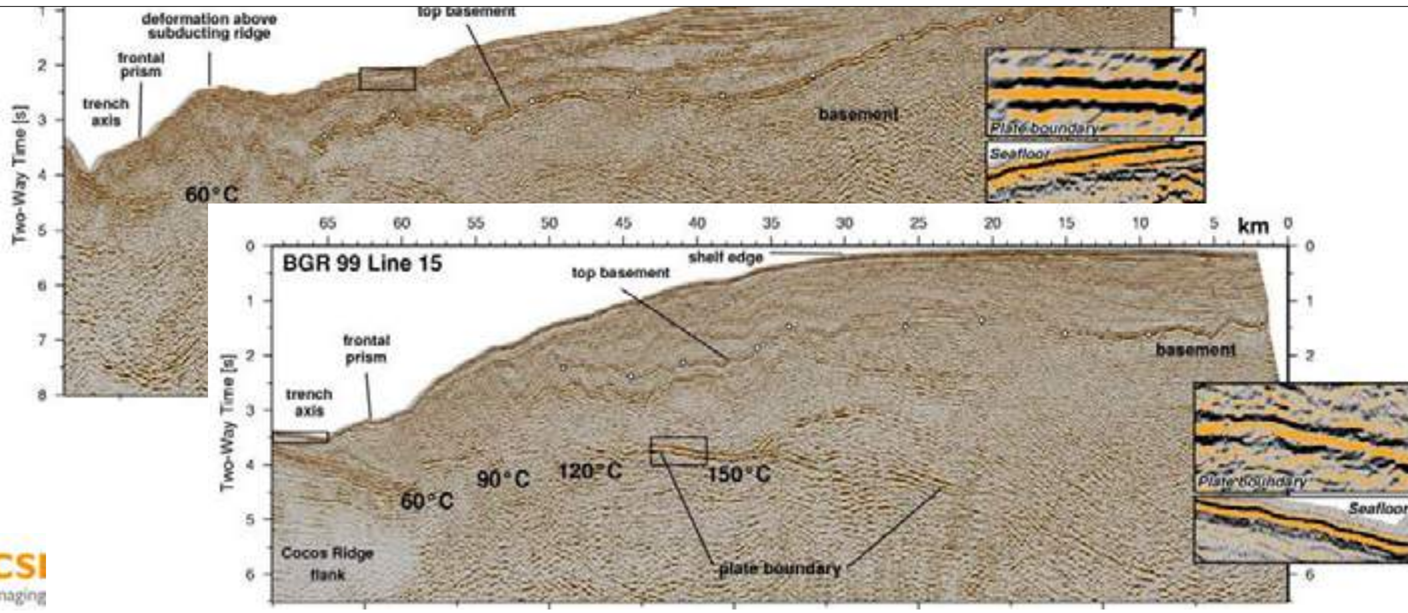

Barcelona CSI
Center for Subsurface Imaging

Modelled flow rates at slope vents based on heat flux measurements

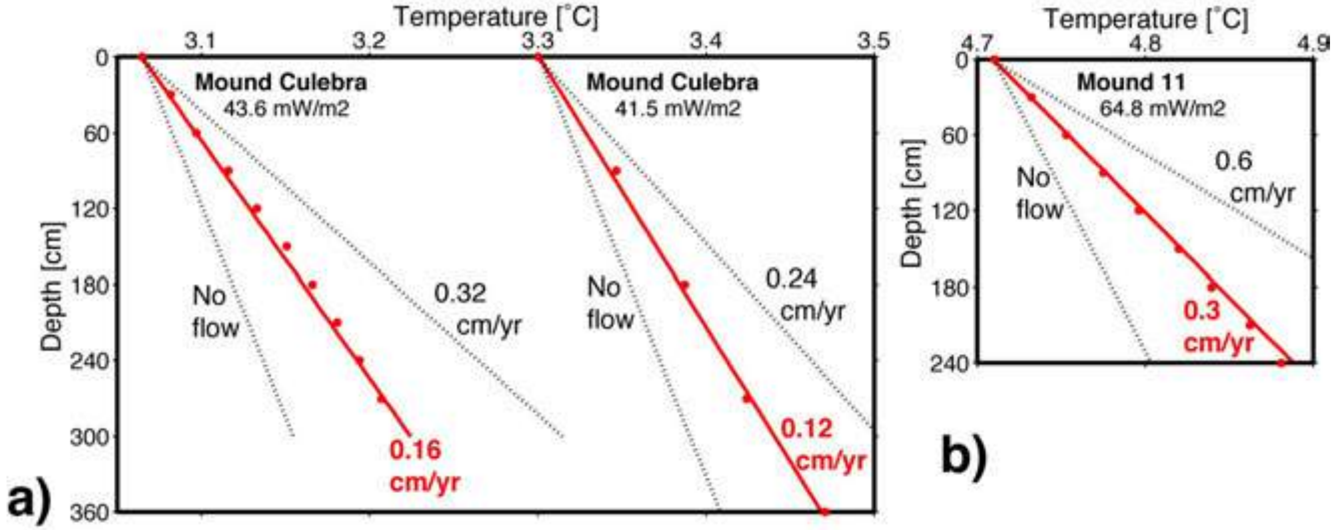

Modelled flow rates at slope vents based on pore water chemistry

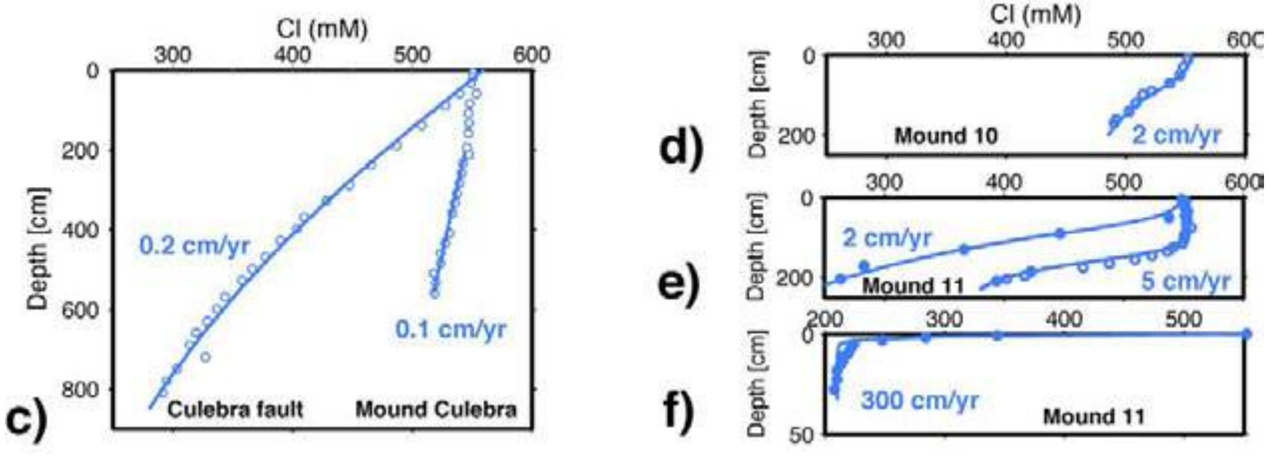

Barcelona CSI
Center for Subsurface Imaging

Average fluxes of dehydration water under the forearc

- **Input:** minera… …wood, 2004)
- **Output at 1 s…**
- **Mapped # of…**

W…

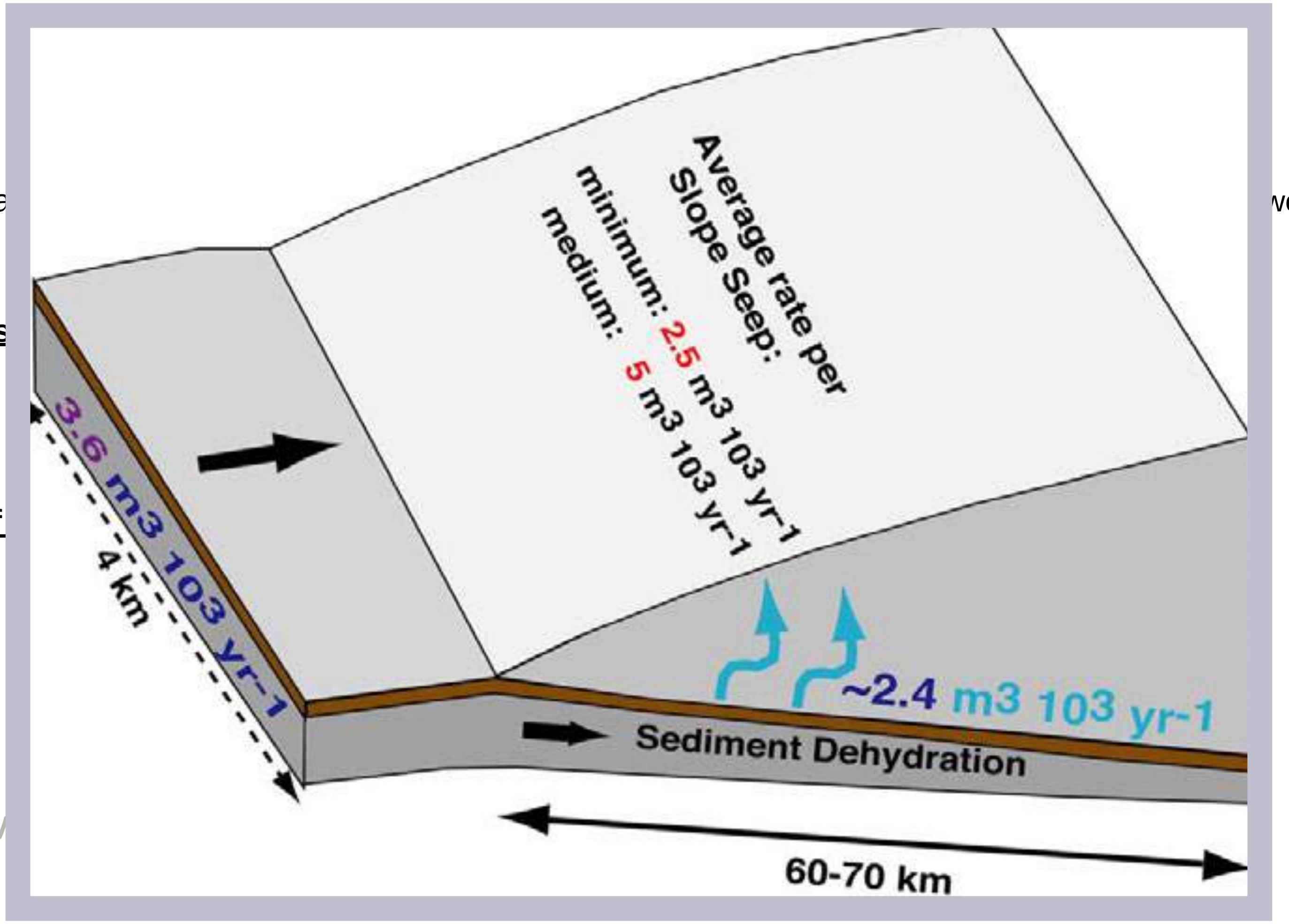

Barcelona CSI
Center for Subsurface Imaging

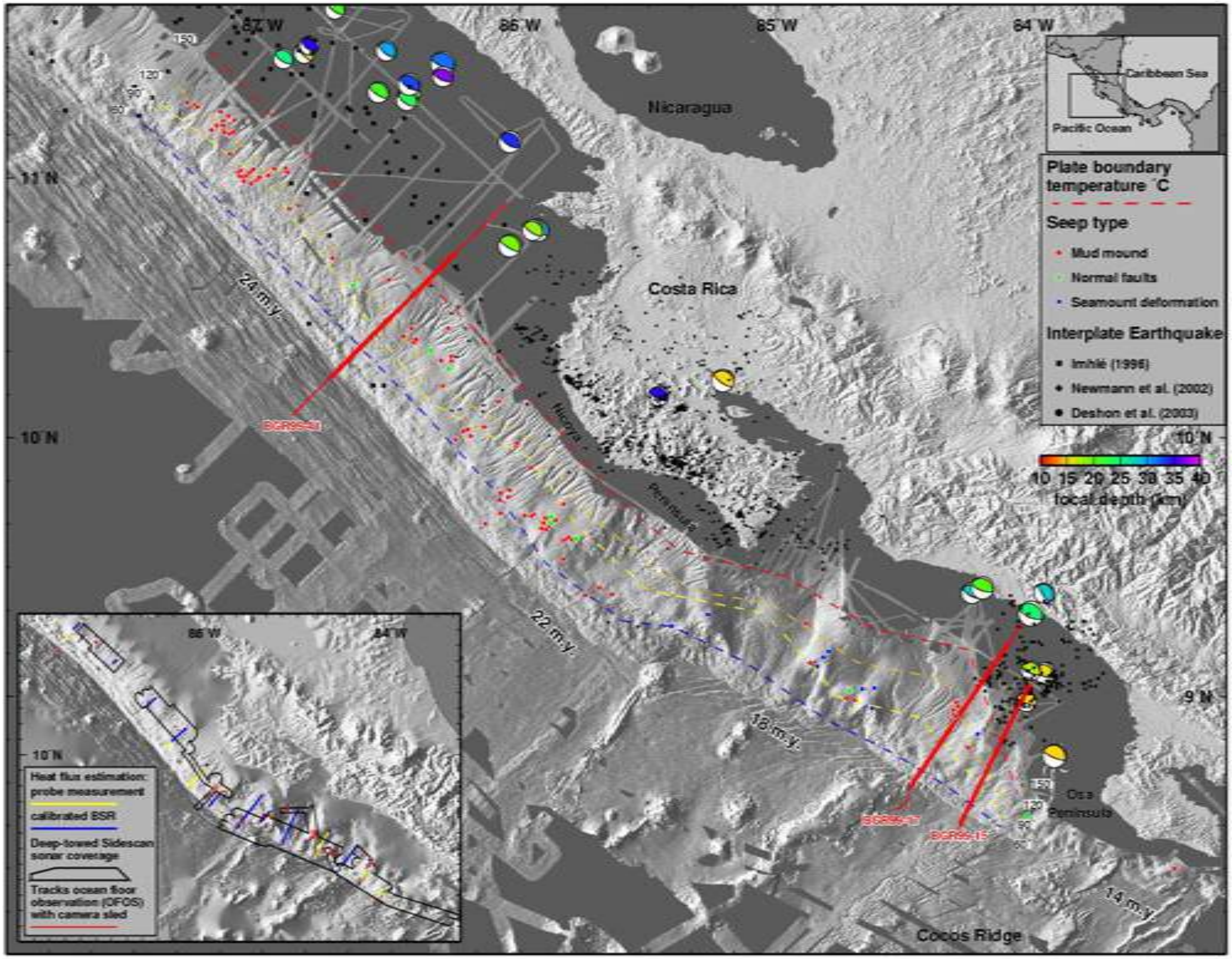

Barcelona CSI
Center for Subsurface Imaging

The forearc fluid and material exchange between lithosphere and hydrosphere

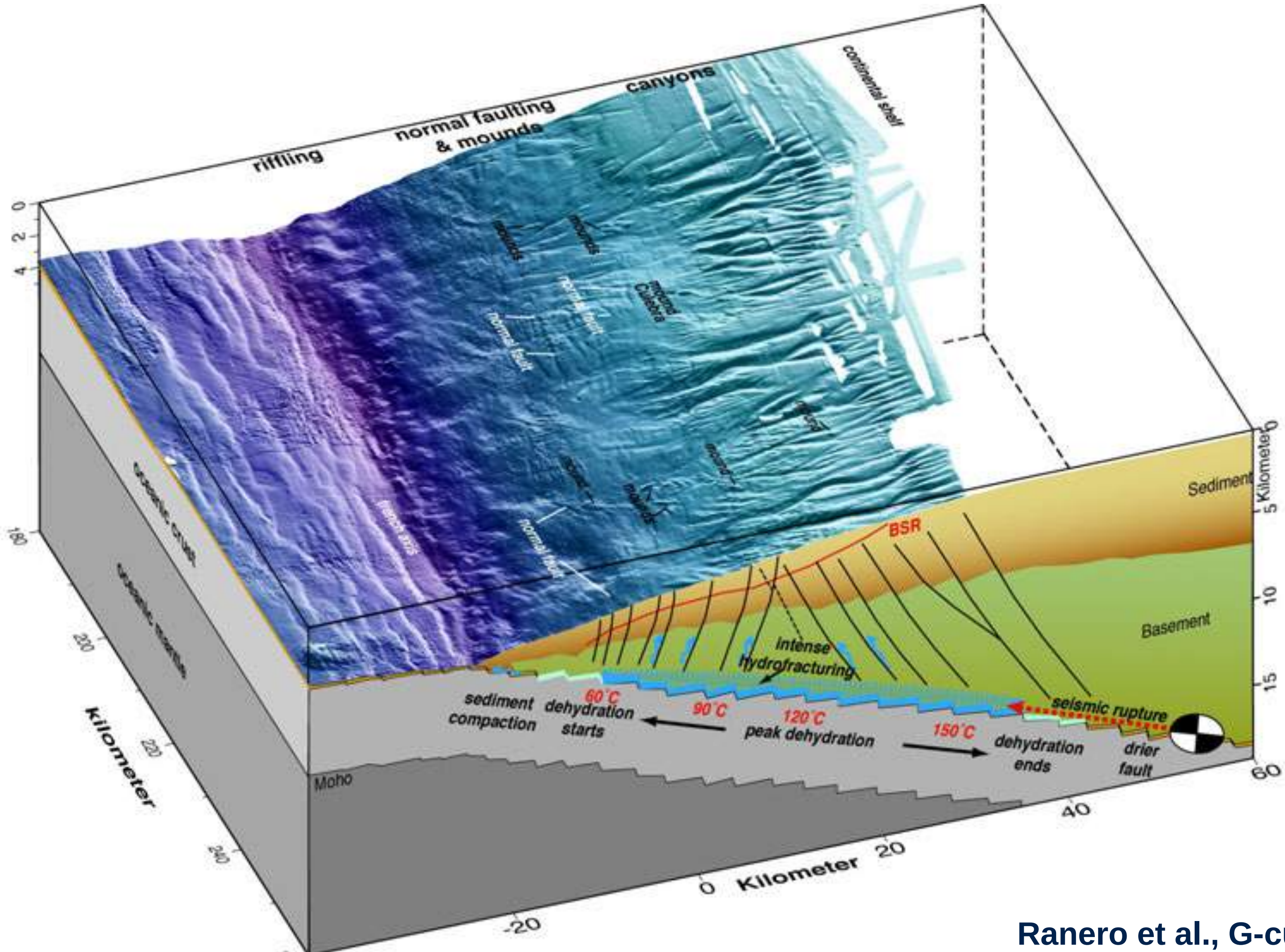

Ranero et al., G-cubed 2008

Correlation between locked patches and fluid-poor fault segments

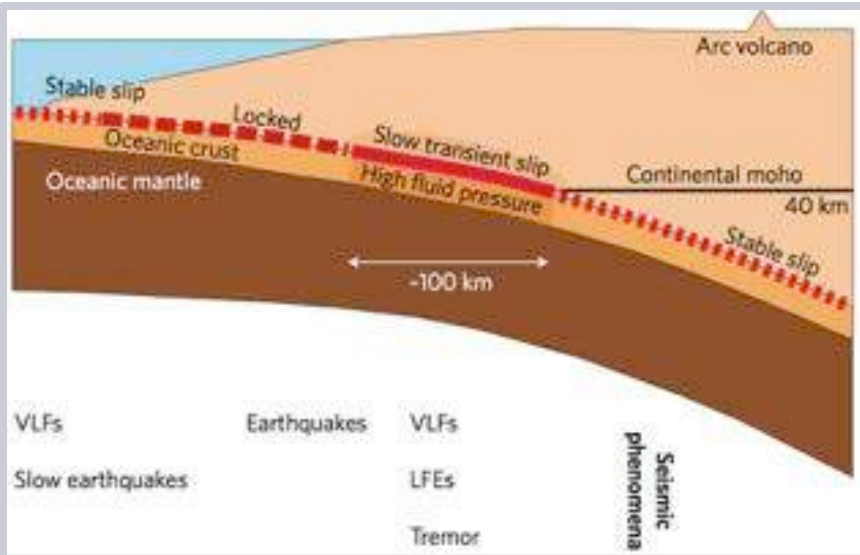

Peng & Gomberg (2010)

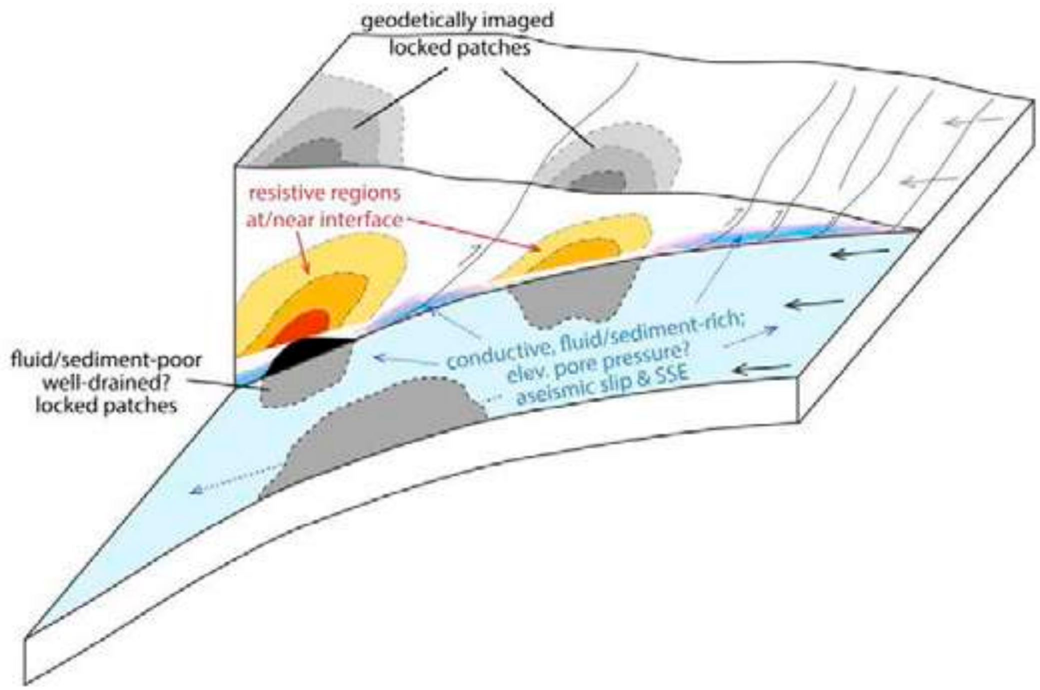

Barcelona CSI
Center for Subsurface Imaging

Saffer, GRL 2013

3. The Incoming plate of subduction zones

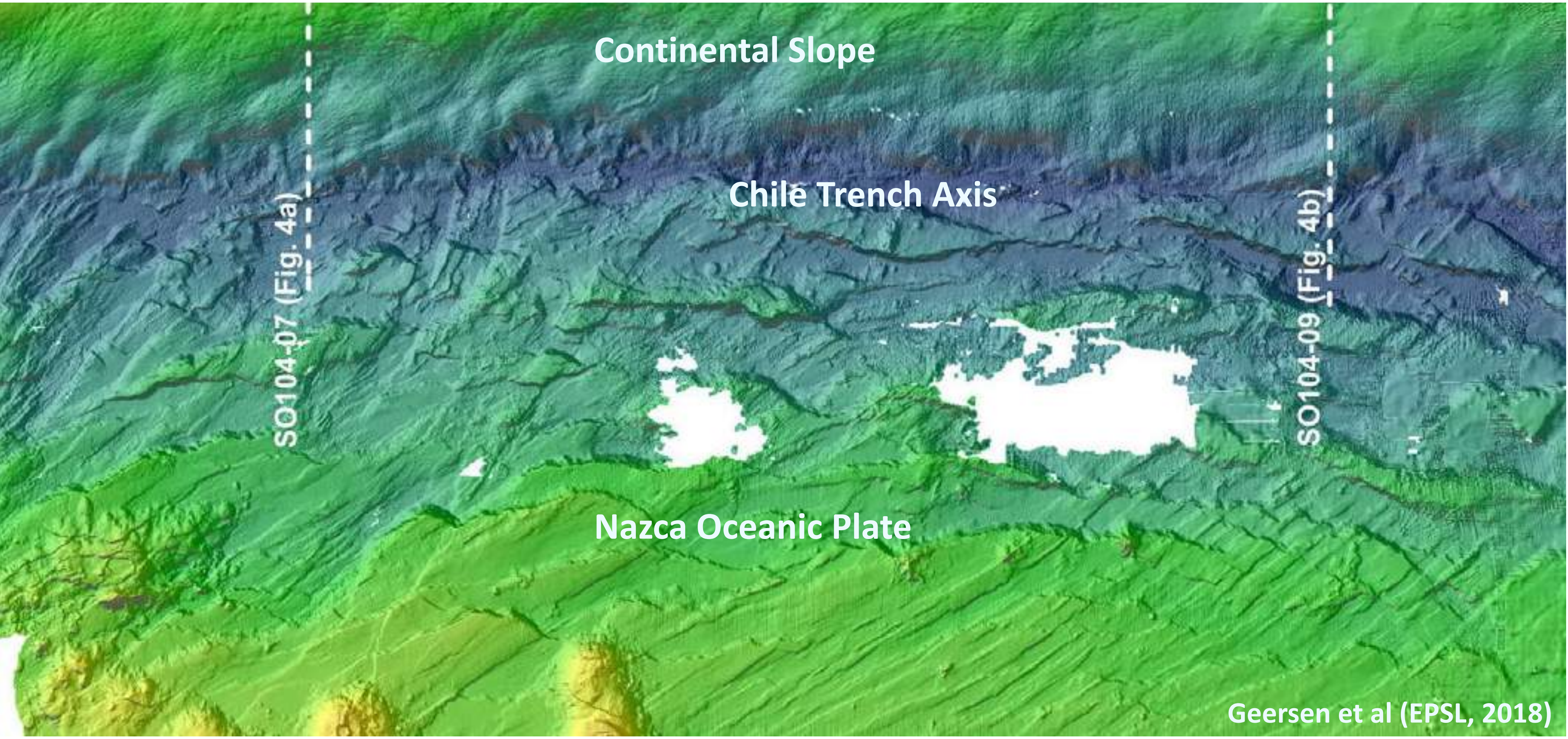

Barcelona CSI
Center for Subsurface Imaging

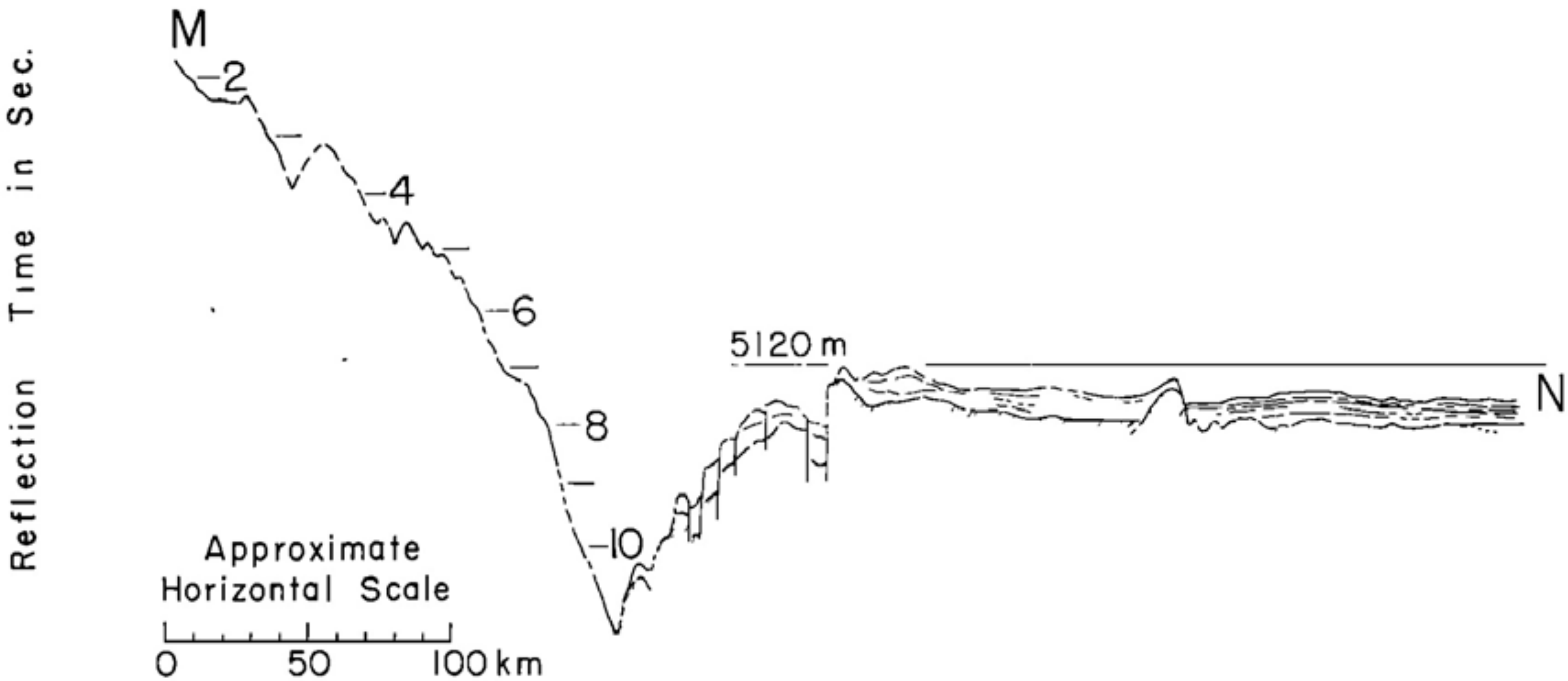

Fig. 8. Seismic reflection profile across the Japan trench extending easterly along 35°N from point M near Japan to point N [after *Ludwig et al.*, 1966]. Vertical scale represents two-way reflection time in seconds (i.e., 1 sec = 1 km of penetration for a velocity of 2 km/sec). Note block faulting along seaward slope of trench demonstrating extension in crust and inclusion of sediments in basement rocks. Also note shoaling of oceanic basement on approaching trench as suggested by work of *Gunn* [1937]. Vertical exaggeration ~25 : 1.

Isacks, Oliver & Sykes, (JGR 1968)

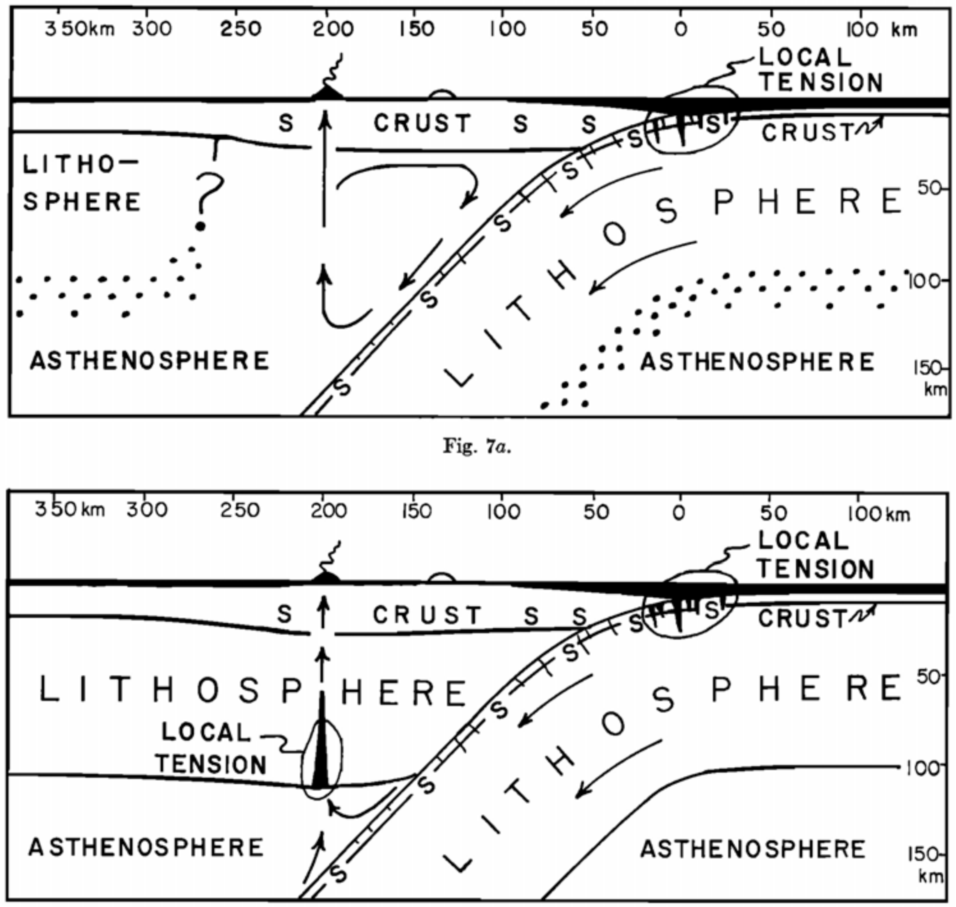

Fig. 7b.

Figure 7 shows vertical sections through an island arc indicating hypothetical structures and other features. Both sections show down-going slab of lithosphere, seismic zone near surface of slab and in adjacent crust, tensional features beneath ocean deep where slab bends abruptly and surface is free. (In both sections, *S* indicates seismic activity.) (*a*) A gap in mantle portion of lithosphere beneath island arc and circulation in mantle associated with crustal material of the slab and with adjoining mantle [*Holmes,* 1965]. (*b*) The overriding lithosphere in contact with the down-going slab and bent upward as a result of overthrusting. The relation of the bending to the volcanoes follows *Gunn* [1947]. No vertical exaggeration.

Isacks, Oliver & Sykes, (JGR 1968)

Barcelona CSI
Center for Subsurface Imaging

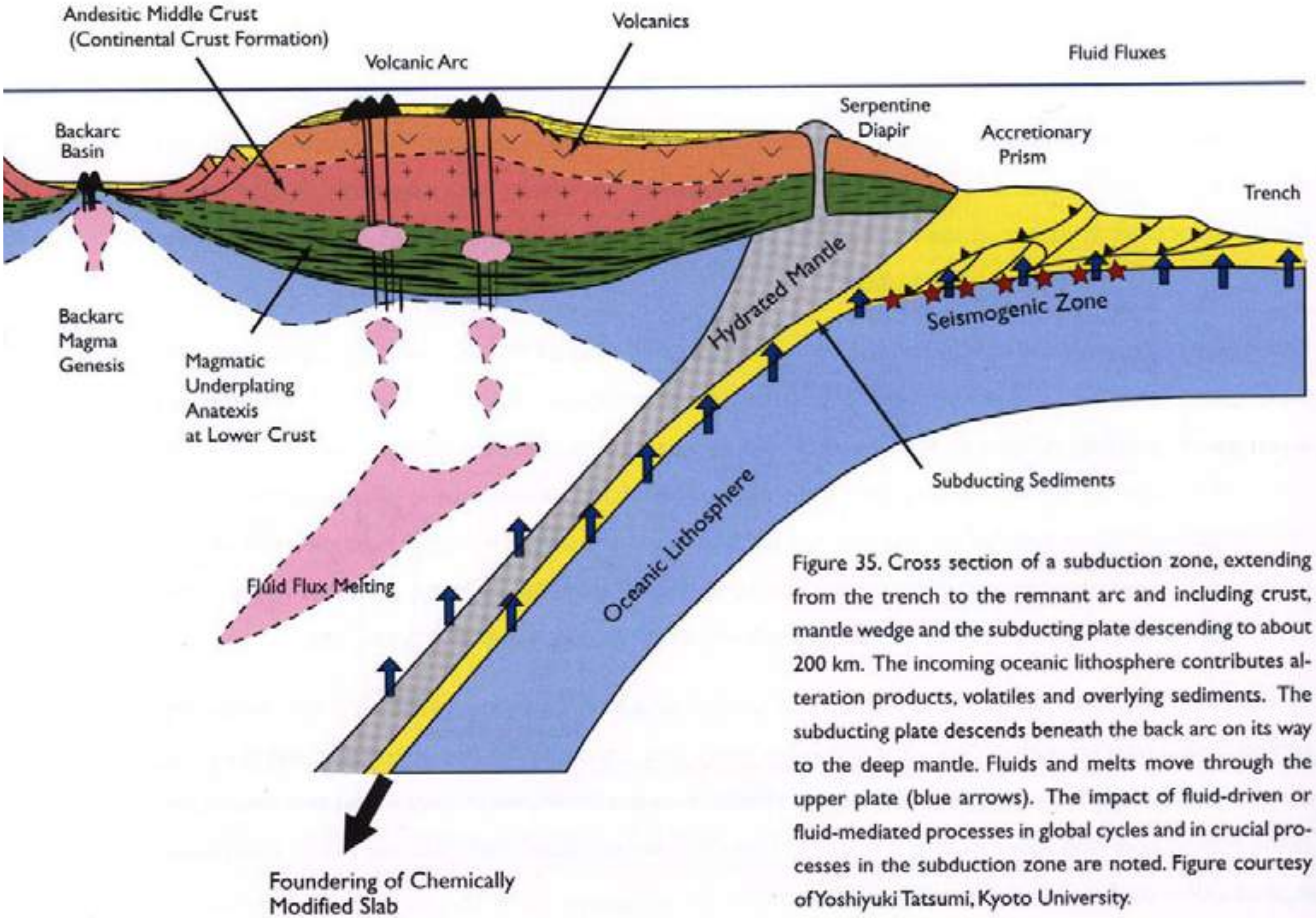

Figure 35. Cross section of a subduction zone, extending from the trench to the remnant arc and including crust, mantle wedge and the subducting plate descending to about 200 km. The incoming oceanic lithosphere contributes alteration products, volatiles and overlying sediments. The subducting plate descends beneath the back arc on its way to the deep mantle. Fluids and melts move through the upper plate (blue arrows). The impact of fluid-driven or fluid-mediated processes in global cycles and in crucial processes in the subduction zone are noted. Figure courtesy of Yoshiyuki Tatsumi, Kyoto University.

Are the lower planes of double seismic zones caused by serpentine dehydration in subducting oceanic mantle?

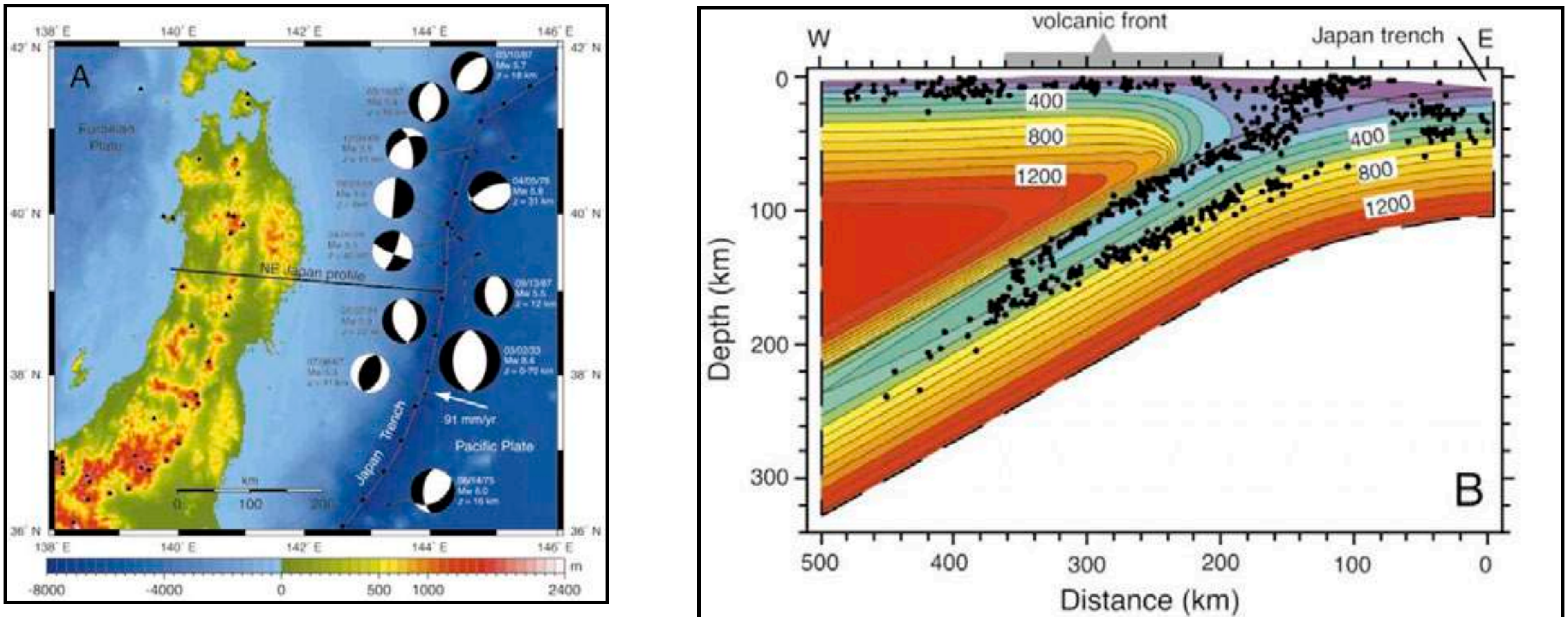

Figure 2. A: Geotectonic map of northeast Japan depicting plate boundaries, location of thermal model, and focal mechanisms for selected outer rise earthquakes (Kanamori, 1971; Seno and Gonzalez, 1987; Engdahl et al., 1998). Solid triangles—Holocene volcanoes; M_W—moment magnitude; *z*—depth below seafloor. B: Cross section through northeast Japan (~39°N) showing earthquake hypocenters (Hasegawa et al., 1994) and calculated thermal structure. Isotherm contour interval = 100 °C.

Peacock (Geology 2001)

Barcelona CSI
Center for Subsurface Imaging

Facts about peridotite serpentinization

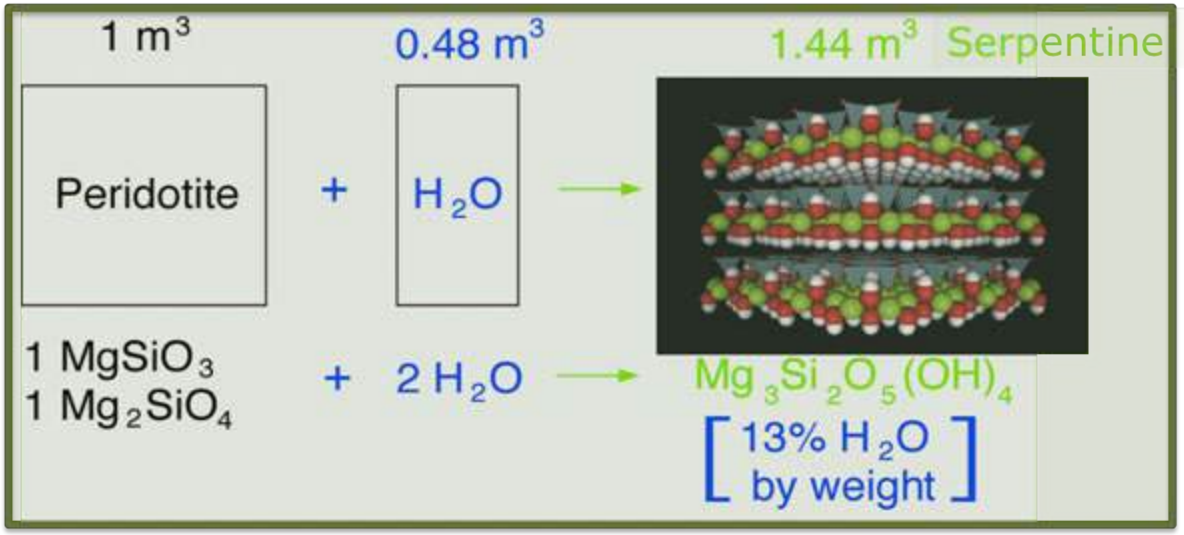

- Only occurs **below ~500-600°C**
- Water uptake up to **13wt.%** for complete transformation
- Latent heat of complete transformation is ~300°C (**Exothermic !!**)
- **V_P decrease** from 8 km/s to 4.5 km/s
- **Density decrease** from 3.3 Mg/m³ to ~2.3 Mg/m³ (~40%)
- **Geologically fast!** diffusion speed is upto 1 km/1 m.y.

Barcelona CSI
Center for Subsurface Imaging

Serpentine (Antigorite) Stability Phase Diagram

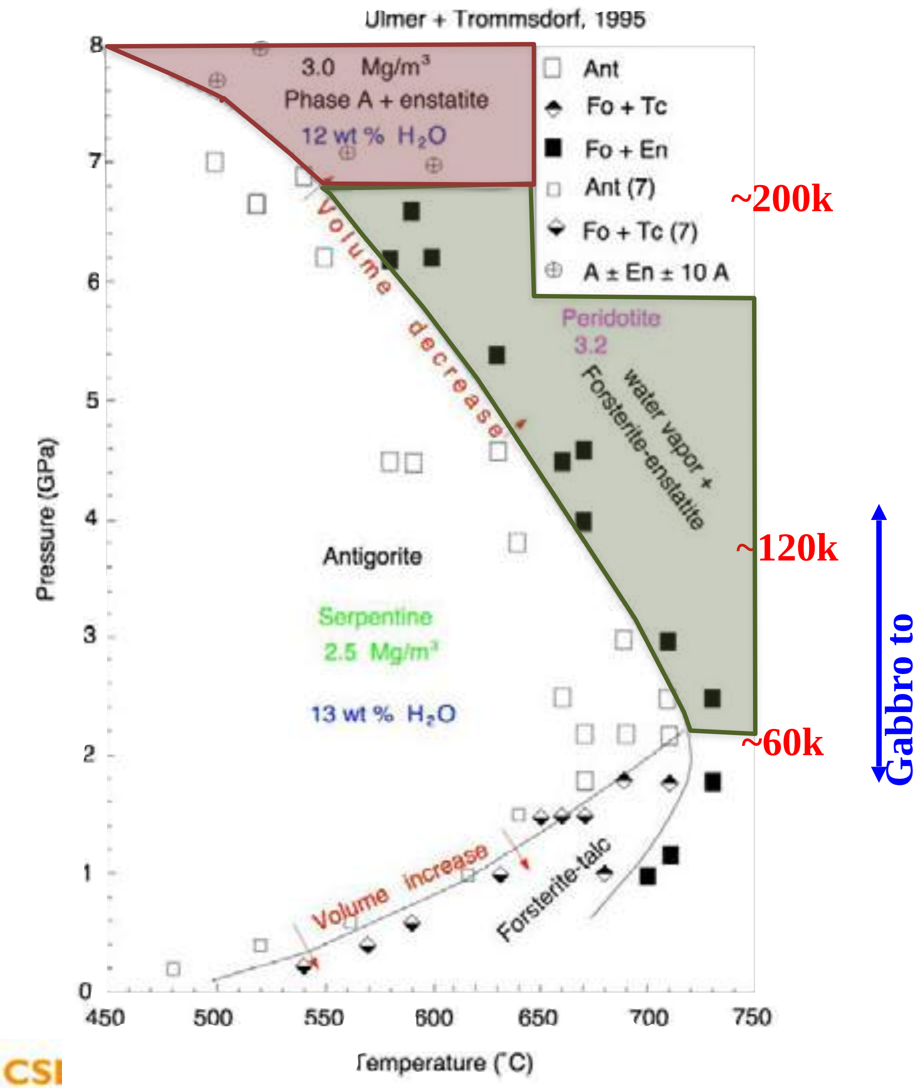

- at *P* corresponding to depths > ~200km: Serpentine transforms to hydrous Phase A *without dehydration* but increase in density.

- at higher *P* or depths > ~60km, *de-serpentinization* occurs with increase in either *P* or *T.*

- at low *P: de-serpentinization* occurs with increase in *T.*

Barcelona CSI
Center for Subsurface Imaging

Serpentinite Seduction, Science, Nov 2002

Kerrick (2002): "Seductive" but extremely unlikely.

Clearly a hydraulic impossibility to get water to such great depths…

"The hypothesis that surface water is drawn to such a depths [double seismic zones] by dilatancy arising from seismic pumping associated with deep earthquakes is difficult to reconcile with hydraulics."

"Propagation of cracks and fractures necessary for fluid ingress would be inhibited by the large increase in rock volume accompanying serpentinization."

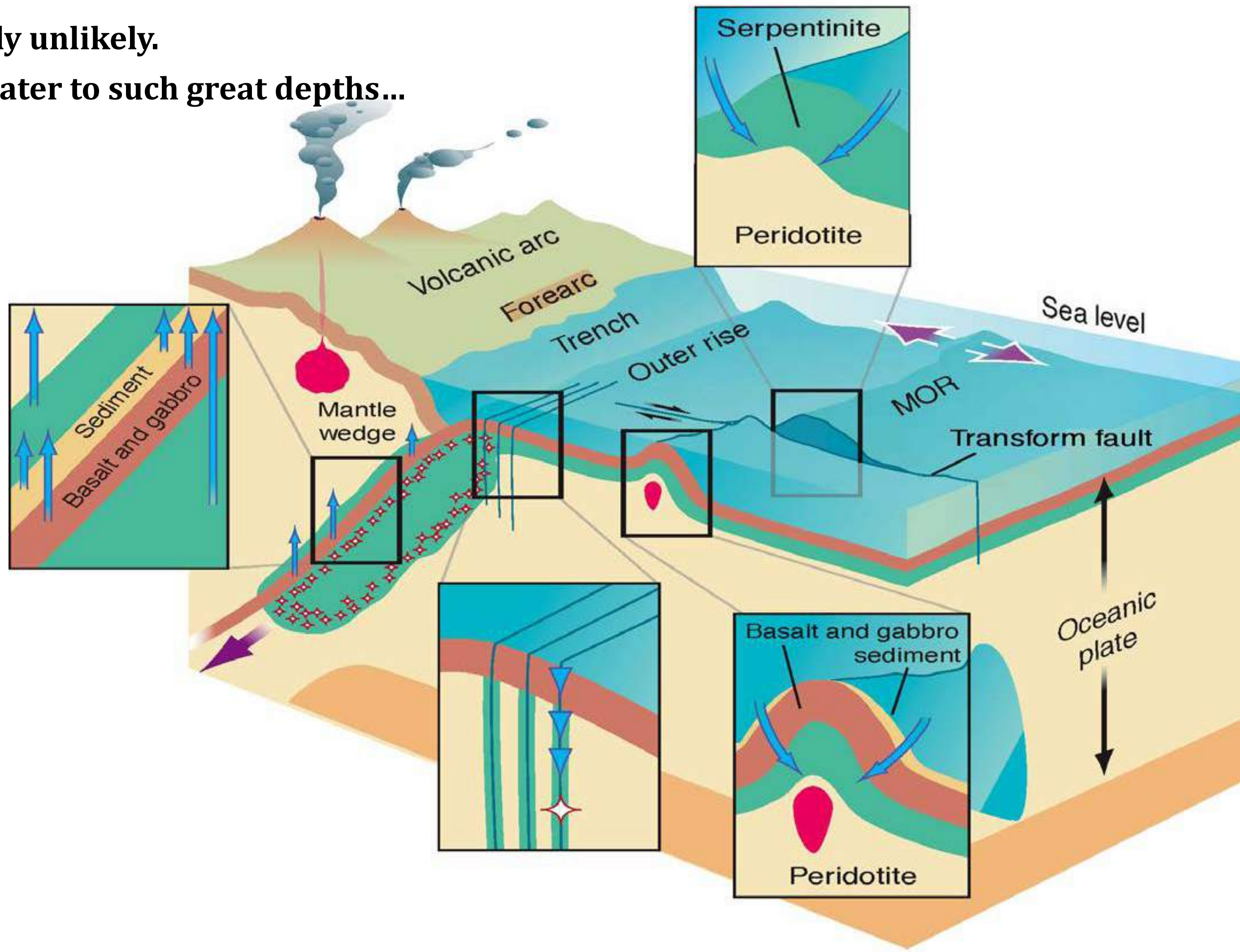

Barcelona CSI
Center for Subsurface Imaging

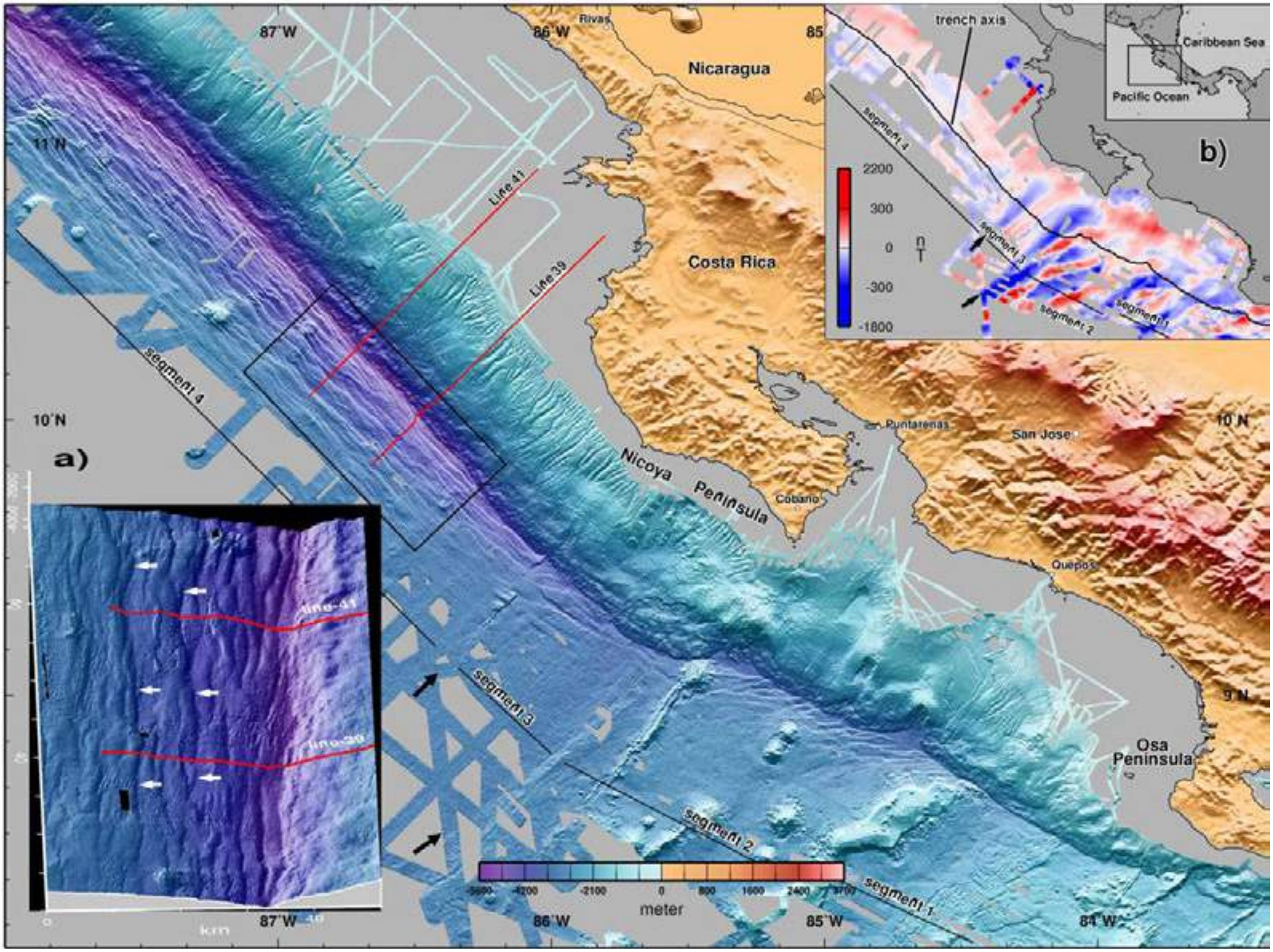

Barcelona CSI
Center for Subsurface Imaging

Pervasive bend-faulting: The mechanism

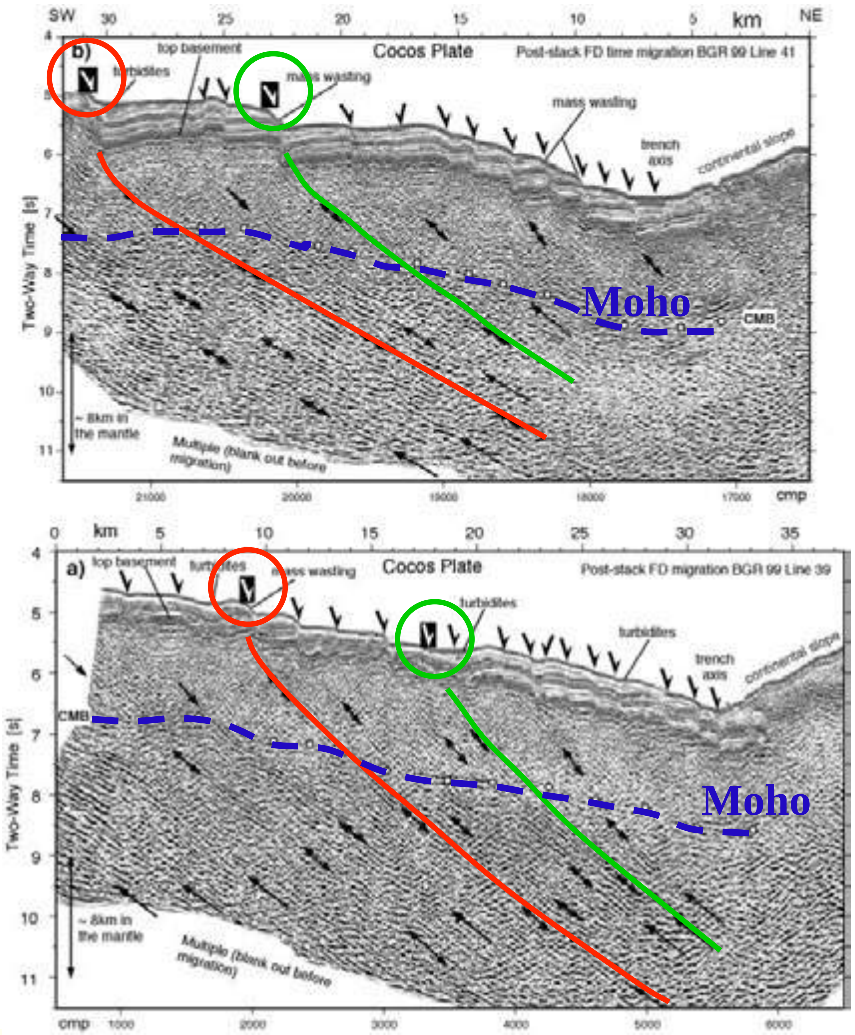

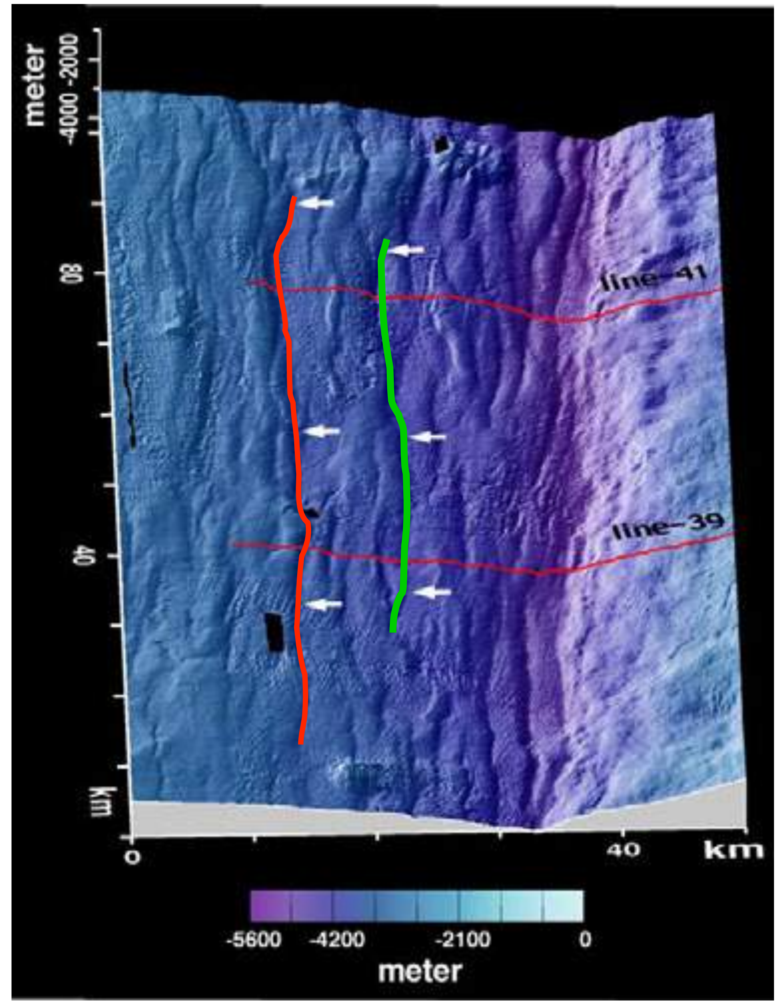

Ranero et al., Nature 2003

Barcelona CSI
Center for Subsurface Imaging

Pervasive bend-faulting: The mechanism

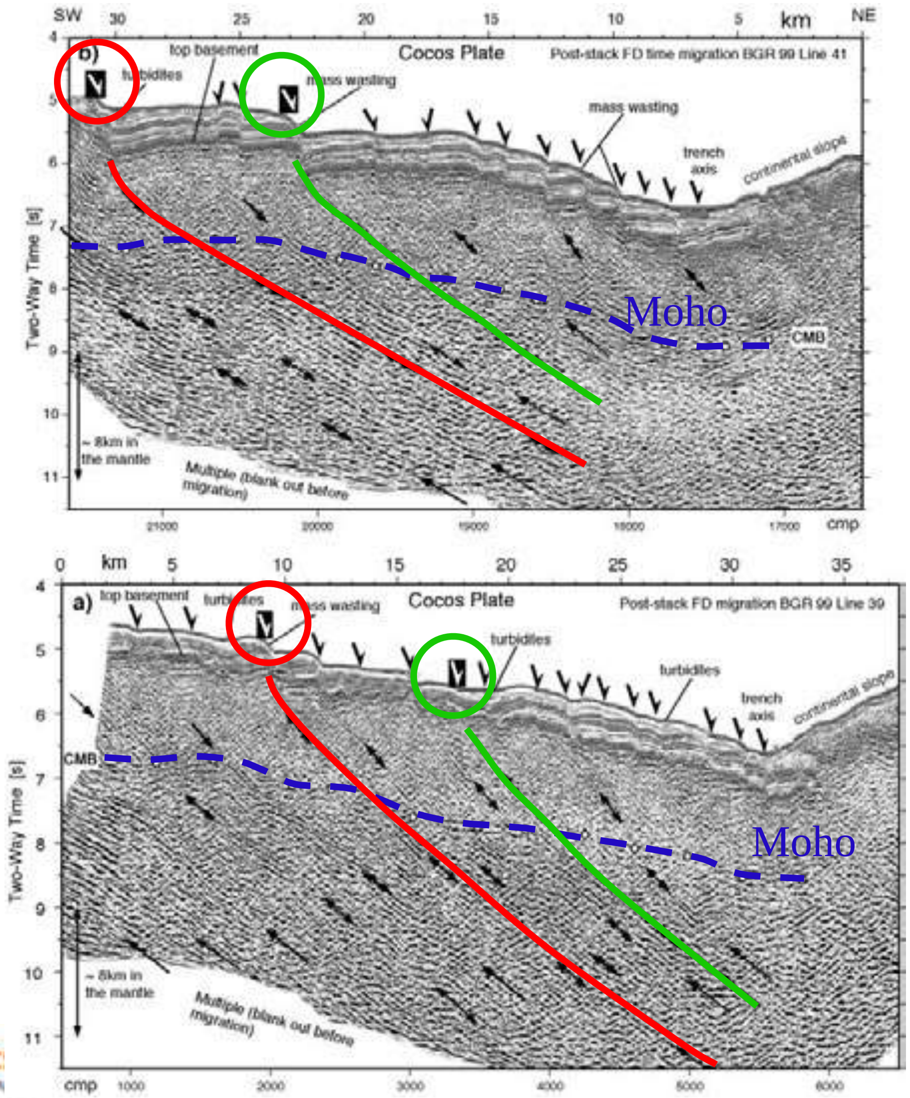

Bend-faulting is a viable mechanism for creation of pervasive water-paths from seafloor to the mantle

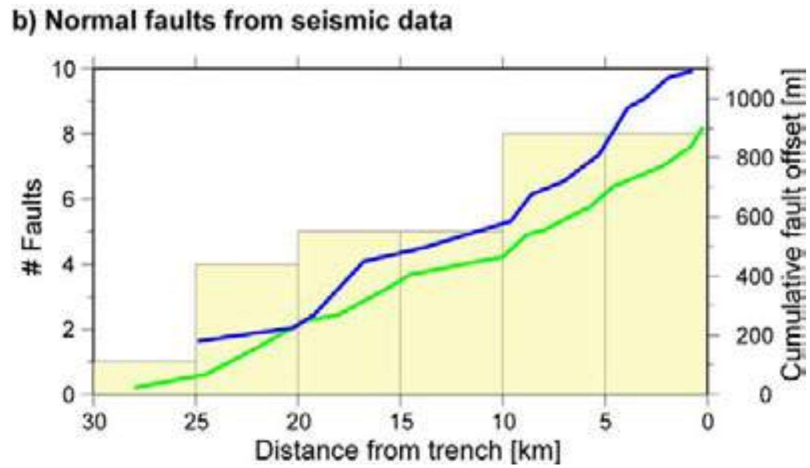

Ranero et al., Nature 2003

Anomalously-low crust and mantle velocities offshore Chile

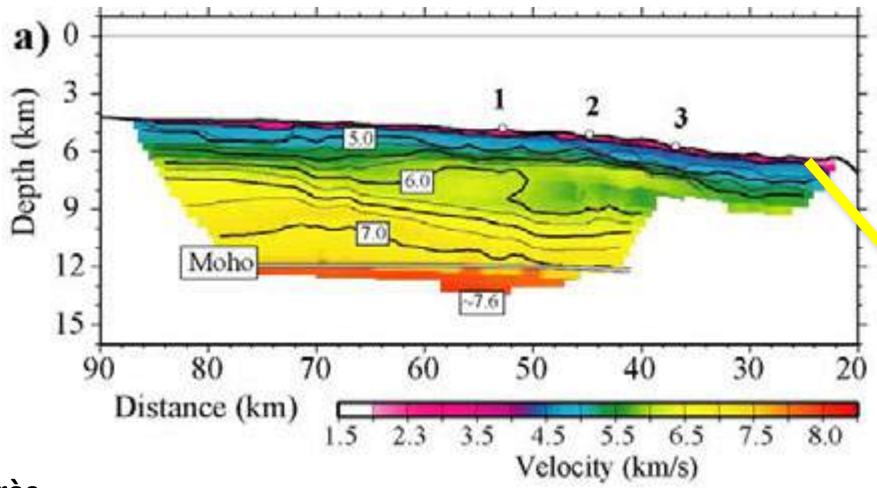

Ranero & Sallarès (Geology, 2004)

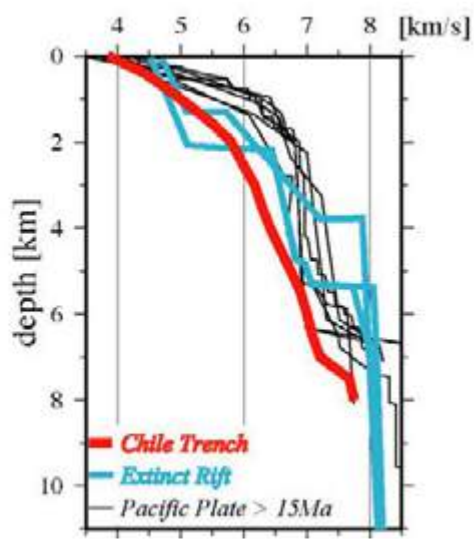

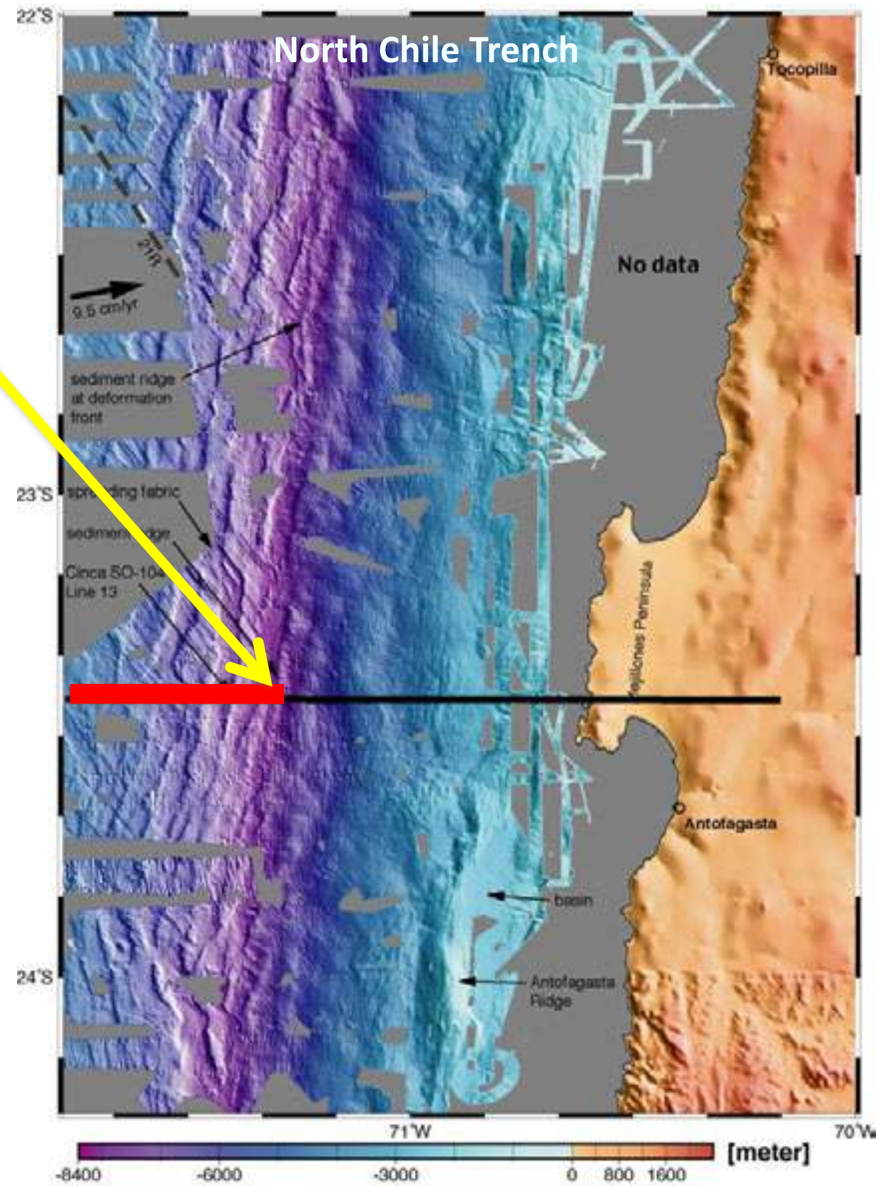

Barcelona CSI
Center for Subsurface Imaging

Heat flux at the trench axis

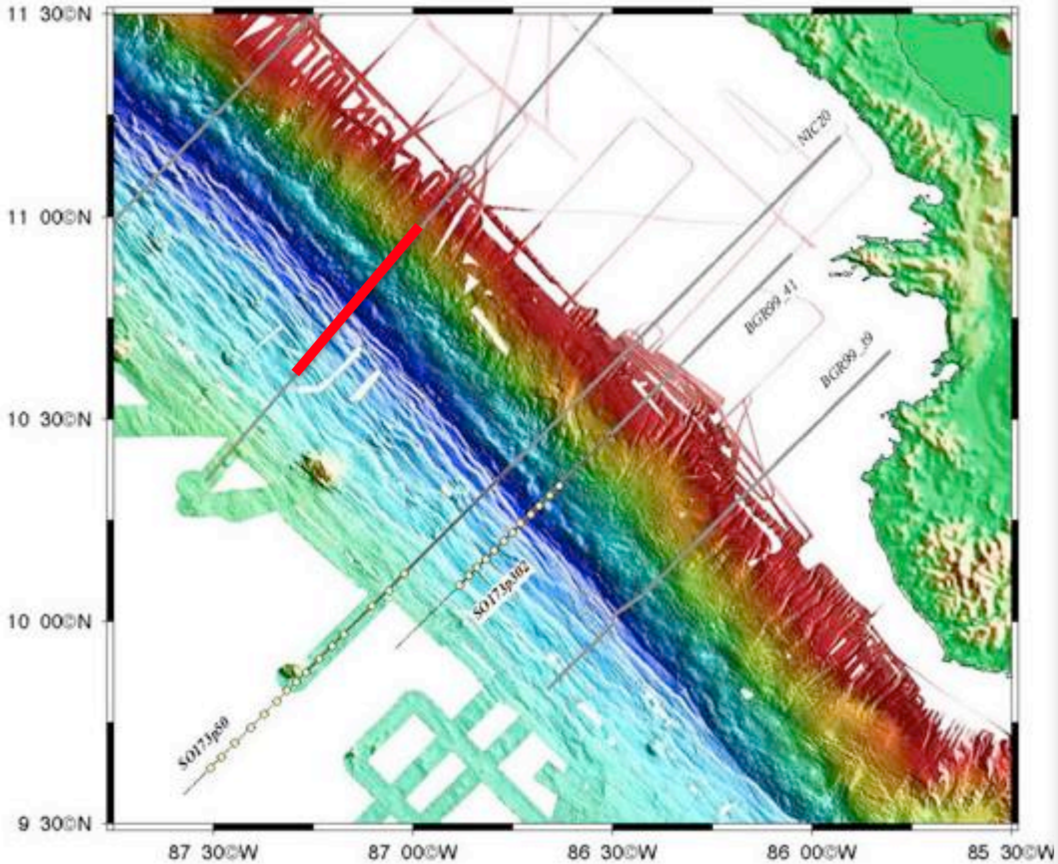

Grevemeyer et al. (EPSL 2005)

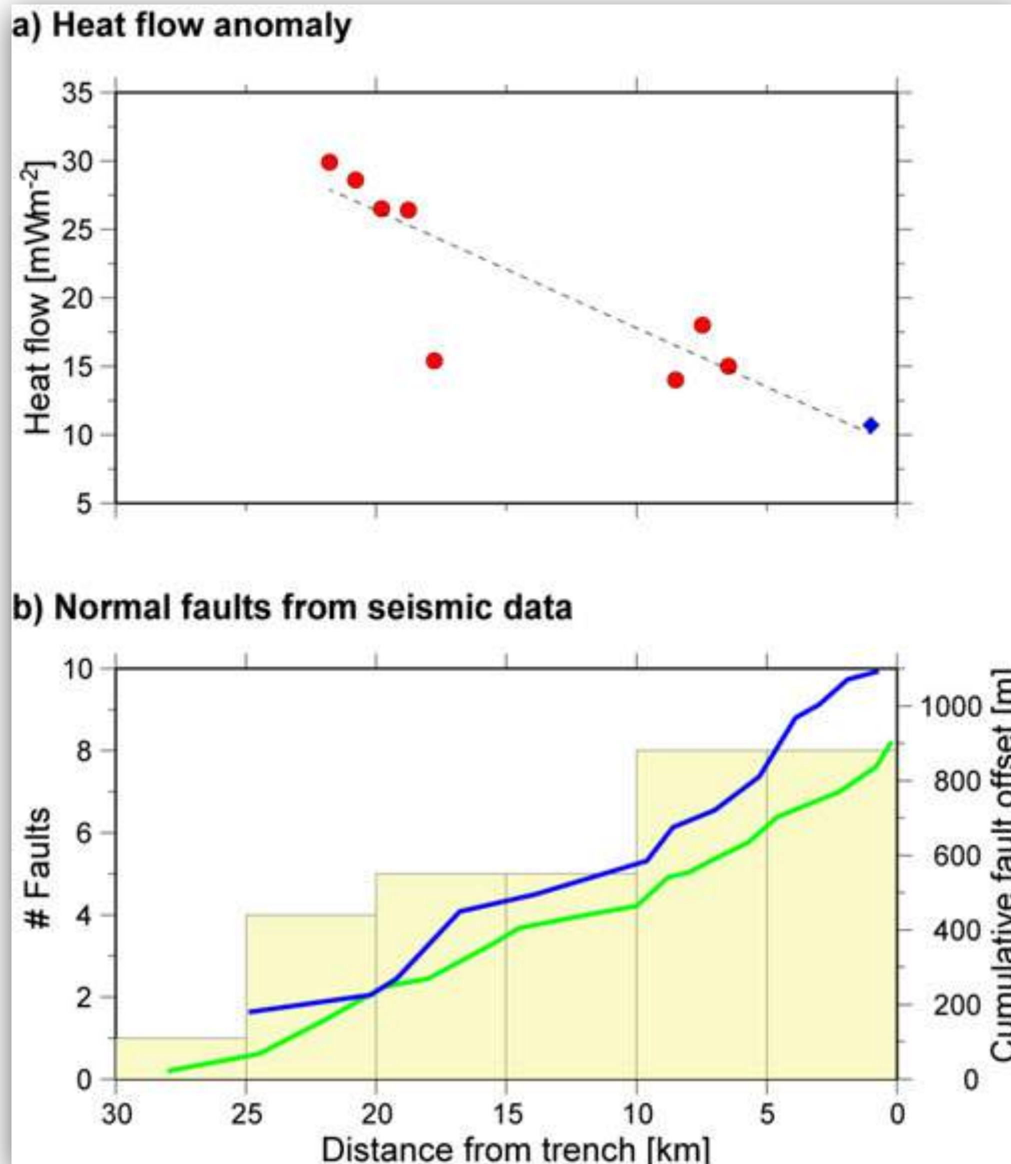

Barcelona CSI
Center for Subsurface Imaging

Wide – Angle Seismic Studies of trenches (2004-2015)

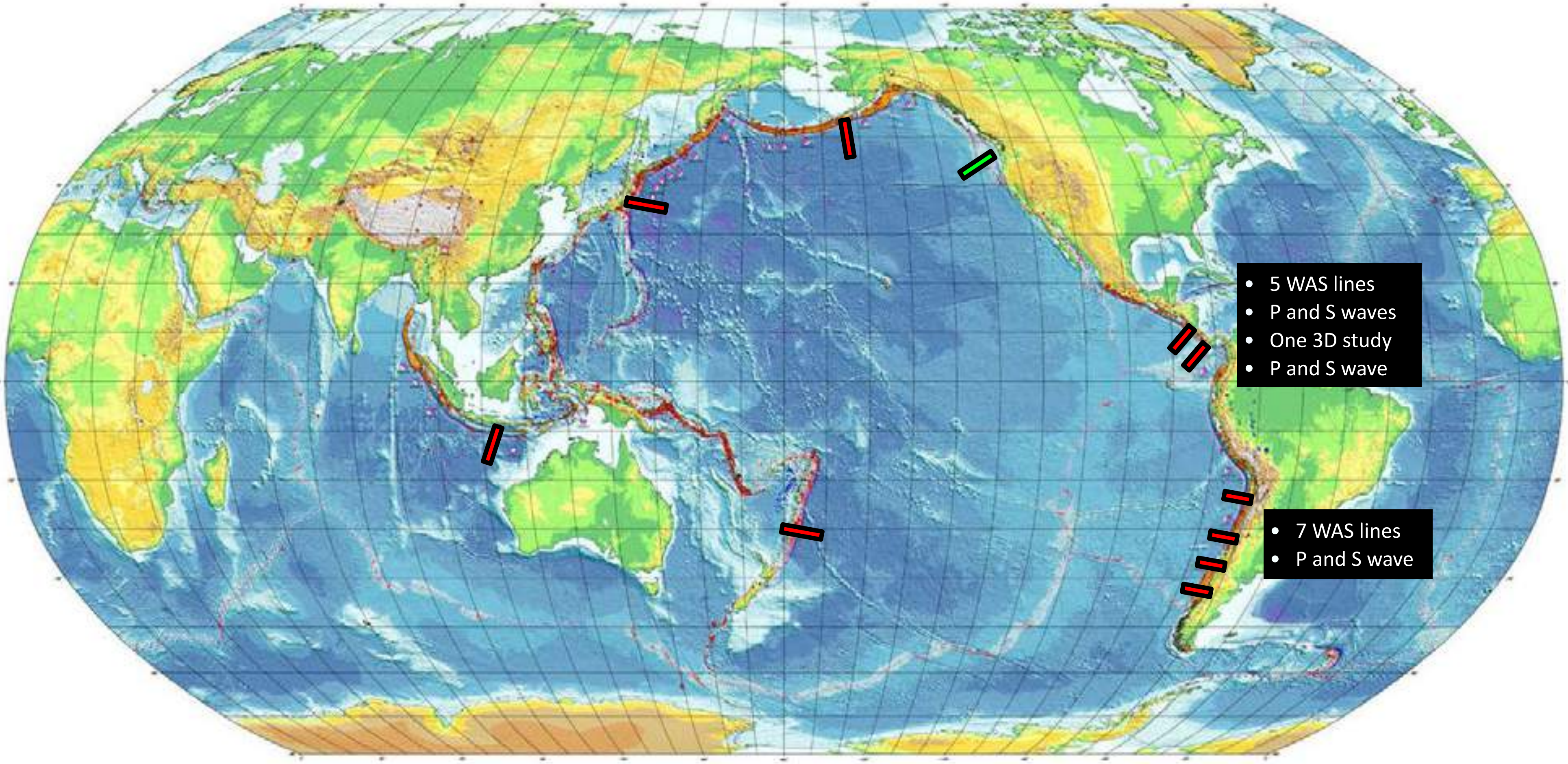

Barcelona CSI
Center for Subsurface Imaging

All modern seismic studies of incoming plates at trenches found low mantle velocities:
Exception: Cascadia -> Plate young and hot (~450°C at Moho)

Compilation of Vp perpendicular to trench axis

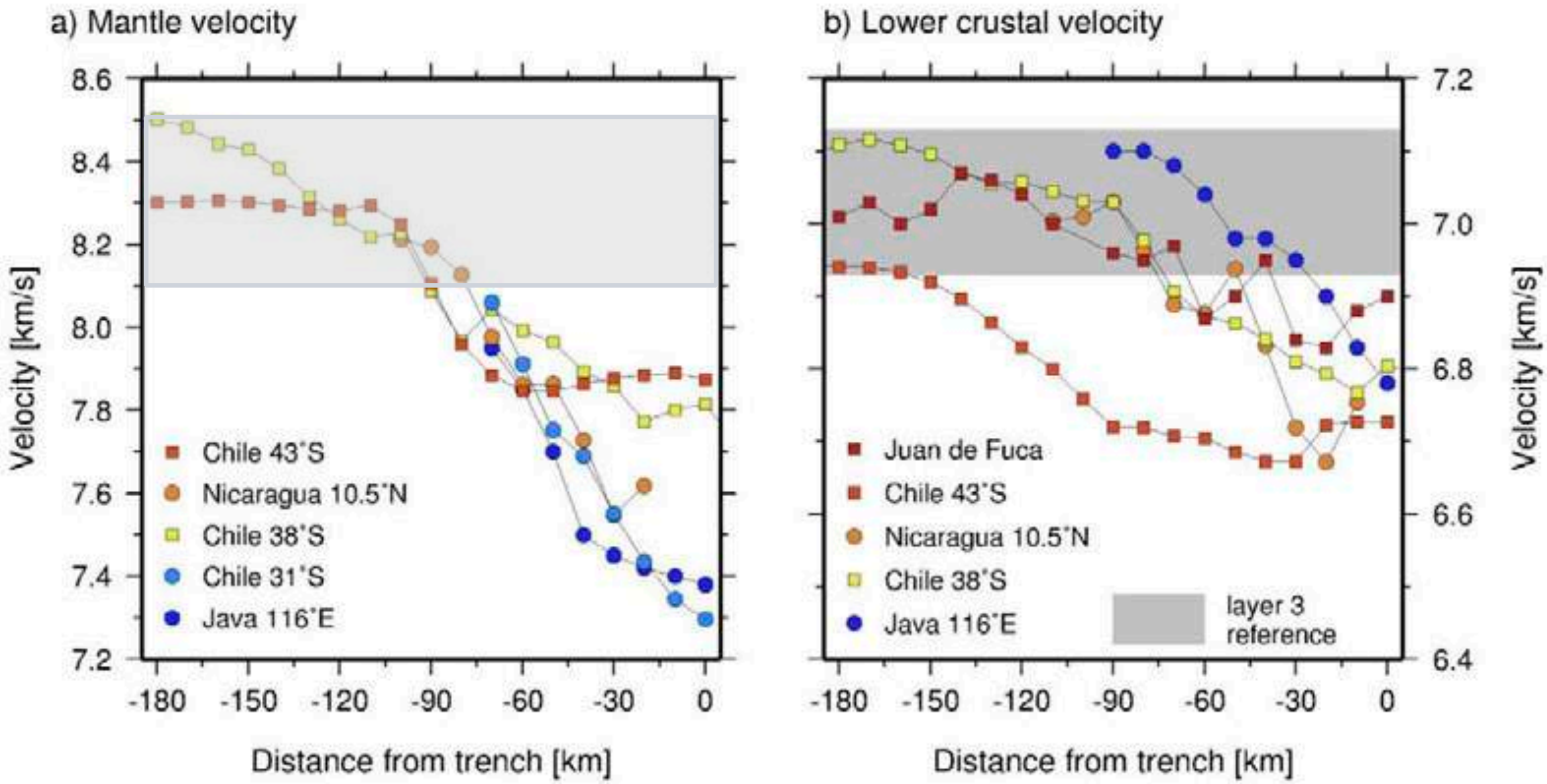

Decreasing VP means fracturaron OR serpentinisation?

Barcelona CSI
Center for Subsurface Imaging

Grevemeyer, Ranero, Ivandich (2018)

NIC-20 wide-angle seismic profile off Nicaragua

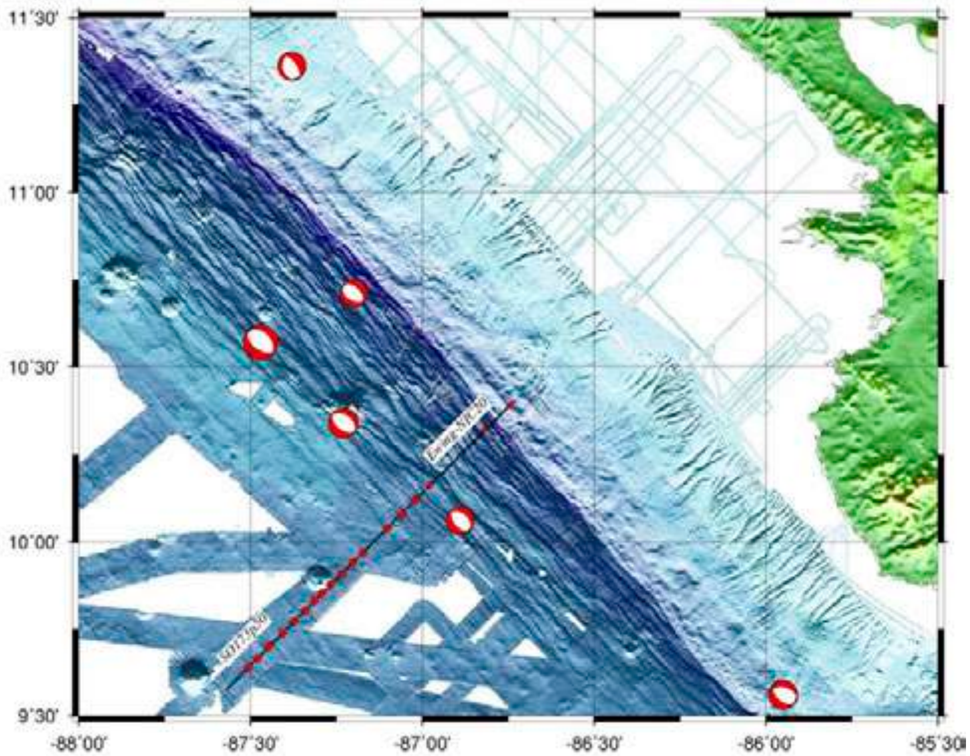

Grevemeyer, Ranero, Ivandich (2018)

Barcelona CSI
Center for Subsurface Imaging

a) **P-wave velocity model**

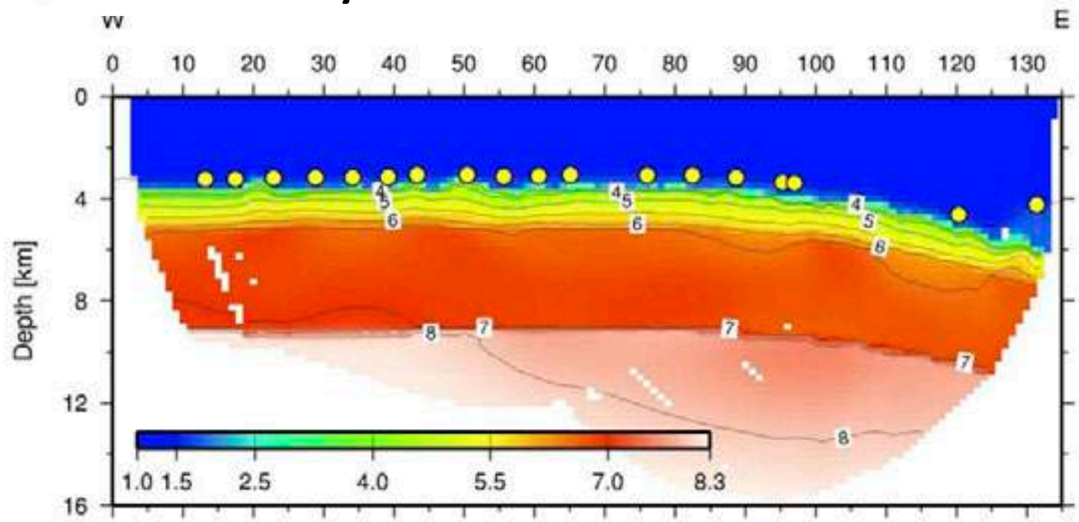

b) **S-wave velocity model**

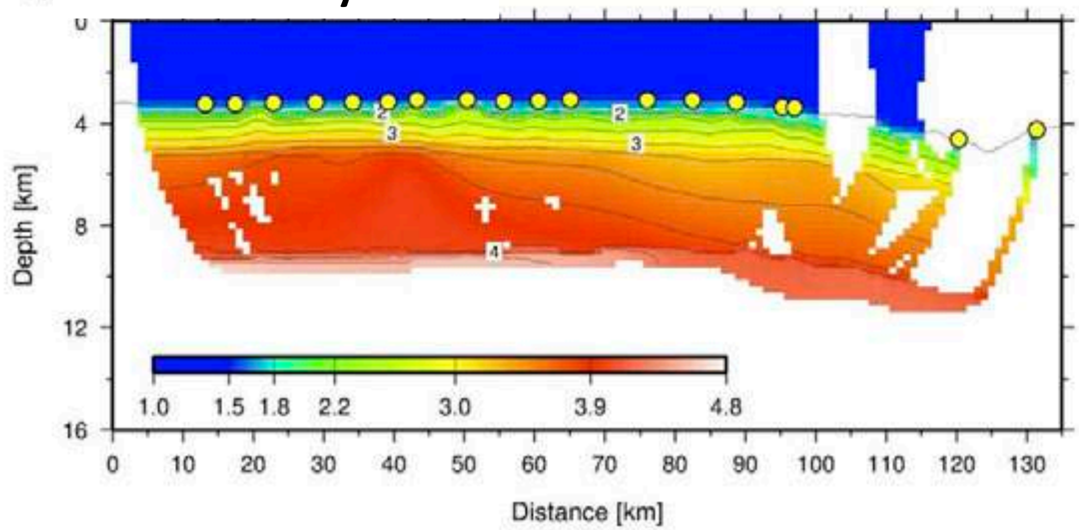

NIC-20 offshore Nicaragua

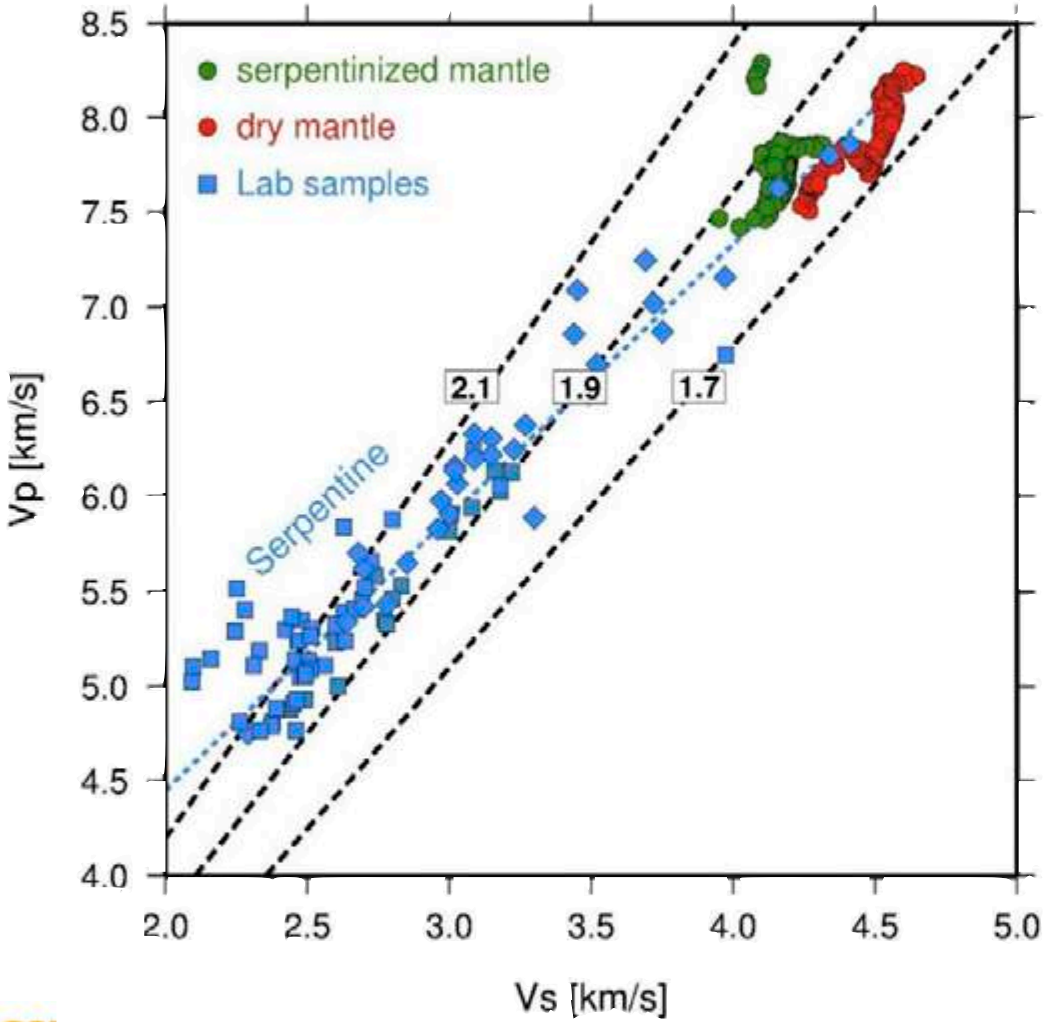

Lab. studies show that **serpentines have high Vp/Vs ratios** compared to dry peridotite:

A **Vp/Vs ratio of >1.8 supports serpentinization** of the mantle of the Nicaragua trench.

Barcelona CSI
Center for Subsurface Imaging

Grevemeyer, Ranero, Ivandich (2018)

How much water is carried in slabs?

The conventional model:

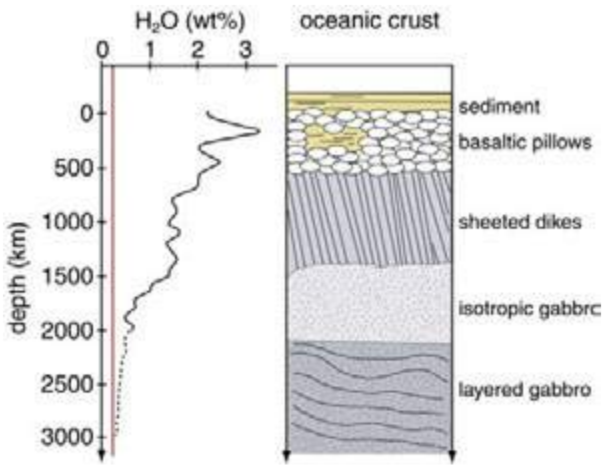

New proposition:

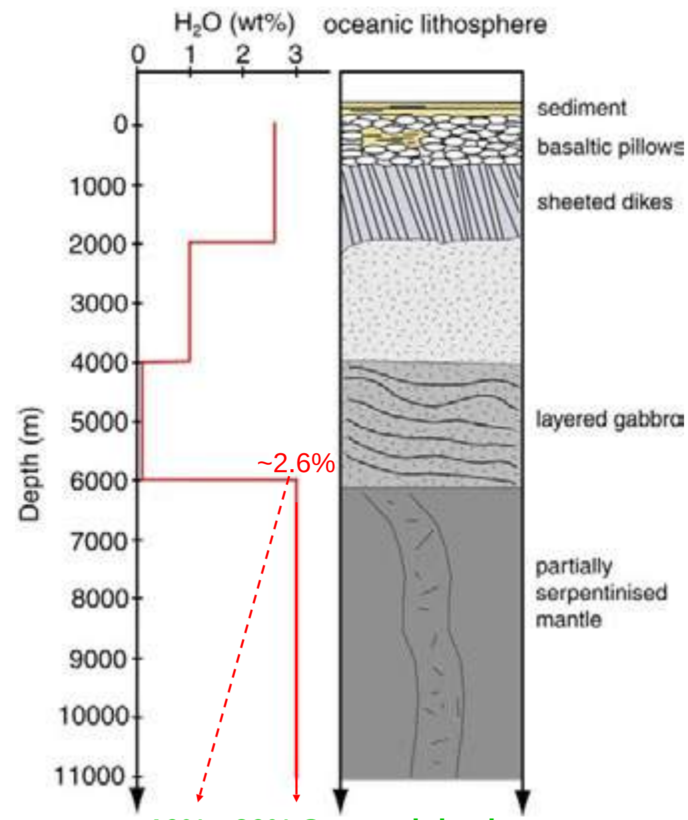

Barcelona CSI
Center for Subsurface Imaging

Water content in oceanic plates at trenches

	Thickness	Bound water ($m^3\ H_20/\ m^2$)
sediment	0.4 km	90
Upper crust	2 km	85
Lower crust	4 km	60
Mantle / 15% serpentine	15 km	~900

The chemically bound water in a 15 km-high mantle column containing 15% serpentine

is equivalent to a

~0.9 km-thick column of water.

The complex structure of incoming plates and down-going slabs

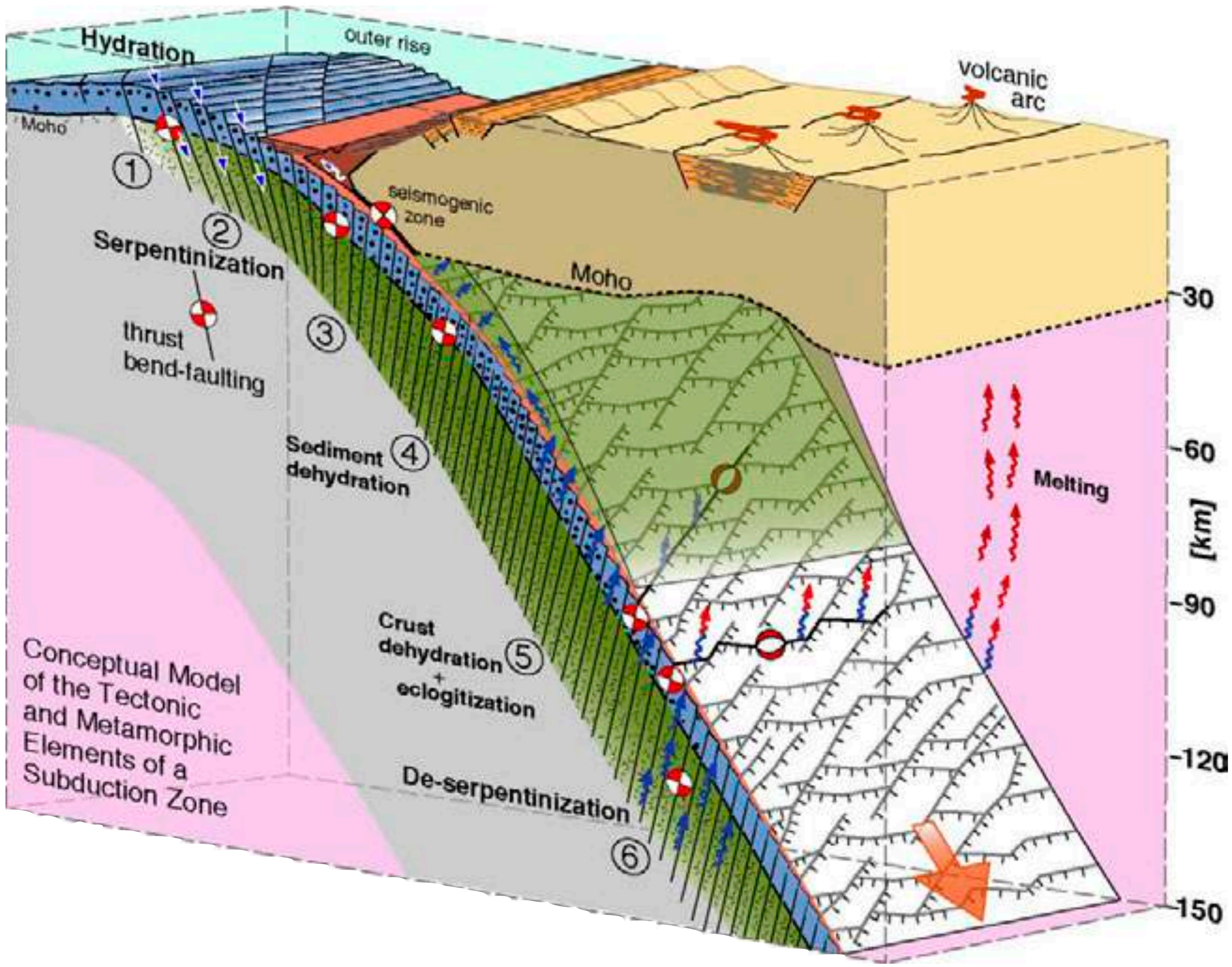

Barcelona CSI
Center for Subsurface Imaging

Ranero et al., G-cubed 2005

Fault-induced seismic anisotropy by hydration in subducting oceanic plates

Manuele Faccenda[1], Luigi Burlini[2], Taras V. Gerya[1] & David Mainprice[3]

(Nature, 2008)

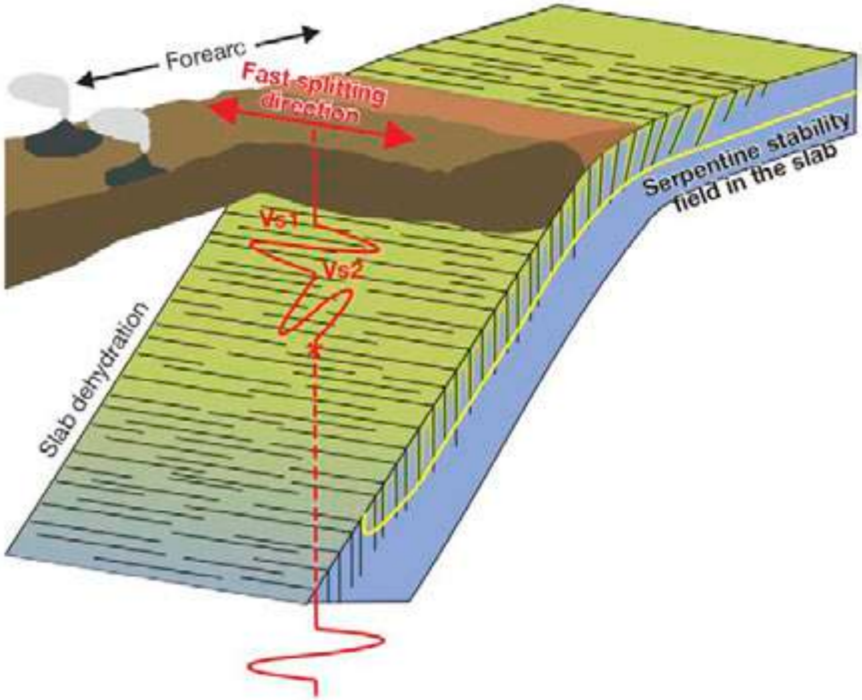

Figure 3 | Schematic diagram of the tectonic and compositional structure of the slab and the inferred splitting behaviour. Vs1 and Vs2 are the fast and slow, orthogonally polarized, shear waves, respectively. The polarization of Vs1 aligns parallel to the strike of the fault set. The colour scheme of the slab is as in Fig. 2a, b.

Deep slab hydration induced by bending-related variations in tectonic pressure

Manuele Faccenda[1]*, Taras V. Gerya[1] and Luigi Burlini[2]

(Nature Geos. 2009)

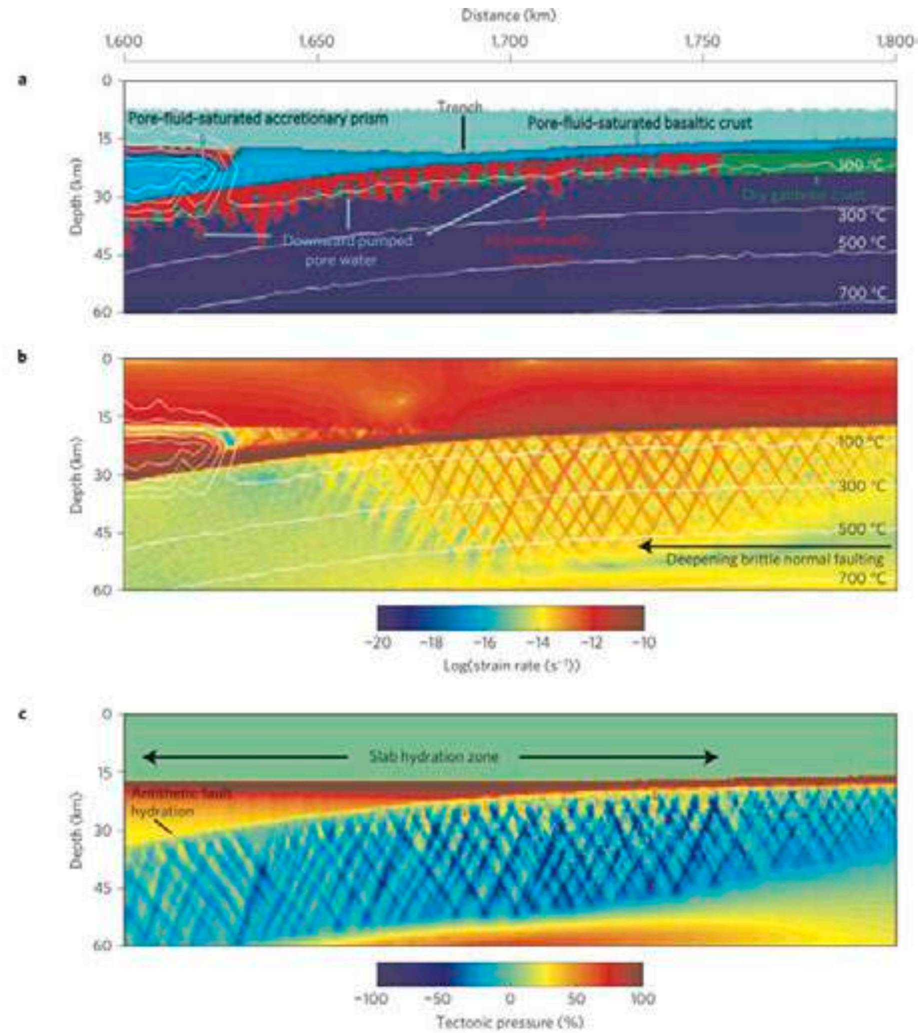

Barcelona CSI
Center for Subsurface Imaging

Seismic evidence of negligible water carried below 400-km depth in subducting lithosphere

Harry W. Green II[1], Wang-Ping Chen[2] & Michael R. Brudzinski[3]

(Nature, 2010)

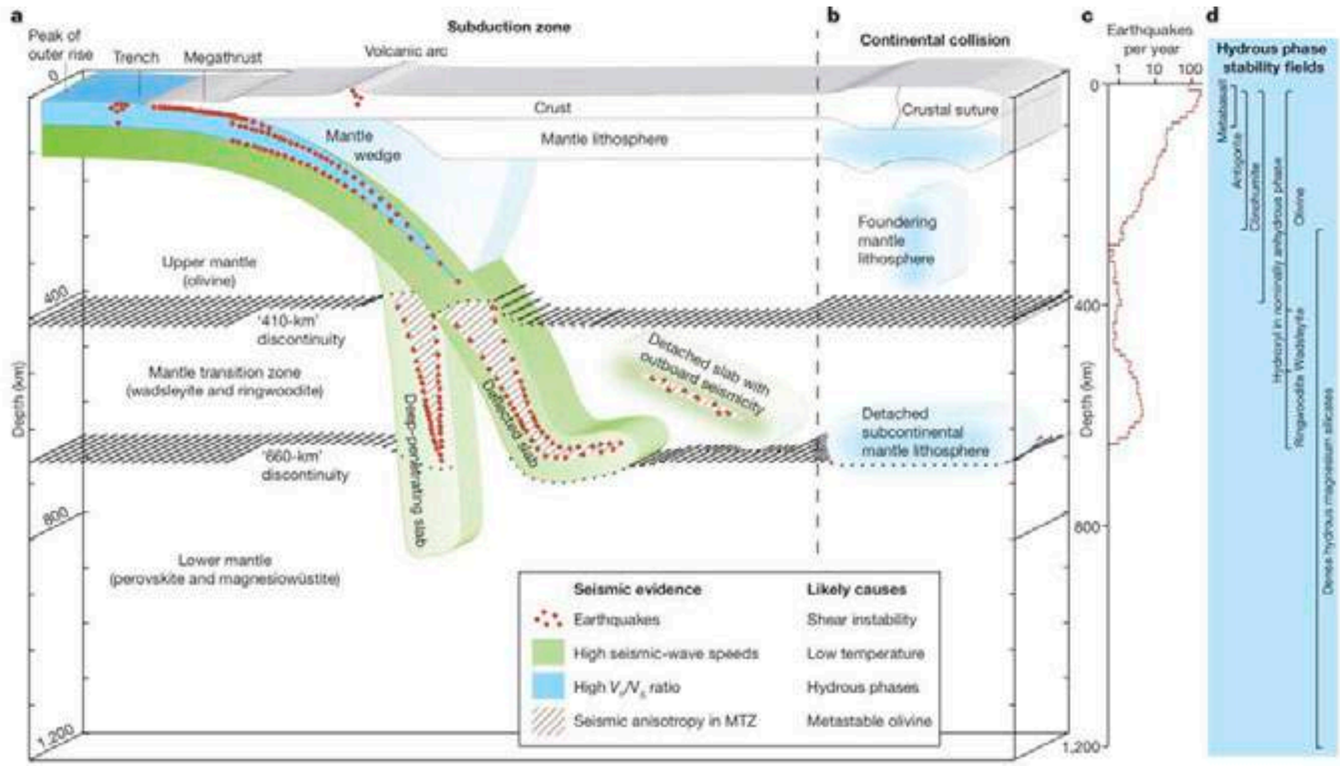

Figure 1 | Schematic summarizing key points presented in this study. **a**, Salient features of subduction zones and overall structures of the upper mantle and the mantle transition zone, with key seismic observations and their likely causes. The most prominent example of deflected and detached slabs is under the back-arc region of the Tonga–Kermadec subduction zone[8], whereas the slab along the steeply dipping Mariana subduction zone seems to penetrate into the lower mantle[27]. Globally, not a single earthquake has been recorded below a depth of about 680 km. **b**, Salient features of a continental collision zone, such as the Himalaya–Tibet collision zone, where Rayleigh–Taylor instability causes thickened subcontinental mantle lithosphere to founder. Before collision, the subcontinental mantle lithosphere was hydrated as part of the mantle wedge along an Andean-type continental margin[33]. **c**, Globally averaged number of earthquakes (body-wave magnitude, ≥5) per year as a function of depth. Notice that the horizontal scale is logarithmic. **d**, Summary of stability of various hydrous phases, emphasizing the effect of depth (or, equivalently, pressure). There is a sequence of dehydration reactions that can account for the concentration of seismicity above depths of about 350 km. In contrast, there is no corresponding dehydration for the concentration of seismicity at greater depths. Moreover, there is no seismicity associated with expected dehydration of nominally anhydrous olivine polymorphs and dense hydrous magnesium silicates at greater depths.

Barcelona CSI
Center for Subsurface Imaging

Seismic constraints on the water flux delivered to the deep Earth by subduction
Savage (Geology 2012)

Large quantities of water penetrate to > 600 km

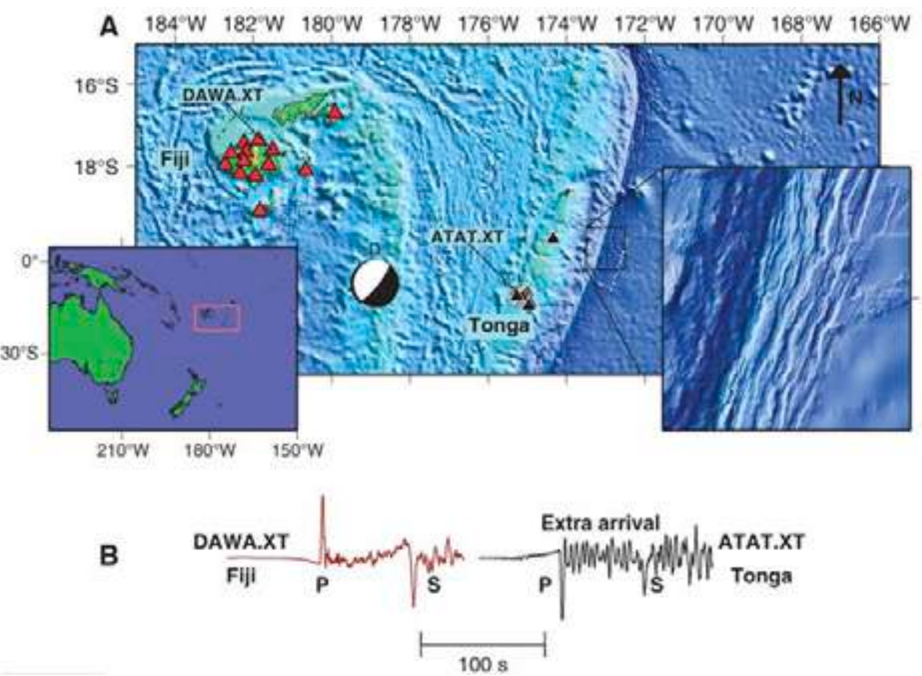

Figure 1. A: Data from deep earthquake (634 km) displayed as lower hemisphere projection recorded at Tonga (black triangles) and Fiji (red triangles) seismic stations. Left inset shows general location of Tonga and Fiji. Right inset is bathymetry image of subducting plate as it enters trench, and shows presence of large offset trench-parallel faults. B: Initial impulsive arrivals are compressional P waves followed by shear or S waves, seen in data from Fiji (red seismogram). Unexpected arrival is visible in Tonga data (black seismogram) with extended duration and large amplitude.

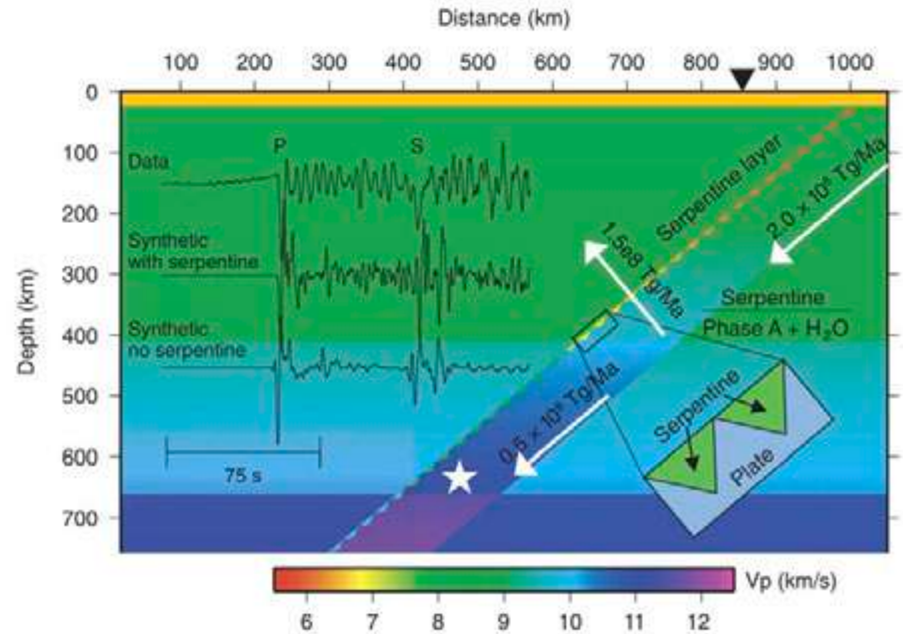

Figure 2. Simplified compressional wave speed model of Tonga-Fiji subduction zone. Subducting plate, dipping to left, is higher wave speed than background mantle model and includes undulating serpentine layer on top of plate. Lower right inset shows plate (blue box) and serpentine layer (green triangles). Comparison between data (top) and synthetic seismograms (middle, bottom) demonstrates that addition of a serpentine layer to top of plate improves fit between data and synthetics. Synthetic earthquake source is located at white star, and seismic station is at inverted triangle (black, at top). White arrows show determined mantle water fluxes into Earth (2.0×10^9 Tg/Ma), expelled due to serpentine conversion to phase A (1.5×10^9 Tg/Ma) and carried to deeper depths by subducting lithospheric mantle (0.5×10^9 Tg/Ma).

Barcelona CSI
Center for Subsurface Imaging

ARTICLES
PUBLISHED ONLINE: 27 FEBRUARY 2017 | DOI: 10.1038/NGEO2902

nature geoscience

Seawater cycled throughout Earth's mantle in partially serpentinized lithosphere

M. A. Kendrick[1]*, C. Hémond[2], V. S. Kamenetsky[3], L. Danyushevsky[3], C. W. Devey[4], T. Rodemann[5], M. G. Jackson[6] and M. R. Perfit[7]

The extent to which water and halogens in Earth's mantle have primordial origins, or are dominated by seawater-derived components introduced by subduction is debated. About 90% of non-radiogenic xenon in the Earth's mantle has a subducted atmospheric origin, but the degree to which atmospheric gases and other seawater components are coupled during subduction is unclear. Here we present the concentrations of water and halogens in samples of magmatic glasses collected from mid-ocean ridges and ocean islands globally. We show that water and halogen enrichment is unexpectedly associated with trace element signatures characteristic of dehydrated oceanic crust, and that the most incompatible halogens have relatively uniform abundance ratios that are different from primitive mantle values. Taken together, these results imply that Earth's mantle is highly processed and that most of its water and halogens were introduced by the subduction of serpentinized lithospheric mantle associated with dehydrated oceanic crust.

Quantifying the global cycles of volatile elements into and out of the mantle is critical for modelling planetary evolution[1-7]. Trace elements and radiogenic isotopes provide important information about mantle heterogeneity, with many features of ocean island basalts (OIBs) commonly attributed to the presence of recycled subducted ocean crust (the HIMU endmember) or sediment (EM endmembers) in their mantle sources[8-10] (Fig. 1). Melts sampling EM (enriched mantle) reservoirs are known to be depleted in H_2O and Cl relative to lithophile elements of similar mantle incompatibility, consistent with the presence of dehydrated sediment or continental crustal material in EM sources[2,4,11-13]. However, the volatile content of HIMU (high-μ, meaning high U/Pb) reservoirs and the relative proportions of recycled versus primordial water in the mantle remain poorly constrained[2,4,11-13].

The current study combines new and published F, Cl, Br, I and

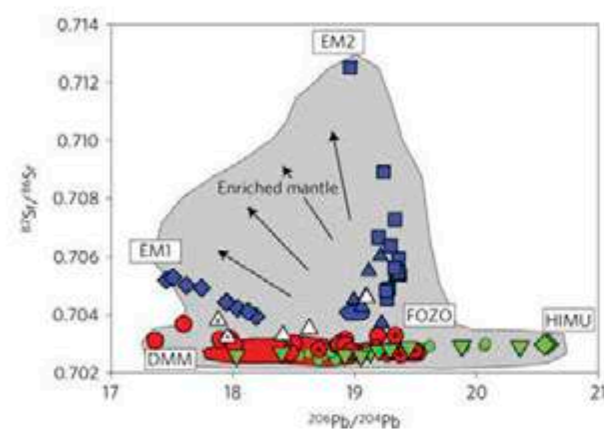

Barcelona CSI
Center for Subsurface Imaging

Growing Evidence of larger-scale transformation of incoming plates

Intense deformation of the lithosphere is **NOT** constrained to **ONLY** the **TRENCH** but occurs in a much broader region extending across the entire **OUTER RISE**.

Barcelona CSI
Center for Subsurface Imaging

Petit Spot : Major transformations?

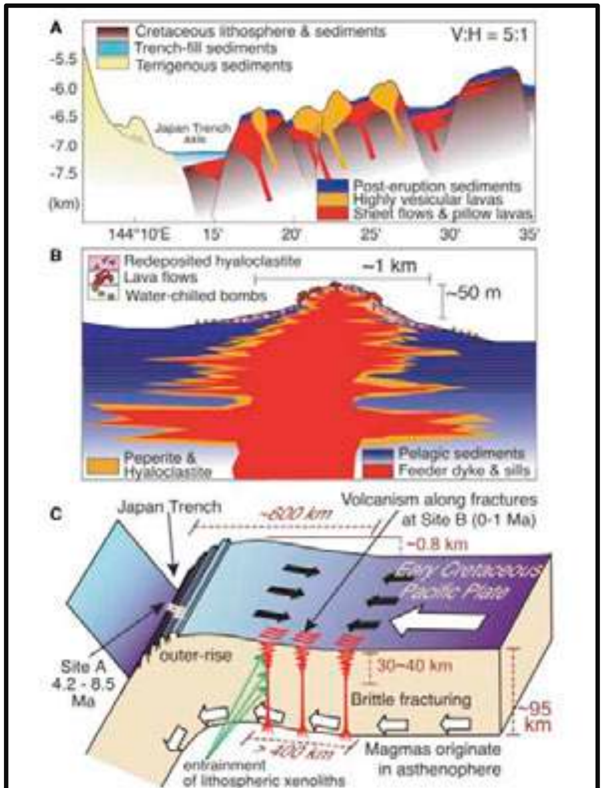

Fig. 3. Geologic interpretations of the lava fields. (**A**) Schematic cross section of site A (red line in Fig. 1, B and C). (**B**) A schematic cross section of a volcano at site B constructed from observations made during dives. (**C**) A conceptual model of petit spot volcanism. Magmas from the asthenosphere escape to the shallow depths because of the extensional environment of the lower lithosphere (*21*) and migrate up through the brittle compressed upper lithosphere by exploiting fractures created by flexure of the plate. Data for the plate and flexure framework are from previous studies (*6, 11, 21, 22*).

Hirano et al., (Science 2008)

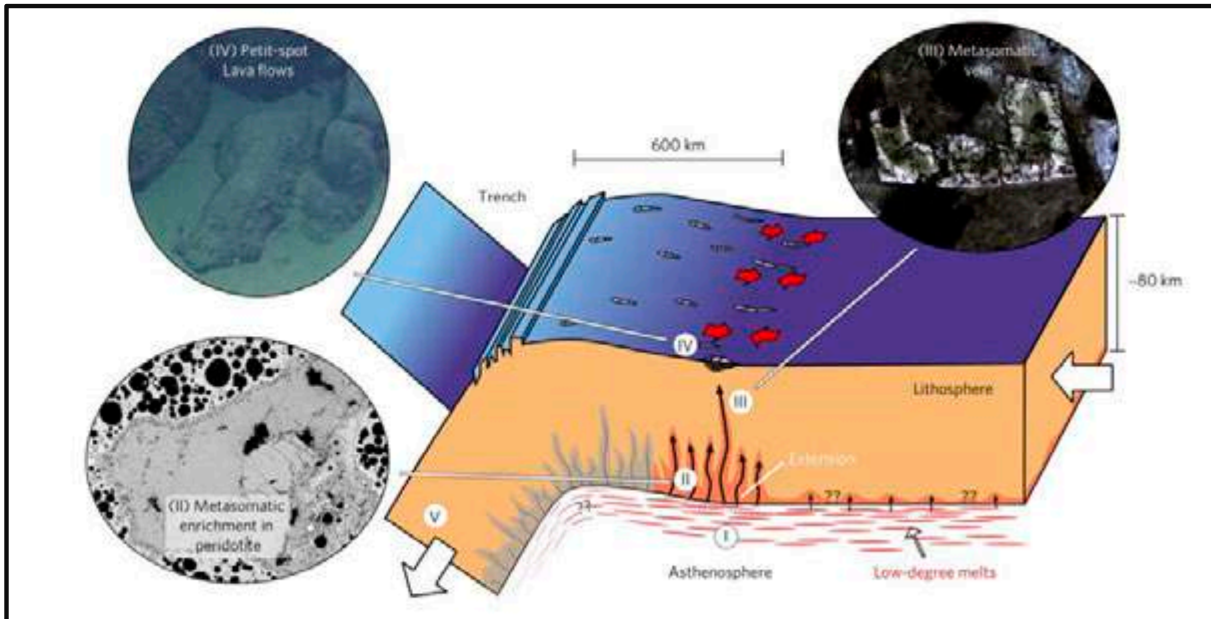

Figure 3 | Schematic model illustrating the metasomatism of the oceanic lithospheric mantle associated to plate flexure. Extension at the base of the lithosphere created by plate flexure allows low-degree melts present at the top ofthe asthenosphere to percolate into the lithospheric mantle (I). The percolation and differentiation of these melts produce various (an-) hydrous metasomatic veins and/or cumulates as a function of pressure and temperature, and cryptic metasomatism in oceanic lithosphere (II–III). In some cases, the reacting low-degree melts could reach the surface and generate the petit-spot sills and lavas (IV). Recycling and storage of oceanic lithosphere into the convecting mantle containing incompatible element-enriched metasomatized domains could produce some of the isotopically enriched components observed in the source of MORBs or OIBs (V).

Pilet et al., (Nature Geos. 2016)

Barcelona CSI
Center for Subsurface Imaging

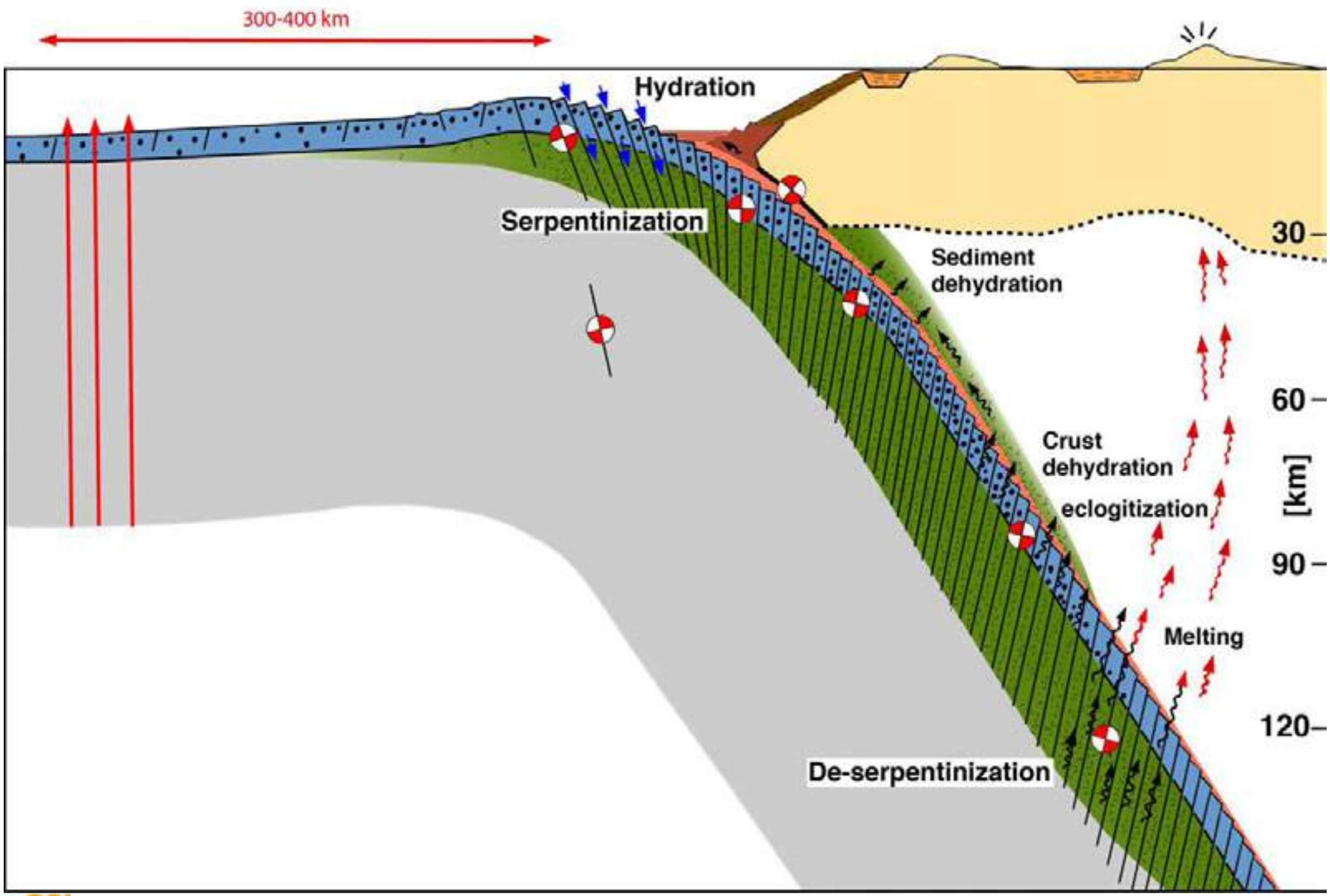

Barcelona CSI
Center for Subsurface Imaging

Significance

Mid Ocean Ridge Systems:

- **~60,000 km long system.**
- **30-40 km width of active deformation and magmatism.**
- **0.5 - 2 m.y. of active deformation.**
- **Max. depth of intense deformation and exchange between hydrosphere and lithosphere reaches to ~10 km.**

Incoming Plate at Subduction Trenches:

- **~55,000 km long system.**
- **300-400 km width of the active deformation, serpentinization & metasomatism.**
- **1 - 4 m.y. of active deformation.**
- **Max. depth of intense deformation and geochemical exchange between hydrosphere and lithosphere may reach ~15-30 km.**

Incoming Plates are a new class of geodynamic setting

Barcelona CSI
Center for Subsurface Imaging

4. What do to next to advance?

Why plate tectonics crystallised in the 1960s?

New Observations from New Technologies (after WWII):

- **Magnetometers** -> Seafloor spreading magnetic lineations
- **Seafloor maps** -> Mid Ocean Ridges and Trenches
- **Worldwide seismological network** -> Slabs in the mantle

1873

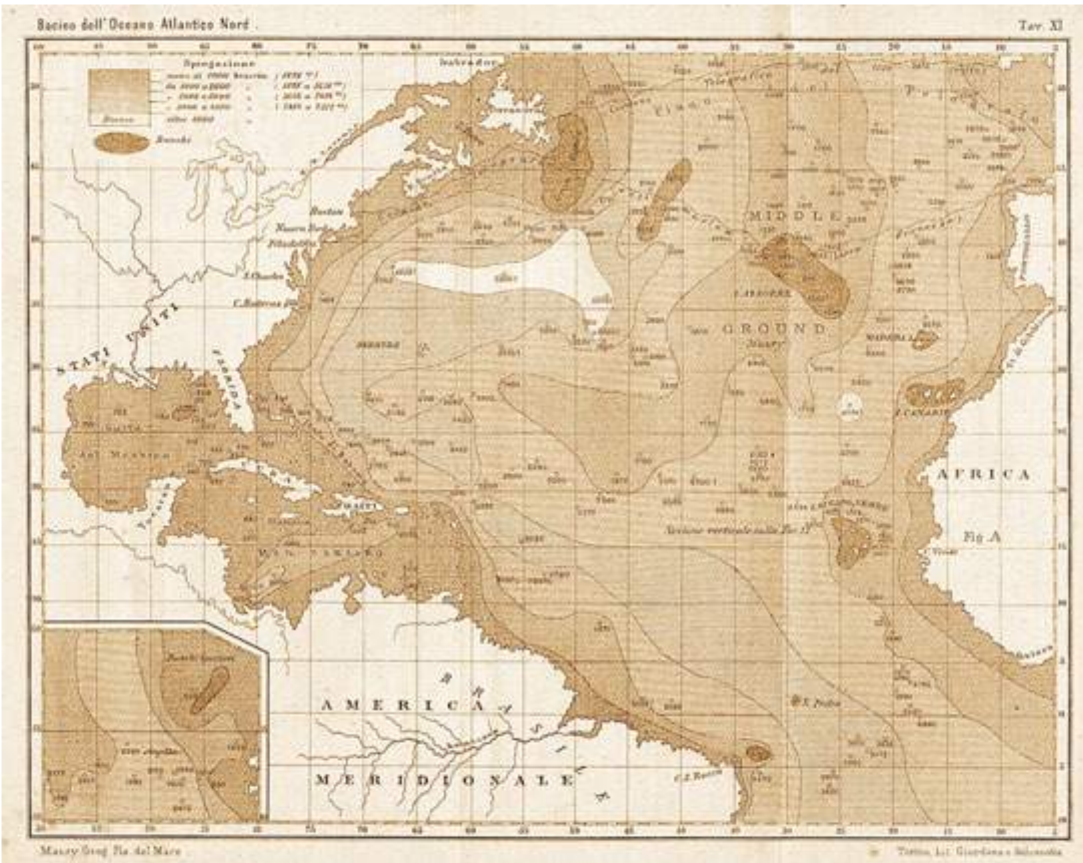

1940

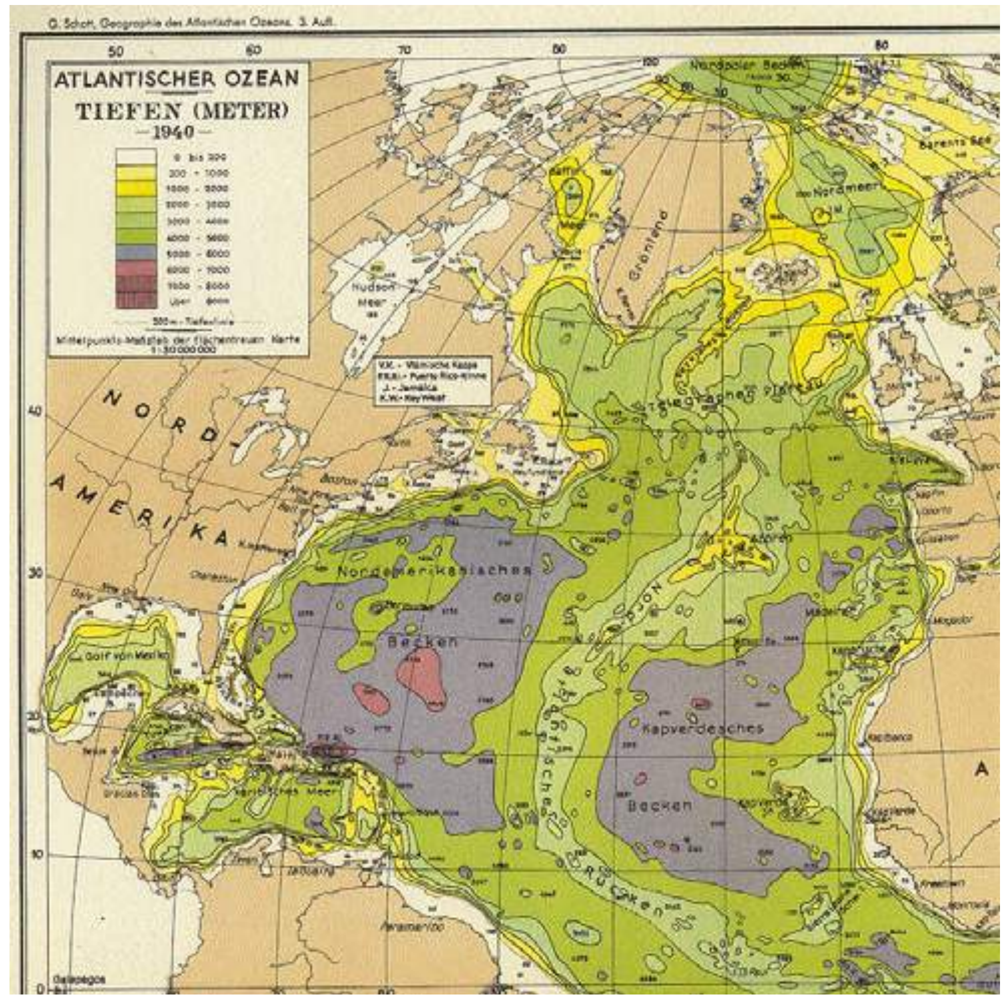

Barcelona CSI
Center for Subsurface Imaging

1950 to 60's **Marie Tharp** maps provided a Key Observation: The MOR system

Barcelona CSI
Center for Subsurface Imaging

~1980’s

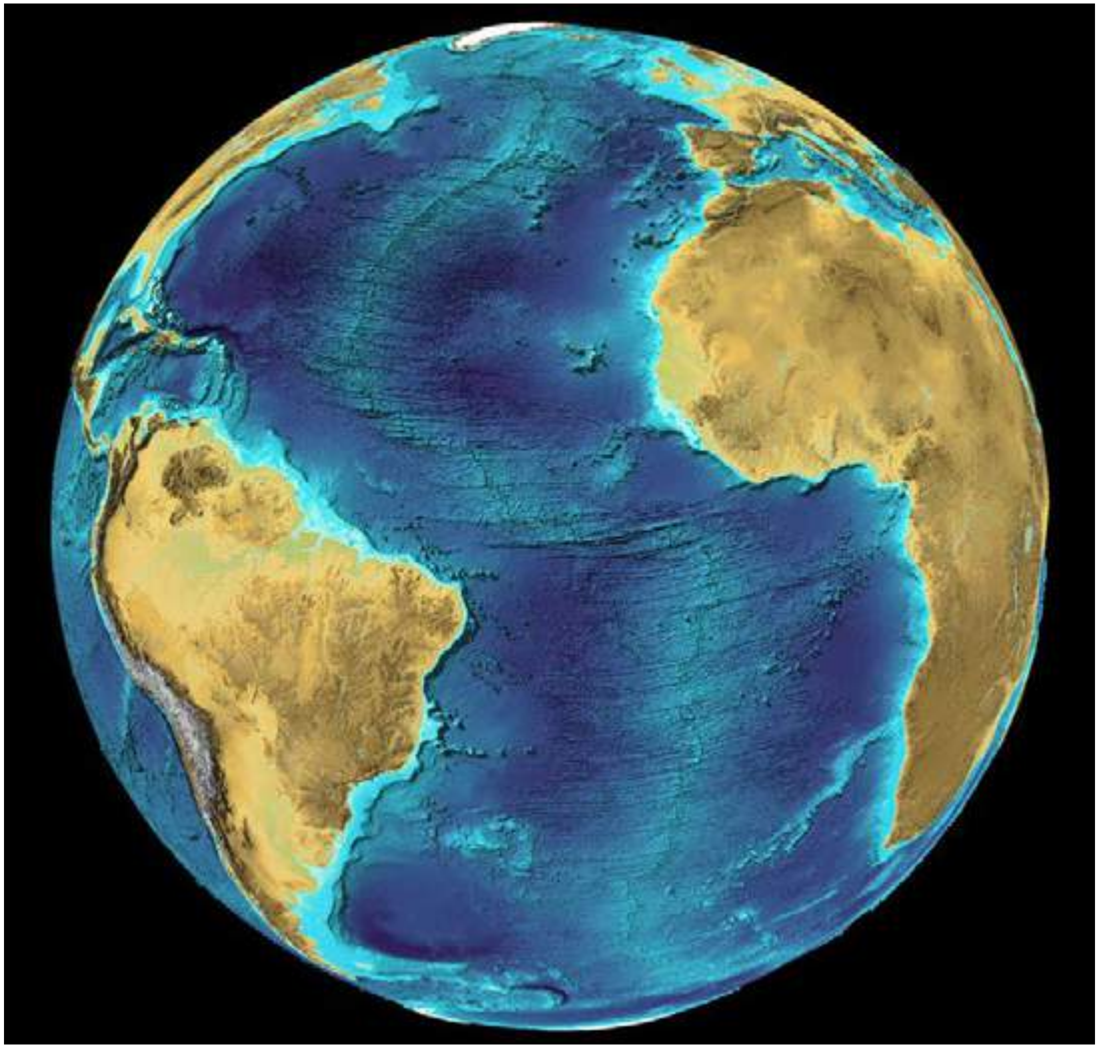

Barcelona CSI
Center for Subsurface Imaging

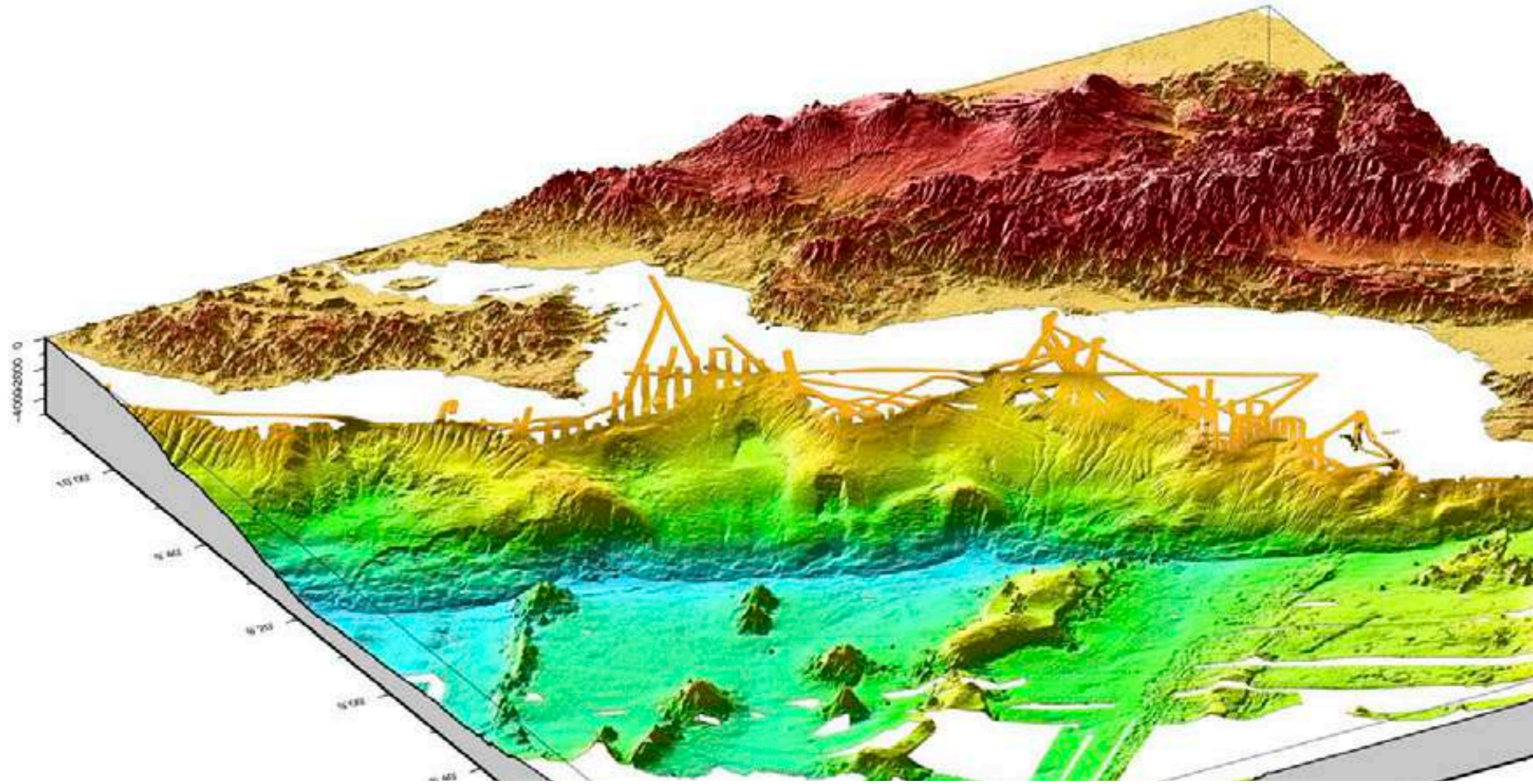

Barcelona CSI
Center for Subsurface Imaging

What do we need to do to image subduction zones?

NEXT
GENERATION
GEOPHYSICS

Barcelona CSI
Center for Subsurface Imaging

Three-dimensional elastic wave speeds in the northern Chile subduction zone: variations in hydration in the supraslab mantle

Diana Comte,[1,2] Daniel Carrizo,[2,3] Steven Roecker,[4] Francisco Ortega-Culaciati[1] and Sophie Peyrat[5]

Geophys. J. Int. (2016)

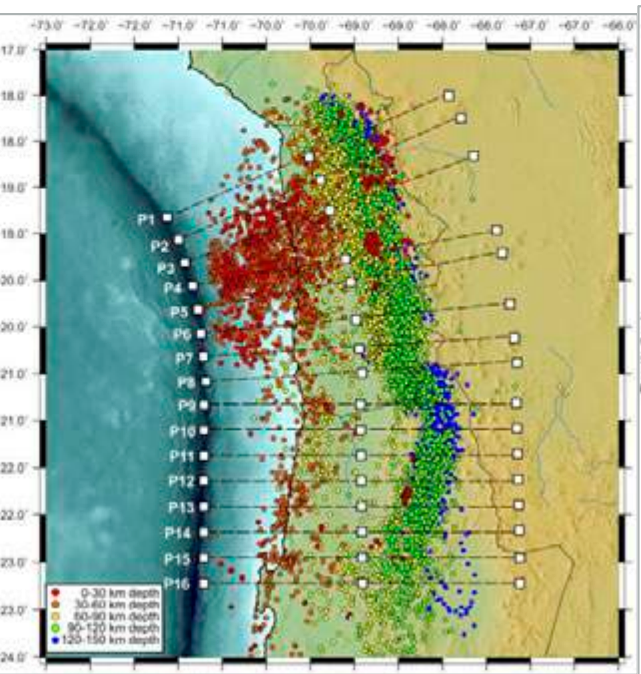

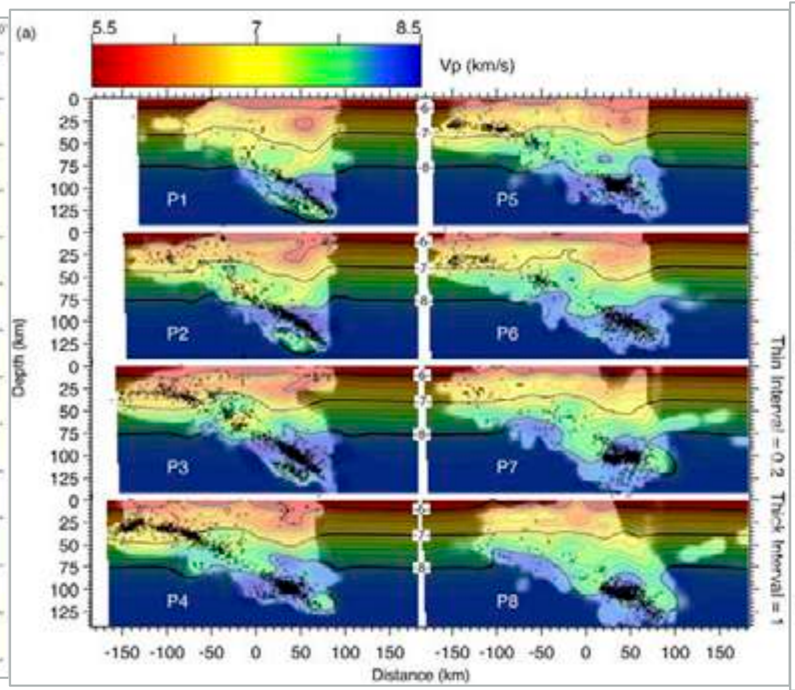

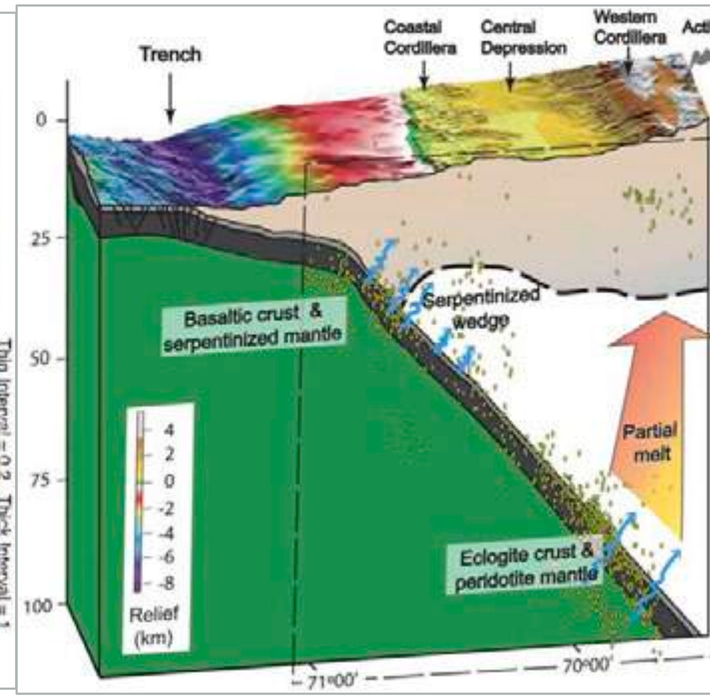

The Seismic Structure and Dynamics of the Mantle Wedge

Douglas A. Wiens, James A. Conder, and Ulrich H. Faul

Annu. Rev. Earth Planet. Sci. 2008

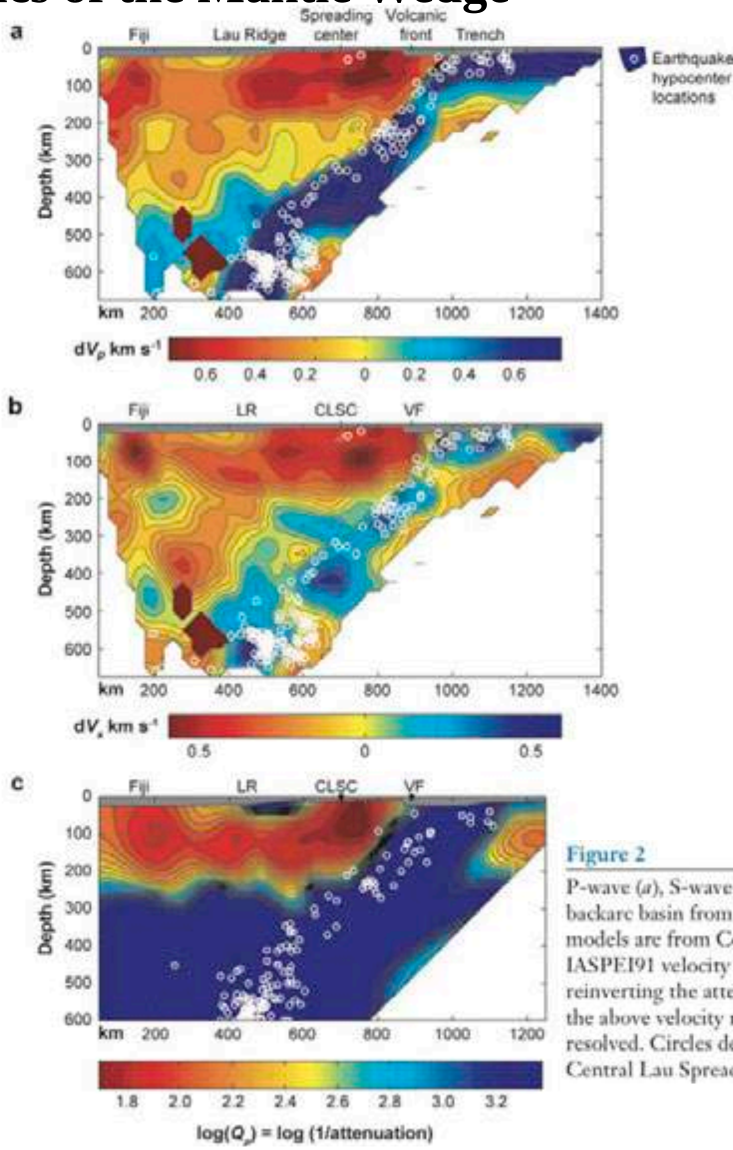

Figure 2

P-wave (*a*), S-wave (*b*), and Q_p (*c*) tomographic models for the Tonga-Lau subduction zor backarc basin from an ocean-bottom seismograph deployment. The P-wave and S-wave models are from Conder & Wiens (2006) and are given as velocity anomalies relative to IASPEI91 velocity model (Kennett & Engdahl 1991). The Q_p structure was determined reinverting the attenuation measurements of Roth et al. (1999) using ray paths calculated the above velocity model. The solutions are masked where the structures cannot be adeq resolved. Circles denote earthquake hypocenter locations. CLSC denotes the position of Central Lau Spreading Center.

Barcelona CSI
Center for Subsurface Imaging

Imaging the source region of Cascadia tremor and intermediate-depth earthquakes

Geoffrey A. Abers[1]*, Laura S. MacKenzie[2], Stéphane Rondenay[3], Zhu Zhang[4], Aaron G. Wech[5], and Kenneth C. Creager[5]

(Geology, 2009)

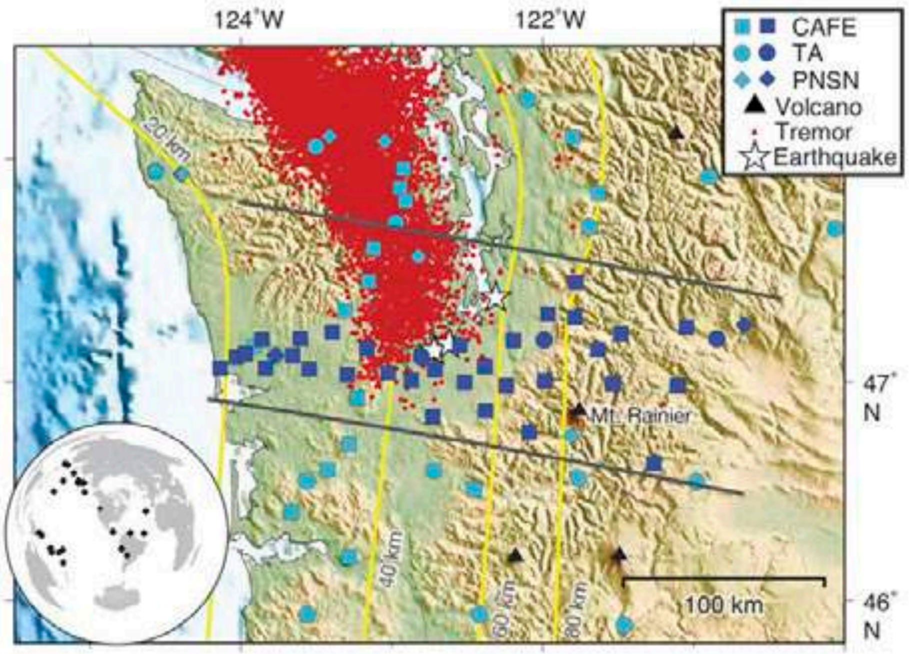

Figure 1. Broadband seismic stations used in this study (blue), tremor (red dots), and contours to slab seismicity (yellow). Stations symbols are dark blue if used in migration image or light blue if only used to estimate incident wavefield and for earthquake location. Symbol shape indicates network (legend): CAFE—Cascadia Arrays for Earthscope; TA—Earthscope Transportable Array; PNSN—Pacific Northwest Seismic Network. Tremors (dots) from 2004, 2005, 2007, and 2008 sequences located by automated detection technique (Wech and Creager, 2008). Contours show depth to Juan de Fuca slab at 20 km intervals (McCrory et al., 2004). Dark lines denote cross-section projection region (Fig. 2). Stars show epicenters of three largest ($M > 6.5$) recorded intraslab earthquakes, in 1949, 1965, and 2001(Data Repository, Section C; see footnote 1). Inset, lower left, shows earthquakes used in migration (diamonds).

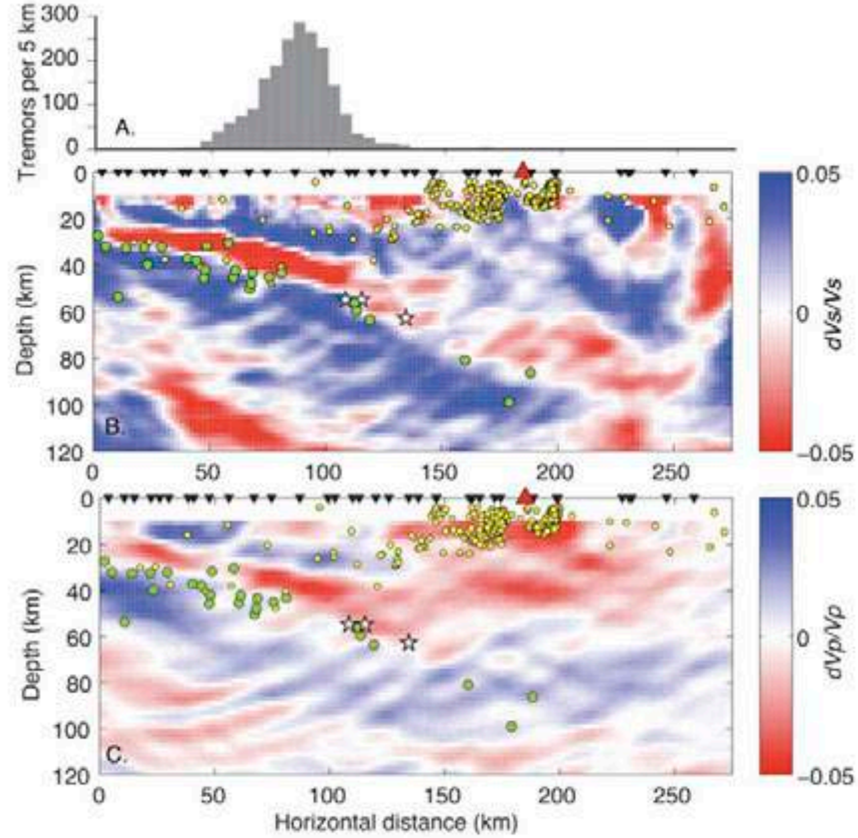

Figure 2. Migration images for central Washington, with seismicity and tremor. Transect location shown on Figure 1; horizontal distance of 0 km corresponds to coastline. A: Histogram of number of tremors shown in Figure 1 between section lines, in bins 5 km wide. B: *S*-wave velocity variations *dVs/Vs*, from migration. Green circles: earthquakes >20 km deep and between 47°N and 48°N latitude, occurring during CAFE and relocated using same velocity model as migration. Yellow circles: select events from local catalog (McCrory et al., 2004). Red triangle: Mt. Rainier volcano. Stars: three largest ($M > 6.5$) recorded earthquakes at waveform-derived depths. C: Same as B, but for *P*-wave velocity variations *dVp/Vp*.

Barcelona CSI
Center for Subsurface Imaging

Pervasive Seismic Wave Reflectivity and Metasomatism of the Tonga Mantle Wedge

Yingcai Zheng,[1] Thorne Lay,[1]* Megan P. Flanagan,[2] Quentin Williams[1]

(Science 2007)

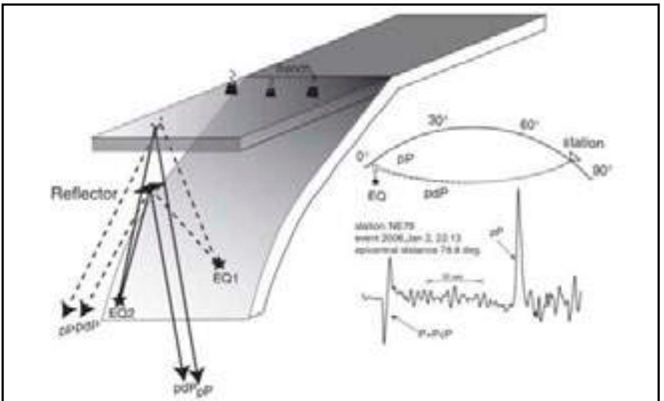

Fig. 1. Schematic of the Tonga mantle wedge imaging geometry. Deep-focus earthquakes within the subducted Pacific plate in the Tonga subduction zone radiate up-going energy that reflects from the underside of Earth's surface (*pP*) or the underside of velocity contrasts at depth *d* above the sources (p_dP) and then travels to teleseismic distances. The p_dP arrivals are precursors to the surface reflections. The inset shows ray paths for p_dP and *pP* to a teleseismic distance of 80°. Data from stations in the range from 40° to 140° were used for imaging the wedge. An example of a vertical-component seismogram is shown on the lower right, with energy between *P* and *pP* mainly caused by underside reflections, which arrive as precursors to *pP*. EQ, earthquake; *PcP*, down-going *P* wave that reflected from the core-mantle boundary.

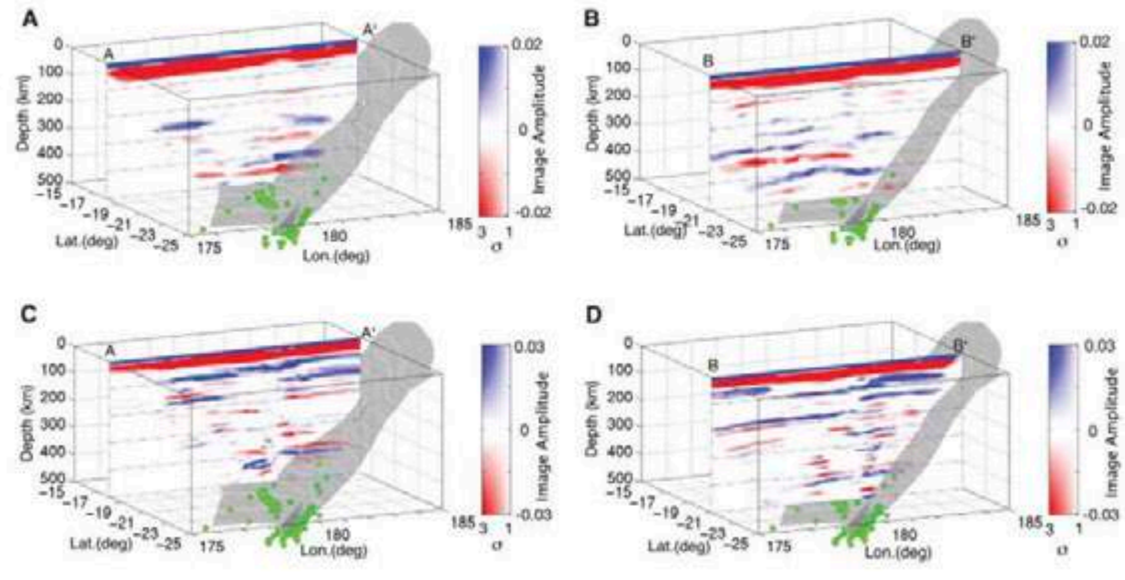

Fig. 4. Vertical west-east profiles in the (**A** and **B**) *P*-wave migration volume and (**C** and **D**) the *SH*-wave migration volume along profiles A to A′ (Fig. 2) at 18°S [(A) and (C)] and B to B′ at 21°S [(B) and (D)]. The period of the Ricker wavelet applied to the data is 16 s for *P* and 20 s for *SH*. Color scales correspond to those in Fig. 3. The strong blue and red stripes near the surface are the images of the *pP* and *sSH* surface reflections. The upper surface of the subducting Pacific plate is indicated by the gray facade. The deep-focus earthquake hypocenters are shown by green dots. The intermittence in the reflectors may be due to non-uniform ray path sampling. In many instances, the reflectors extend to the westward edge of our field of illumination.

State of the art geophysics for 3D higher-resolution physical properties determination

Target:

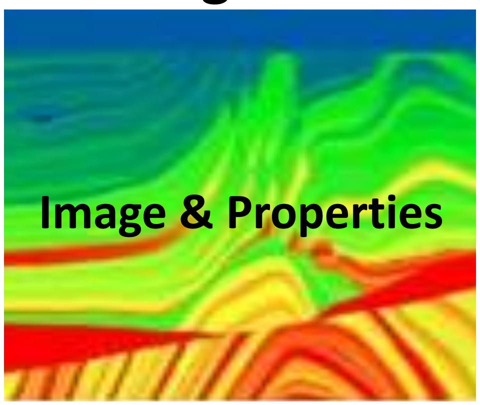

Pre-Stack Depth Migration

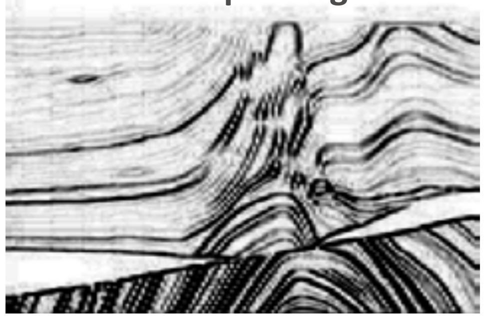

- Pre-stack **Depth migration** of Seismic reflection data (relatively short offsets)
- Excellent definition of boundaries and geometry (e.g. RTM)
- Limitations to determine physical properties **> need velocity model building (TTT)**

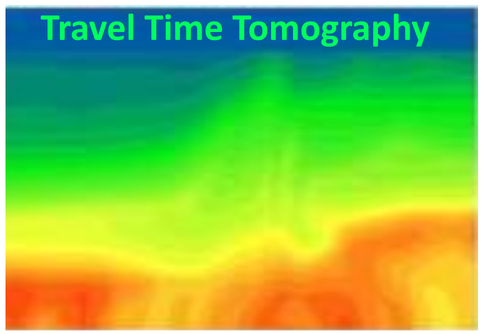

- **Travel Time Tomography** (Inversion) using arrival time of refracted + reflected phases.
- Ray theory > Resolution ~$(\lambda d)^{1/2} \approx 10^3$ m
- Moderately non-linear > robust; moderate computational cost; limited resolution.

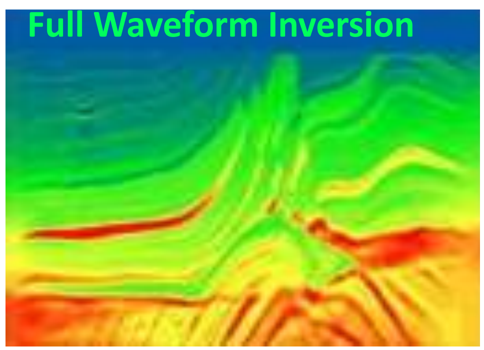

- **Full waveform inversion** (phases and amplitudes) > Advantages TTT & PSDM.
- Wave equation > Resolution ~$\lambda/2 \approx 10^1$-10^2 m (similar to MCS+PSDM).
- Strong non-linearity > Initial model, low freq, noise, source, computational cost.

Barcelona CSI
Center for Subsurface Imaging

State of the art geophysics for 3D higher-resolution physical properties determination

Full azimuth 3D data

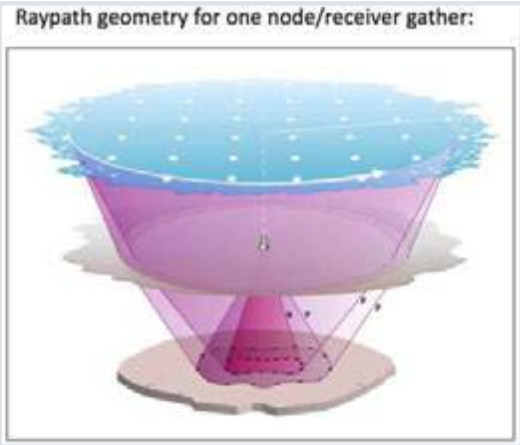

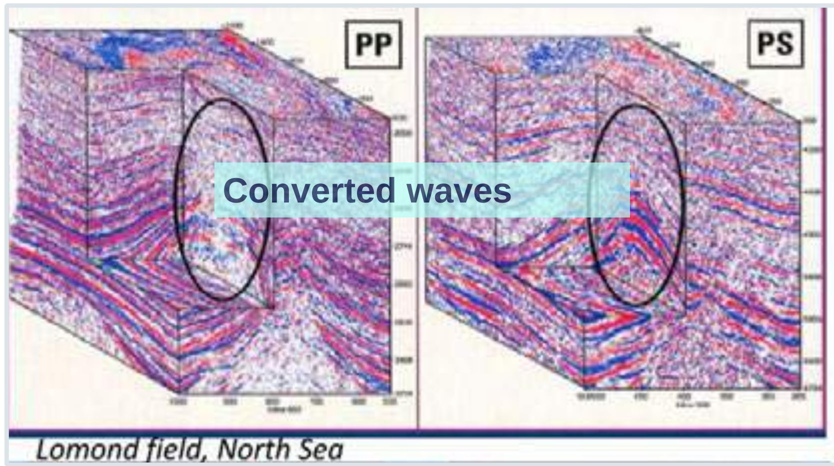

Converted waves

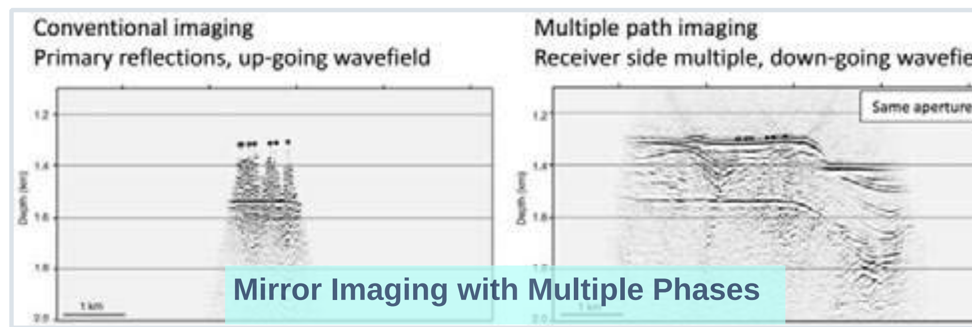

Mirror Imaging with Multiple Phases

Barcelona CSI
Center for Subsurface Imaging

Three major topics of subduction zones for the 21st century

- **Earthquakes and Slow Slip Phenomena at the mega-thrust interplate fault.**
- **Fluids and their relation to deformation.**
- **The incoming plates and slab structure.**
- **New technologies (instruments and algorithms)**

End presentation

Thank You!